TECHNISCHE UNIVERSITÄT DRESDEN

16th German Ferrofluid Workshop

Dresden
July 17th – 19th.
2017

Ferrofluid Workshop

Book of Abstracts

Program of the 16th German Ferrofluid Workshop

Dresden, July 17th –July 19th 2017

Sunday, July 16th

17:00 – 20:00 **Get together**

Monday, July 17th

09:00 **Opening**

09:20 **Synthesis**

09:20	B. J. Ravoo *Photo- and magnetoresponsive self-assembly of nanoparticles*	15
09:45	M.U. Witt, J. Strebe, S. Hinrichs, M. Hermes, B. Fischer, A. Schmidt, R.v. Klitzing *The influence of the microgel structure on the distribution of magnetic nanoparticles*	17
10:10	S. Hinrichs, N. Lucht, B. Fischer *Anisotropic magnetite particles and their incorporation into thermoresponsive hydrogels*	13

10:35 ***Coffee Break & Posters***

11:15 **Medical applications and biotechnology**

11:15	M. Pöttler, E. Scheiber, C. Bohr, M. Döllinger, C. Alexiou, S. Dürr *Magnetic tissue engineering of the vocal fold: generation of 3D cell constructs using superparamagnetic iron oxide nanoparticles*	112
11:40	C. Gräfe, I. Slabu, A. Weidner, E. Schreiber, R.P. Friedrich, F. Wiekhorst, C. Alexiou, S. Dutz, A. Hochhaus, J. H. Clement *The passage of SPIONs through an in vitro blood-brain barrier is dependent on the SPIONs' surface charge*	102
12:05	M. Liebl, D. Baumgarten, U. Steinhoff, L. Trahms, F. Wiekhorst *How to speed up magnetorelaxometry tomography*	104
12:30	M. Zhou, R. Müller, A. Dellith, T. Heinze *Meltable magnetic biocomposites for controlled release*	122

13:00 ***Lunch***

14:30 **Liquid crystals**

14:30	M. Kundt, K. Koch, O. Utan, N. Diklić, A. M. Schmidt *Improving the interaction of colloidal particles with a thermotropic nematic phase*	29
14:55	M. Hähsler, I. Appel, A. Eremin, R. Stannarius, S. Behrens *Stable suspensions of magnetic nanoparticles in thermotropic liquid crystals*	27
15:20	T. Potisk, D. Svenšek, H. Pleiner, H. R. Brand *Fundamental eigenmodes and rheological properties of a ferromagnetic nematic liquid crystal*	31

15:45 ***Coffee Break & Posters***

16:30 **Theory, modelling and simulation**

16:30	A.O. Ivanov, S.S. Kantorovich, E.A. Elfimova, V.S. Zverev, A.V. Lebedev, A.F. Pshenichnikov, P.J. Camp *Concentration-dependent zero-field magnetic dynamic response of polydisperse ferrofluids*	77
16:55	K. A. Kalina, J. Brummund, P. Metsch, M. Kästner *Modeling and simulation of hystereses in MREs filled with NdFeB particles*	78

17:20 ***Postersession***

Tuesday, July 18th

09:00 **Experimental**

09:00	E. Dohmen *Experimentally based finite element simulation of magnetorheological fluids with field dependent anisotropy*	37
09:25	J. Landers, S. Salamon, H. Remmer, F. Ludwig, H. Wende *Mössbauer spectroscopy as an instrument for simultaneous determination of particle mobility and orientation*	50
09:50	F. Ludwig, C. Balceris *The anisotropy of the ac susceptibility of magnetic nanoparticle suspensions*	52
10:15	T. Ilzig, S. Odenbach *Flow control in magnetic fluids*	48

10:40 ***Coffee Break & Posters***

11:20 ***Award ceremony for the Price of the Ferrofluid Society Germany***

Lectures of the awardees

12:40 ***Lunch***

14:00 **Experimental**

14:00	M. Hermes, E. Roeben, A. M. Schmidt *Size effects on magnetic particle nanorheology in complex fluids*	44
14:25	M. Gratz, A. Tschöpe *Rotational dynamics of Ni nanorods in polymer solutions*	40
14:50	H. Schmidt, G. K. Auernhammer *Interaction of magnetic chains in soft gels*	61

15:15 ***Coffee Break & Posters***

16:00 **Applications**

16:00	S.G.E. Lampaert, R.A.J. van Ostayen *Hydrostatic bearing with MR texturing*	94
16:25	T.I. Becker, J. Chavez Vega, V. Böhm, Yu.L. Raikher, O.V. Stolbov, S. Dutz, M. Zhou, S. Odenbach, K. Zimmermann *Investigations of magneto-sensitive elastomers in context of actuator and sensor applications*	92
16:50	O. Baun, P. Blümler *Mag-Guider: A permanent magnet system to guide and image super-paramagnetic nanoparticles*	90

19:00 ***Workshop Dinner***

Wednesday, July 19th

09:00 **Theory, modelling and simulation**

09:00	A. Zubarev, L. Iskakova *To the theory of shear elasticity of magnetic gels*	88
09:25	P. Ilg *Equilibrium magnetization and magnetization relaxation of multi-core magnetic nanoparticles from computer simulations*	75
09:50	M. Puljiz, S. Huang, G. K. Auernhammer, A. M. Menzel *Coupled displacements and rotations of magnetic particles in elastic environments in bulk and near rigid substrates*	82
10:15	N. Roth, R. Weeber, C. Holm *Towards the simulation of dynamic processes in magnetic gels*	84

10:40 ***Coffee Break & Posters***

11:20 **Ferrogels**

11:20	M. T. Lopez-Lopez, A. B. Bonhome-Espinosa, J. D. G. Duran, A. Zubarev *Biopolymer ferrogels. The role of nanoparticle concentration*	19
11:45	E. I. Wisotzki, K. Jazxhi, P. Tempesti, E. Fratini, S. G. Mayr *High energy crosslinking of gelatin ferrogels towards the development of a bioactuator*	25
12:10	S. Schatte, W.Grunert, S. Prévost, M. Gradzielski *Worm-like micellar gels connecting magnetic nanocubes*	23

12:35 **Closing**

20 Ferrofluid Workshop

ABSTRACTS

Abstracts

Material Synthesis

Ferrogels

Liquid Crystals

Experimental Techniques and Results

Theory

Technical Applications

Medical Applications

Advances towards responsive nanocomposites with supramolecular activity

L. Fruhner[1], M.Kruteva[1], J. Allgaier[1], W. Pyckhout-Hintzen[1], R. Koll[2], H. Heller[2], A. Feld[2], H. Weller[2]

[1] *Jülich Centre for Neutron Science, Forschungszentrum Jülich GmbH, 52425 Jülich, Germany*
[2] *Institute of Physical Chemistry, University of Hamburg, Grindelallee 117, 20146 Hamburg, Germany*

Recently, we published our results concerning homogeneously distributed superparamagnetic iron oxide nanoparticles (SPIONs) with a diblockcopolymer shell consisting of polybutadiene (PB) and poly(ethylene oxide) (PEO) in a PEO matrix. [1] Here, we present these results next to our recent advances towards responsive nanocomposites with supramolecular activity.

Motivation

Nanocomposites consisting of inorganic nanoparticles and polymer matrices are an important class of smart and adaptive materials. Unfortunately, the immiscibility between these two components leads to problems in their synthesis and handling. By shielding the particles with polymer hairs consisting of the same polymer as the matrix we were able to overcome this difficulty and achieve highly stable and monodisperse nanocomposites which can be seen in Figure 1. Staining the sample with phosphotungstic acid allows the display of the polymer shell around the nanoparticles.

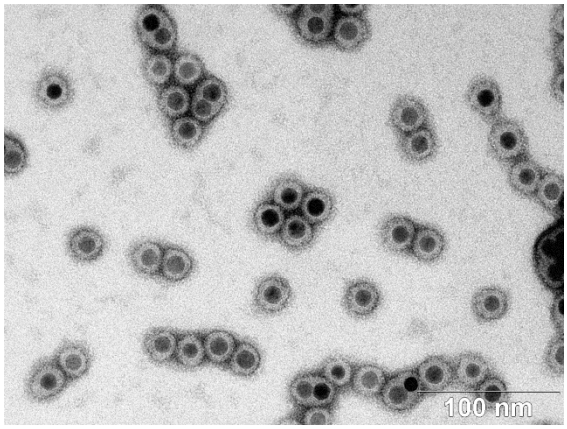

Figure 1 TEM image of nanocomposites

Synthesis improvements

The SPIONs are coated with a polymer multishell to stabilize them against aggregation (Figure 2). For this purpose, PB-PEO diblockcopolymers are prepared via anionic living polymerisation and used for micellar encapsulation of the SPIONs. While the PB part of the polymers is crosslinked via the thiol-ene click reaction to provide a dense shell structure, the PEO hairs form an outer corona which allows the nanocomposites to be well dispersed in water.

Although having achieved a highly homogeneous distribution of nanoparticles already, we are still aiming at improving the synthesis procedure. Using phosphonate groups instead of amino groups to attach the polymer ligands to the nanoparticles' surface, decreases the amount of ligand needed to provide a stable shell considerably.

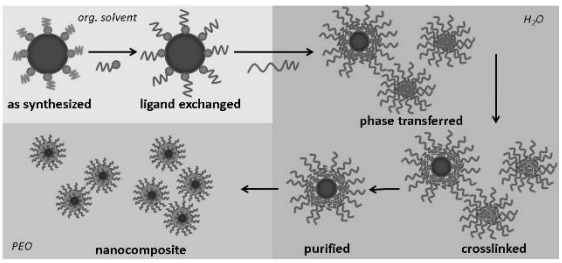

Figure 2 Synthesis procedure for nanocomposites

To avoid the high temperatures necessary during the radically initiated crosslinking of the inner polymer shell, we successfully tried to use UV light to initiate the thiol-ene click reaction. The so obtained samples' distribution of nanoparticles is comparable to the results of the normal procedure.

Longer polymer chains lead to even better distributions than before, making it possible to describe the data obtained via small-angle X-ray scattering (SAXS) with a spherical form factor only (Figure 3).

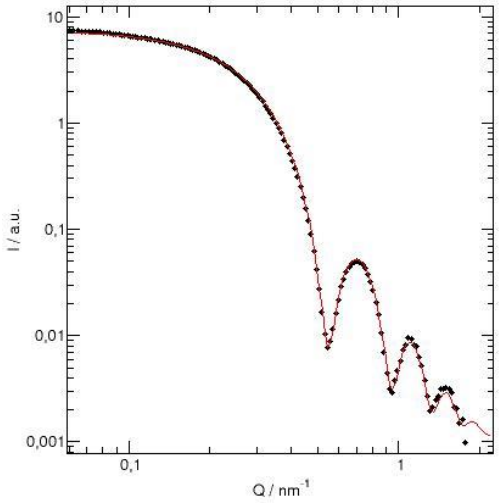

Figure 3 SAXS data of nanocomposite

Magnetic properties

Investigating our nanocomposites with magnetometry shows an excellent superparamagnetic behaviour, evidence for which can be found in the zero-field-cooled (ZFC) and field-cooled (FC) curves displayed in Figure 4.

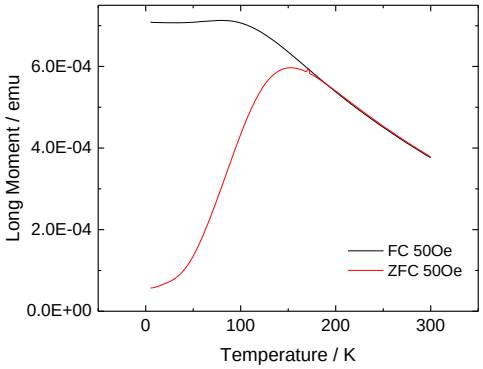

Figure 4 ZFC/FC curves of nanocomposite

When exposed to a magnetic field, the nanoparticles reveal an anisotropic scattering image. Using small-angle neutron scattering (SANS), it is possible to detect the magnetic contribution of the scattering of the nanoparticles.

Supramolecular functionalisation

Attaching supramolecular functionalities to the end of the polymer hairs leads to equally good distribution of nanoparticles in the polymer matrix. Additionally, functionalising also the matrix itself arises new interactions between particle and matrix.

Acknowledgments

Financial support is gratefully acknowledged from DFG-SPP 1681 “Feldgesteuerte Partikel-Matrix-Wechselwirkungen”.

References

[1] A. Feld, R. Koll, L. Fruhner et al, *ACS Nano*, **2017**, *11* (4), pp 3767–3775

Anisotropic magnetite particles and their incorporation into thermoresponsive hydrogels

S. Hinrichs[1], N. Lucht[1], B. Fischer[1]

[1] *University of Hamburg, Department of Physical Chemistry, Grindelallee 117, 20146 Hamburg.*

Hydrogels that respond to more than one stimulus are called multi-responsive hydrogels. A hydrogel consisting of a thermoresponsive polymer loaded with (anisotropic) magnetic particles is presented in this work. Special attention is paid to the synthesis and characterization of the thermo-responsive and magnetic properties.
The magnetic cores consist of magnetite particles coated by a silica shell of tunable thickness. The magnetic particles are synthesized by different methods to achieve different degrees of anisotropy and phase purity.
The polymer network material is *N*-isopropylacrylamide (Nipam) which undergoes a phase transition from a free elongated structure towards a coiled-globule formation around the human body temperature (~32 °C).

Synthesis of isotropic magnetic particles

To compare the effects of the particle shape on the properties of the hydrogels isotropic (spheric) as well as anisotropic (rhomboedric) particles were synthesized.
The synthetic scheme for spherical particles was based on the work of Zou et al.[1]. The reaction is a modified coprecipitation mechanism. Iron salts are added dropwise to a mixture of water, ammonia and hydrazine at 90 °C. To stabilize the particles in aqueous media citrate is added. The saturation magnetization lies at about 375 kA/m.
The silica shell can be added by dispersing the particles in water and adding a silica precursor, namely tetraethyl orthosilicate (TEOS), and again hydrazine as a catalyst. The thickness of the silica shell can be tuned from 6 nm (Figure 1a,b) to more than 20 nm by changing the content of TEOS.

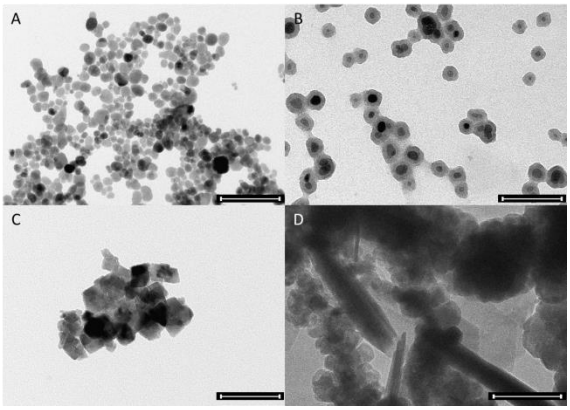

Figure 1: TEmicrographs of the particles synthesized in this work. A: Isotropic particles synthesized by the two phase method. B: The particles from A with a silica shell with a thickness of about 8 nm. C: Particles synthesized by reduction and aging in TMAH. D: Detail of Particles synthesized according to C but in a magnetic field. The scale bar in all images is 100 nm.

Synthesis of anisotropic magnetic particles

Anisotropic particles were synthesized by a hydrothermal approach in a twostep reaction.[2] In a first step precursors of β-FeOOH are synthesized which are subsequently reduced to magnetite by hydrazine. The magnetite particles grow in the shape of rhombohedra with a diameter of about 25 nm and are very phase pure.[3] The saturation magnetization lies at 363 kA/m. These particles can also be stabilized by citrate. (Figure 1c)
Another approach is the synthesis directly in a magnetic field.[4] Iron salts get reduced with or without the presence of a field of up to 180 mT and after that tetramethylammonium hydroxide (TMAH) is added and the precursor seeds are aged. The

aging step removes any impurities left in the system during the reduction step.
In Figure 1d a TEmicrograph of a detail from a sample prepared in a magnetic field by the aging method is displayed. Anisotropic shapes are produced by this method, but the ratio anisotropic:isotropic should be increased by further optimization.

Ferrogels

To obtain multi-responsive ferrogels the Fe_3O_4@Si particles are used as a basis for a free radical polymerization of Nipam. The Nipam strains get crosslinked by a bifunctional acrylamide to form a microgel. The thermoresponsive and magnetic properties of the microgel were characterized. The microgelbeads were crosslinked to a macrogel by utilizing glutaraldehyde.[5] The macrogel retains its thermoresponsive properties and responds to a magnetic field. (Figure 2) When comparing the magnetic response of the hydrogel to that of the pure particles it can be approximated that the hydrogel consists of roughly 0.8 wt% magnetic particles.

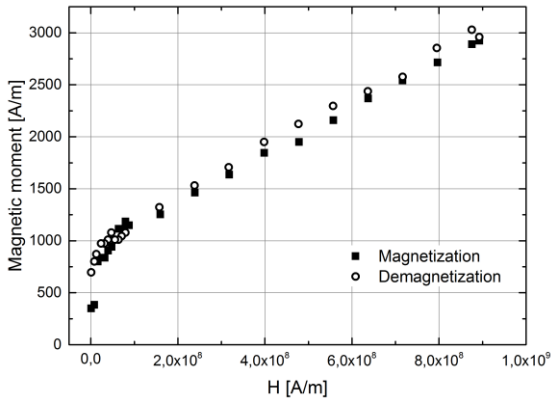

Figure 2: Magnetization curve of a microgel prepared with 25 nm particle diameter. The saturation magnetization lies at 3 kA/m suggesting a particle concentration of approximately 0.8 wt% of.

Acknowledgments

The author thanks the University of Hamburg program for doctoral scholarships for financial support.
The authors acknowledge the Deutsche Forschungsgemeinschaft (DFG) viathe priority program SPP 1681 "Feldgesteuerte Partikel-Matrix-Wechselwirkungen".

References

[1] Zou, J. et al., *RSC Advances* 4.19 **(2014)**: 9693-9700
[2] Peng, Z. et al., *Chem. Lett*. 34 **(2005)**: 636–637
[3] Hinrichs, S., Fischer, B., et al., *J. Magn. Magn. Mater*. 431 **(2016)**: 237-240
[4] Deshmukh, R. et al., *J. Nanopart. Res.* 19.1 **(2017)**: 13
[5] Nun, N., Fischer, B. et al. **(2017)** submitted

Photo- and magnetoresponsive self-assembly of nanoparticles

Bart Jan Ravoo

[1] *Organic Chemistry Institute and Center for Soft Nanoscience, Westfälische Wilhelms-Universität Münster, Germany. Email: b.j.ravoo@uni-muenster.de*

Self-assembly is emerging as a superior method to prepare adaptive and responsive nanomaterials. The structure and function of these materials is determined by the dynamic and weak interactions of the constituent "building blocks" of the material. Since the inherent interactions are weak, these versatile materials readily respond to even small changes and stimuli in their environment. In this contribution, we will highlight our newest findings concerning the preparation of photoresponsive and magnetoresponsive materials by self-assembly of nanoparticles. These structures are photoresponsive since the particles interact through photoresponsive host-guest interactions of cyclodextrins. Moreover, they are magnetoresponsive since they contain superparamagnetic nanoparticles.

We have prepared "magnetic vesicles" that self-assemble in microscale linear aggregates in aqueous solution under the influence of a magnetic field.[1] A noncovalent and photoresponsive azobenzene cross-linker can stabilize the metastable linear aggregates, which can be photoisomerized between an adhesive and a nonadhesive configuration. Thus, the hybrid soft material responds to magnetic field as well as to light and a stable self-assembled structure can only be obtained in a magnetic field in the presence of the cross-linker.

Furthermore, we explored arylazopyrazoles (AAPs) as a new light-responsive motif.[2] Compared to azobenzenes, AAPs offer quantitative photoisomerization in both directions and longer half-life times of the E-isomer. We have applied AAPs in photoresponsive clustering of nanoparticles. Moreover, we have prepared Janus silica particles (diameter 6 micron) by sandwich microcontact printing of an ATRP initiator and subsequent growth of polymer brushes exclusively in the printed caps of the Janus particles. AAPs can be included in the polymer brush caps and the resulting "guest" Janus particles form linear aggregates in the presence of superparamagnetic "host" nanoparticles coated with cyclodextrins.[3] These anisotropic aggregates can be manipulated in a magnetic field.

Finally, we have recently shown that the photoisomerization of azobenzenes and AAPs can be mediated by near-infrared irradiation of upconversion nanoparticles.[4] Currently, we investigate the photo- and magnetoresponsive assembly of multifunctional nanoparticle clusters containing metal, upconversion and superparamagnetic nanoparticles.

Acknowledgments

This research was funded by the Volkswagen-Foundation and the Deutsche Forschungsgemeinschaft.

References

[1] Schenkel, J.H.; Samanta, A.; Ravoo, B.J. *Adv. Mater.* **2014**, 26, 1076.

[2] Stricker, L.; Fritz, E.C.; Peterlechner, M.; Doltsinis, N.L.; Ravoo, B.J. *J. Am. Chem. Soc.* **2016**, 138, 4547.

[3] Samanta, A.; Ravoo, B.J. *Angew. Chem. Int. Ed.* **2014**, 53, 12946.

[4] Möller, N.; Hellwig, T.; Stricker, L.; Engel, S.; Fallnich, C.; Ravoo, B.J. *Chem. Commun.* **2017**, 53, 240.

Influence of the temperature gradient of the syntheses of monodisperse magnetic nanoparticles by thermal decomposition on the magnetically active particle volume

E. Siebert, S. Odenbach

Chair of Magnetofluiddynamics, Measuring and Automation Technology, Technische Universität Dresden, Dresden 01062, Germany

Introduction

The synthesis of monodisperse magnetic nanoparticles is of key-importance for understanding the interaction processes between different fractions of nanoparticles, by varying their size ratios and volume portions. It has been observed that the magnetically active particle volume can strongly differ from the hydrodynamic size of the particles and thus, leading to strongly decreased interactions among them. This could be examined by the decrease of the magnetoviscous effects in ferrofluids accordingly. In contribution to the conference it will be shown how the temperature gradient of the synthesis of monodisperse magnetic nanoparticles has an influence on the magnetically active particle volume.

Synthesis

Iron oxide nanocrystals has been obtained by a thermal decomposition reaction using the reaction pattern for 12 nm particles by Park et al. [1]

Methods

For measuring and controlling the temperature of the reaction the temperature controller LC6 from JULABO has been used. The controlling parameters have been optimized so that the temperature gradient can be hold constant over the whole reaction process.

The heating-up process for the first reaction has just been executed by full power heating until reaching the boiling point of the solution at approximately 320°C. Figure 1 shows the received temperature gradient.

For the second reaction the heating-up process has been set to a constant temperature gradient of 3.3°C/min until the temperature of 320°C is reached.

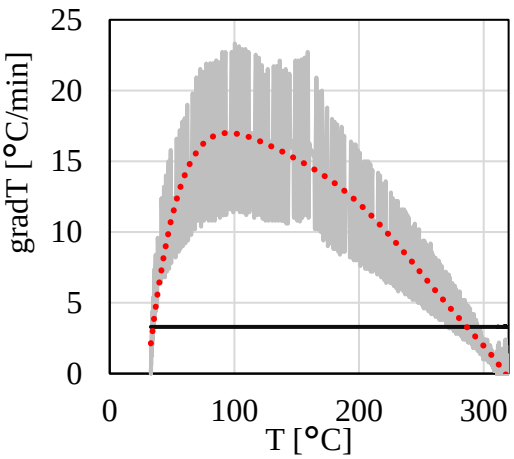

Figure 1: *Temperature gradient of the uncontrolled heating up (grey dots) with fit (red dots) and the controlled heating (black dots) over the reaction temperature.*

Results

The results lead to the assumption that the high temperature gradient of the uncontrolled heating up process is leading to a smaller magnetically active particle volume, while the constant slow heating is providing the possibility for the particles to grow magnetically “healthy”.

References

[1] Park, J. et. Al. (2004) *Nature materials* **3(12)**

The Influence of the Microgel Structure on the Distribution of Magnetic Nanoparticles

M.U. Witt[1], J. Strebe[1], S. Hinrichs[2], M. Hermes[3], B. Fischer[2], A. Schmidt[3], R.v. Klitzing[1]

[1] *Technische Universität Darmstadt, Institut für Festkörperphysik, Alarich-Weiss-Straße 10, 64287 Darmstadt*
[2] *Universität Hamburg, Institut für Physikalische Chemie, Grindelallee 117, 20146 Hamburg*
[3] *Universität zu Köln, Institut für Physikalische Chemie, Luxemburger Straße 116, 50939 Köln*

The following work is focused on the distribution of magnetic nanoparticles (MNP) inside of N-Isopropylacrylamid (NIPAM) microgel particles.

Introduction

In the field of multifunctional microgels the variability of systems is large. Starting from the built-in of co-monomers to get a system that is sensitive to the pH, over the incubation of gold nanoparticles to use light as an external stimuli. In this study we are using magnetic nanoparticles (MNP) to add a magnetic response [1].

Sample Preparation

The synthesized microgel consists of N-Isopropylacrylamid (NIPAM), N,N′-Methylenebis- (acrylamide) (BIS), Allylamine (AA). Two different synthesis routes are used to grow microgels with different internal structures. Both are surfactant free precipitation polymerisations. The first route was published by Pelton and Chibante [2] resulting in a heterogeneous microgel structure. In a heterogeneous microgel the amount of cross-linker BIS decreases with increasing distance from the particle center leading to a denser core and a fluffy shell. The second route is published by Acciro et al. [3]. Here the reactants are feeded into the reaction. In this way the concentration of BIS and AA in the reaction was constant. The constant concentration results in a homogeneous distribution of BIS and therefore in a constant mesh size over the whole scale of the microgel particle.
The MNP consist of Cobaltferrite. Two different batches are used. The first one is synthesized by the group of A. Schmidt (Universität zu Köln) and the second one by B. Fischer (Universität Hamburg).

Results

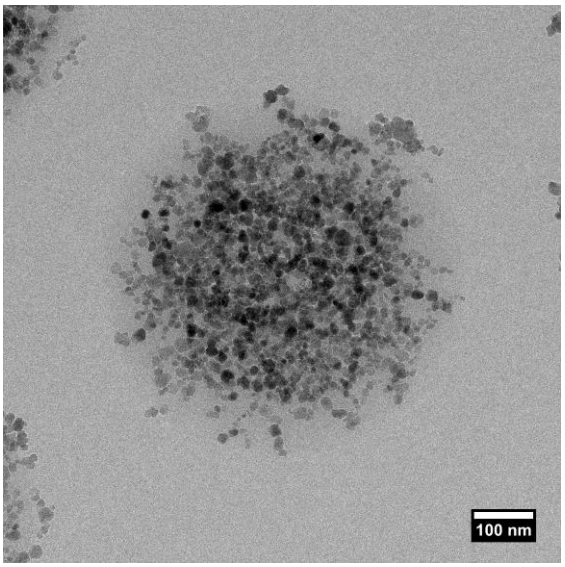

Figure 1: TEM picture of PNIPAM Microgel loaded with MNP.

Transmissions electron microscopy (TEM) images give information about the distribution of MNP inside the microgel. Fig. 1 shows such a TEM image. The picture shows the MNP distribution. The circular arrangement of the particles is originated in the shape of the microgel.

Fig. 2 shows the distribution of MNP inside the microgel as a cut through of the gel. The black pixel frequency gives the grey value distribution for a section of the hybrid particle.

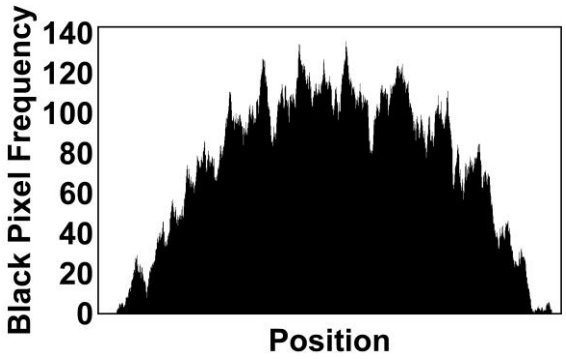

Figure 2: Histogram for the distribution of MNP inside the microgels derived from the TEM Image.

From the two dimensional projection, the three dimensional distribution of the MNP can be estimated.
The Gaussian distribution of the black values over the radius originates from a homogenous MNP distribution. The density of the MNP is constant over the gel. The electrons in the TEM have to travel a bigger Volume in the center of the gel, leading to a higher black value in the center.

The next measurements include the observation of the volume phase transition temperature (VPTT) using dynamic light scattering (DLS) and the change in the electrophoretic mobility (ZetaSizer). The measurements show that the well-known shrinking and swelling behavior of the microgels is preserved, even after the incubation of MNP.
In cooperation with A. Schmidt the magnetization is measured and compared to the magnetization of single MNP, improving the understanding of the coupling between MNP and microgel.

Outlook

Additional measurements are covering the response of the hybrids to external constant magnetic fields in bulk solution and at the surface.
A perspective is to use the microgels in order to form magnetic materials. These materials are easy to prepare, even at non-planar surfaces and show a fast reponse to outer stimuli.

References

[1] S. Backes, M. U. Witt, R. v. Klitzing, J. Phys. Chem. B **2015**, *119*, 12129-12137
[2] R. Pelton, P. Chibante, Colloids Surf. A, **1986**, *20*, 247-256
[3] R. Acciaro, Langmuir, **2011**, *27,* 7917-7925

Biopolymer ferrogels. The role of nanoparticle concentration

M. T. Lopez-Lopez[1], A. B. Bonhome-Espinosa[1], J. D. G. Duran[1], A. Zubarev[2]

[1] *Department of Applied Physics, University of Granada, Granada, Spain.*
[2] *Department of Mathematical Physics, Ural Federal University, Ekaterinburg, Russia.*

Hydrogels are 3-D networks of polymer chains in which the dispersion medium is an aqueous solution. Due to the versatility of the properties (mechanical, chemical, biocompatibility degree) of hydrogels, different applications have been reported for these materials in several fields, including biomedical applications [1].

Hydrogels can be endowed with exceptional properties by addition of synthetic materials. For example, the inclusion of magnetic particles in polymer gels enables the generation of magnetic hydrogels or ferrogels [2]. The magnetic character of ferrogels allows their control by noncontact magnetic forces, which represents an interesting feature for applications [3-5]. Furthermore, the fundamental investigation of the physical properties of ferrogels presents special challenges, due to phenomena such as changes in structure provoked by mechanical or magnetic stimuli [6].

In this work, we analyze the effect of nanoparticle concentration on the physical properties of ferrogels consisting of biopolymer networks with embedded magnetic particles, swollen by a water-based solution. We prepared these magnetic hydrogels by crosslinking of the biopolymer precursors in the presence of magnetic nanoparticles. We used two different protocols for the preparation of the ferrogels differentiated by the application in one of them of a magnetic field at the beginning of the crosslinking process. Both protocols resulted in the formation of macroscopically homogeneous ferrogels.

From the microscopic point of view, ferrogels crosslinked without field application presented some cluster-like knots that were connected by several polymer threads, whereas ferrogels crosslinked under a field presented alternating parallel bands of low and high concentration of polymers, aligned in the direction of the applied magnetic field. By contrast, non-magnetic hydrogels presented a homogeneous net-like structure with only individual connections between pairs of fibers.

Differences in the microstructure correlated well with the mechanical properties. Indeed, ferrogels presented a huge enhancement of the mechanical properties as the concentration of magnetic nanoparticles was increased. We studied, by using Winter Chambon criterion [7], the kinetic of the crosslinking process of the hydrogels and found that the characteristic gelation time diminished as the magnetic nanoparticles content increased.

From all this we can conclude that nanoparticles favor the crosslinking process, serving as nucleation sites for the attachment of the polymer chains. Attraction between the positive groups of the monomers and the negative surface groups of the magnetic nanoparticles justifies the enhancement role played by the nanoparticles on the mechanical properties of the ferrogels.

Finally, we developed a theoretical model that semiquantitatively explains the experimental results by assuming the indirect attraction among monomers through the attached nanoparticles. Due to this attraction, the monomers condense into nuclei of the dense phase. At the end of the polymerization process the nuclei (knots) of the dense phase crosslink the fibrin threads, so strengthening their structure and enhancing their mechanical properties.

Acknowledgments

This study was supported by project FIS2013-41821-R (Plan Nacional de Investigación Científica, Desarrollo e Inno-

vación Tecnológica, Ministerio de Economía y Competitividad, Spain, co-funded by ERDF, European Union). A. Z. is also grateful to the Russian Fund for Basic Research, 16-58-12003, the Program of Russian Federation Ministry of Science and Education, project 3.1438.2017/PCh.

References

[1] E. Caló, V. V. Khutoryanskiy: Biomedical applications of hydrogels: A review of patents and commercial products. European Polymer Journal 65, 252–267 (2015).

[2] M. T. Lopez-Lopez, J. D. G. Duran, L. Yu Iskakova and A. Yu Zubarev: Mechanics of Magnetopolymer Composites: A review. Journal of Nanofluids 5, 479-495 (2016).

[3] G. Pessot, P. Cremer, D. Y. Borin, S. Odenbach, H. Löwen and A. M. Menzel.: Structural control of elastic moduli in ferrrogels and the importance of non-affine deformations. The Journal of Chemical Physics 141, 124940 (2014).

[4] M. T. Lopez-Lopez, G. Scionti, A. C. Oliveira, J. D. G. Duran, A. Campos, M. Alaminos and I. A. Rodriguez: Generation and characterization of novel magnetic field-responsive biomaterials. PLoS One 10, e0133878 (2015).

[5] L. Rodriguez-Arco, I. A. Rodriguez, V. Carriel, A. B. Bonhome-Espinosa, F. Campos, P. Kuzhir, J. D. G. Duran and M. T. Lopez-Lopez: Biocompatible magnetic core–shell nanocomposites for engineered magnetic tissues. Nanoscale 8, 8138-8150 (2016).

[6] A. B. Bonhome-Espinosa, F. Campos, I. A. Rodriguez, V. Carriel, J. A. Marins, A. Zubarev, J. D. G. Duran and M. T. Lopez-Lopez: Effect of particle concentration on the microstructural and macromechanical properties of biocompatible magnetic hydrogels. Soft Matter 13, 2928-2941 (2017).

[7] F. Chambon and H. H. Winter: Linear viscoelasticity at the gel point of a crosslinking PDMS with imbalance stoichiometry. Journal of Rheology 31, 683-697 (1987).

Magnetic Hydrogels: Exploiting the Stabilizing Silica Shell to Tailor the Mechanical Properties of the Gel

N. Lucht[1], S. Hinrichs[1], B. Fischer[1]

[1] *University of Hamburg, Department of Chemistry, Institute of Physical Chemistry, Grindelallee 117, 20146 Hamburg*

Stimuli-responsive hydrogels are cross-linked polymers that are able to react to certain applied stimuli. The typical stimuli that are applied are temperature and pH value.[1] A modern approach is the introduction of nanoparticles to tune the properties of the gel. Hydrogels with embedded magnetic cores are commonly called ferrogels.[2]

The typical synthetic route for ferrogels starts with the synthesis of a stable watery ferrofluid. To increase the stability in solution and to prevent ripening of the magnetic particles a stabilizer is needed. One possibility is the use of surfactants like sodium citrate. In our case we synthesize a silica shell which is synthetically more complex but very robust on the upside. The second major step is the polymerization and cross-linking of the polymer matrix. The used polymerization technique is typically a free radical polymerization. The primary advantage of this technique is its simplicity and applicability for most polymer systems. The inherent disadvantage of this technique is the low degree of reaction control. Nonetheless ferrogels created by this method show remarkable magnetic and – depending on the matrix material - temperature or pH responsivity. These very promising mechanical and chemical properties are subject to further research.

One point of interest that has not yet been excessively studied is the silica shell. Usually the silica shell is used as stabilizer as well as 'linker' between magnetic particle and gel interface. To achieve this 'linkage' a small shell is sufficient in most cases. Our new approach makes use of a huge silica shell with roughly the quadruple

Figure 1: Sketched inside-out etching mechanism of a silica shell (grey) with magnetic core (black).

diameter of the magnetic core. This enables direct manipulation of the shell. Acetic acid and sodium hydroxide are reagents that can dissolve the shell while leaving the magnetic core untouched.[3] Sodium hydroxide is the 'fast & easy' approach which typically does not need special conditions and can be tuned solely by the concentration of sodium hydroxide in the system. The inherent disadvantage of this system lies in the possibility of recondensation of the dissolved silicium oxide derivatives leading to possible agglomeration during the etching process. Acetic acid etching on the other hand is the 'slow & complicated' approach which has the big advantage of inhibiting the mentioned recondensation process while being much slower and synthetically more complex than the sodium hydroxide approach.[3] Independently of the used synthetic treatment the mechanism of the etching process remains in principle the same. Silica spheres or in our case silica shells are synthesized in a base catalyzed condensation reaction of the quadrivalent tetraethyl orthosilicate (TEOS). Two TEOS molecules have basically two possible types of interaction. On the one hand two Si-OH groups can interact via hydrogen bonding on the other hand via a condensation reaction to Si-O-Si with the latter being a more stable but much slower process. The particle formation includes a rapid nucleation that leaves no time for the formation of condensed Si-O-Si bonds. The shell growth process is much slower in

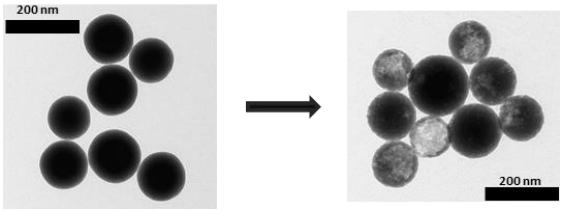

Figure 2: Transmission electron microscopy image of pure silica spheres (left) etched with acetic acid forming hollow spheres (right) as model system.

comparison which decreases further with a growing shell leaving the TEOS more time to condense. The etching agent is able to break the condensed Si-O-Si bonds and therefore dissolves the particle network. The 'rule of thumb' for this process: The lower the condensation grade of the TEOS the more effective the bond breakage while a fully condensed TEOS cannot be dissolved under typical experiment conditions. Therefore the particles are etched in an inside-out mechanism while leaving the surface of the silica particle untouched preserving the structural integrity of the silica shell/particle (see Figure 1). This etching process in combination with a magnetic particle filled hollow silica sphere embedded in a gel matrix allows the particle to move freely inside the etched cavity (see Figure 2). As a first interesting application to exploit this high degree of freedom in comparison to the 'fixed' gel solution would be the application of an AC magnetic field to heat up the gel via induction and force a phase transition of the thermoresponsive gel matrix.

Another project for the future will be the surface functionalization of the silica shell to link a chain transfer agent (CTA) to the surface to allow controlled radical polymerization directly on the particle surface.[4] This polymerization technique allows the synthesis of a highly ordered gel matrix possibly increasing the mechanical and magnetic properties of the ferrogel.

Acknowledgements

The author thanks the Deutsche Forschungsgemeinschaft (DFG) for funding our project inside the Schwerpunktprogramm 1681 (SPP 1681) "Feldgesteuerte Partikel-Matrix Wechselwirkungen".

References

[1] M. Krekhova, G. Lattermann, H. Schmalz, T. Lang and R. Richter, *Physcs Proc*, 2010, **9**, 224-228.

[2] A. P. Safronov, O. M. Samatov, I. S. Tyukova, E. A. Mikhnevich and I. V. Beketov, *J Magn Magn Mater*, 2016, **415**, 24-29.

[3] H. L. Ding, Y. X. Zhang, S. C. Xu and G. H. Li, *Nano Res*, 2016, **9**, 3632-3643.

[4] C. Li, J. Han, C. Y. Ryu and B. C. Benicewicz, *Macromolecules*, 2006, **39**, 3175-3183.

Worm-like micellar gels connecting magnetic nanocubes

S. Schatte[1], W.Grunert[1], S. Prévost[2], M. Gradzielski[1]

[1] *Institut für Chemie, Technische Universität Berlin, Straße des 17. Juni 124. D-10623 Berlin, Germany.*
[2] *Institut Laue-Langevin, D11, 71 avenue des Martyrs, F-38000 Grenoble, France.*

Introduction

Comprehending the interplay between self-assembled networks and (cubic) nanoparticles (MNP) in thermoresponsive aqueous ferrogels is essential. It is essential because responses to mechanical stress, temperature and magnetic field can be manipulated. Most ferrogels result from adding polymeric gelators to an existing ferrofluid.[1] Pockets of the original ferrofluid are encapsulated by domains of polymer molecules on a colloidal scale. Thus, such systems exhibit no synergistic response due to the missing interplay between matrix and particles. A more elaborated ferrogel, which responds to stimuli, is thereby constructed.
We use small angle scattering techniques (SAXS, SANS) to get a detailed picture of the interplay between monodisperse silica coated MNPs incorporated into a gel network. In static SAS we can observe particle and gel fiber arrangement at nanoscale, while time-resolved SAS shows us the kinetics of such systems (relaxation time and pathway of particles and network).

Worm-like micellar gels

A new class of gels is based on combining fatty acids with basic amino acids. Such gels are eco-friendly, non-toxic and cheap. They present attractive rheological and temperature-dependent properties. The viscosity changes reversibly over orders of magnitude by heating/cooling shown in Fig. 1.
By concentration changes, the network density can be influenced. By pH changes, the system can be switched from a vesicle gel to a viscoelastic network formed by worm-like micelles, tuning structure and properties elegantly (Fig. 5, bottom).

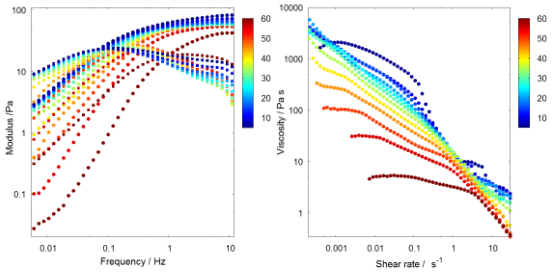

Fig. 1: T dependent rheology measurements: left: storage (●) & loss (■) modulus:; right: viscosity as a function of shear rate

Cubic magnetic nanoparticles

Highly monodisperse Fe_3O_4, $CoFe_2O_4$ (hard ferrite) and $Mn_xZn_{1-x}Fe_2O_4$ (soft ferrite) nanocubes in a size range of 7 to 17 nm (edge length, 10 to 30 nm space diagonal) were synthesized using a thermal decomposition route.[2] The large scale reaction's particles (2-3 g) are shown in Fig. 2 and 5.

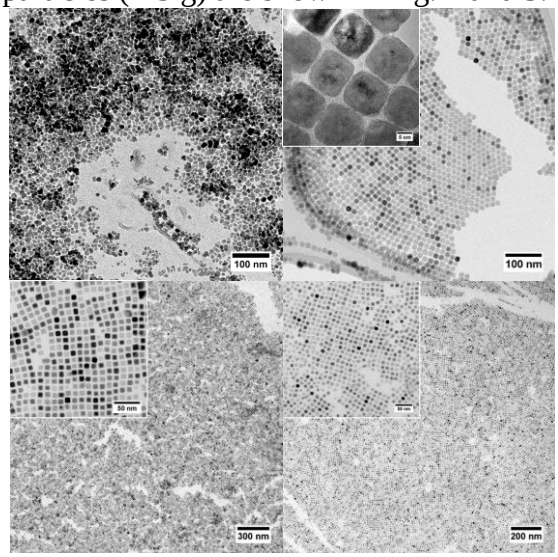

Fig. 2: TEM images of a commercial ferrofluid; as synthesized Fe_3O_4, $CoFe_2O_4$ and $Mn_{0.5}Zn_{0.5}Fe_2O_4$ nanocubes (from top left to bottom right).

Such monodisperse nanoparticles are required for detailed structural investigations (SAS). Commercial ferrofluids are unsuitable due to high polydispersity, (Fig. 2, top left).

The final nanoparticles are coated with a stabilizing hydrophobic oleate shell as seen from infrared spectroscopy and thermogravimetric analysis (Fig. 3).

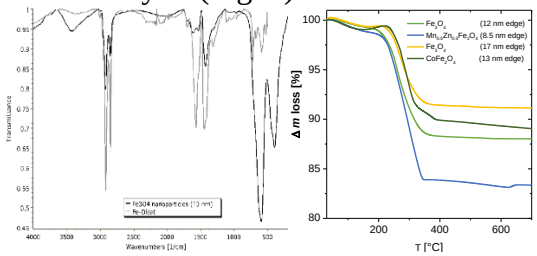

Fig. 3: left: IR spectroscopy of precursor (light grey) and final particles (black); right: TGA curves of differently sized particles.

Silica coating

For enhancing colloidal stability and integrating these hydrophobic MNPs into a hydrogel network, they need to be surrounded by a hydrophilic and protective shell that can be modified chemically. This shell is obtained by a silica coating via a reverse µ-emulsion reaction.[3]

The coated particles are hydrophilic and hence water dispersible with homogeneous shells. The shell thickness can be tuned 4 to 15 nm. (Fig. 4) We enhanced the synthesis in literature towards improved homogeneity and up scaled it by a factor of ~50.

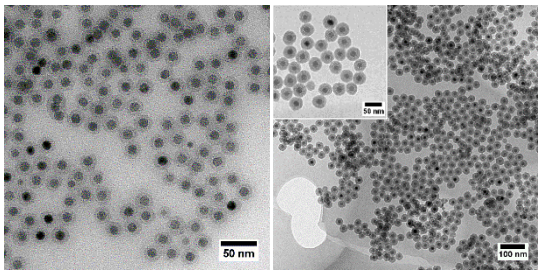

Fig. 4: TEM images of different silica shell thicknesses with the same magnetic core.

Ferrogel modification/Perspective

Aiming at a responsive ferrogel as a versatile system, we intend to combine MNPs and gels. The properties of these ferrogels cannot only be controlled by pH, temperature and composition, but also by a possible hydrophobic shell modification.

These ferrogels will be further characterized in dynamic SAS measurements with magnetic field.

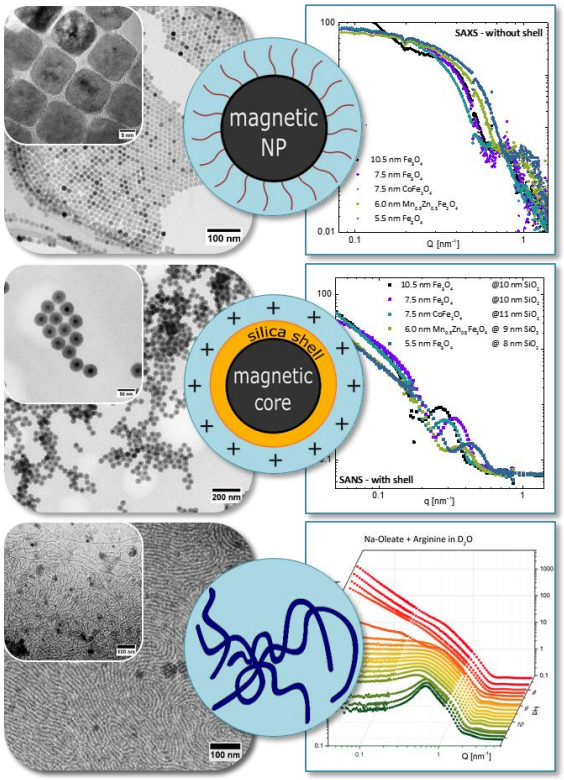

Fig.5: Summary of magnetic core, silica shell and micellar gel characterized by (cryo)-TEM, SAXS and SANS (in D_2O, core matched).

The particles are currently investigated in combination with spider silk to create magnetic filter systems (C. Grill, Universität Bayreuth). The gel system will be observed in ACS measurements, taking advantage of viscosity changes with temperature (H. Remmer, T. Viereck, S. Draack, TU Braunschweig).

Acknowledgments

This work is supported by DFG PR-1473/1 and GR-1030/18-2 within the Priority Program SPP1681. The authors would like to thank the following large scale facilities for beam times: HZB (U.Keiderling), FRMII (M.-S.Appavou), PSI (J. Gavilano), LLB (L.Noirez), ILL (I. Grillo), ESRF (S.Prévost); the following facilities for TEM: FHI (G.Clavel), ZELMI (S.Selve), Uni Jena (M.v.d.Lühe).

References

[1.] Krekhova & Lattermann, *J. Mater. Chem.* **18,** 2842 (2008).
[2.] Park *et al.*, *Nat. Mater.* **3,** 891 (2004).
[3.] Ding *et al.*, *Chem. Mater.* **24,** 4572 (2012).

High energy crosslinking of gelatin ferrogels towards the development of a bioactuator

E. I. Wisotzki[1], K. Jazxhi[1], P. Tempesti[2], E. Fratini[2], S. G. Mayr[13]

[1] *Leibniz Institute of Surface Modification (IOM), Permoserstr. 15, 04318, Leipzig, Germany.*
[2] *Department of Chemistry "Ugo Schiff" and CSGI, University of Florence, via della Lastruccia 3, 50019, Sesto Fiorentino (FI), Italy.*
[3] *Faculty of Physics and Earth Sciences, Leipzig University, Germany.*

In biomedicine, there is significant interest in ferrogels as magnetically responsive composites with potential applications in active drug delivery, actuation and sensing. This project is centered on the synthesis and optimization of radiation crosslinked gelatin ferrogels to design a biocompatible, biodegradable actuator. Modification of gelatin ferrogels with high energy electron irradiation is aimed at achieving magneto-mechanical coupling between particles and the matrix, particularly above the native gelatin sol-gel transition [1]. For such applications, it is critical to understand the coupling and interactions between the magnetic nanoparticles (MNPs) and surrounding matrix. Here, the local network structure as relevant to nano- and microparticles was investigated using scattering and microscopy techniques, in comparison with macroscopic analysis based on rheology and swelling ratios.

SAXS analysis of irradiated hydrogels

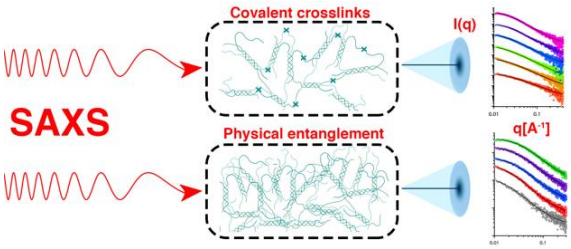

Figure 1: SAXS revealed ranging structural differences in physically entangled and irradiation-crosslinked gelatin hydrogels.

Small-angle X-ray scattering (SAXS) was used to investigate the network structures of gelatin hydrogels with increasing irradiation dose in contrast to gels of increasing physical entanglement [2]. Both increasing irradiation dose and polymer concentration resulted in higher macroscopic shear moduli and reduced swelling ratios due to additional chemical and physical crosslinking, respectively [3]. Fitting the Ornstein-Zernike function with an open Lorentzian exponent indicated that the irradiated gels exhibited increasingly branched and globular structures. Similarly, power law fits revealed the fractal dimension of the irradiated gels increased from values expected for swollen polymer coils to those of branched polymers and chemical gel networks.

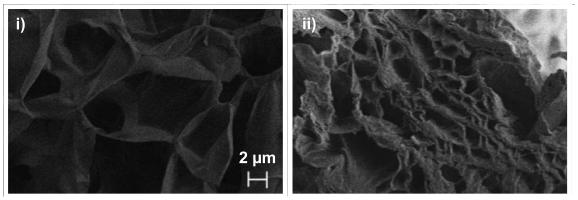

Figure 2: Micrographs of freeze-dried 4 wt% gelatin hydrogels i) unirradiated and ii) irradiated with 10 kGy.

In contrast, the physically entangled gels of increasing concentration reduced the fractal dimension towards those of a rigid linear object, corresponding to an increase in the triple helical content of the networks. Although both radiation and concentration had similar effects on the network macroscopically, SAXS profiles revealed differences in the network structures on the nanoscale. Changes to the porosity of the microstructure were also observed with scanning electron microscopy (SEM) of the freeze-dried hydrogels.

From SAXS-obtained mesh sizes, the network shear modulus was predicted using

several flexible and semi-flexible models, then compared to the macroscopically determined shear moduli. Overall, differences in the scaling behavior of the networks was apparent, highlighting fundamental differences in the entangled and chemically crosslinked gel networks.

Magnetic response of irradiated ferrogels

The next stages of the project are focusing on achieving magneto-mechanical coupling between MNP and irradiated gelatin networks to demonstrate potential as a magnetically-controllable bioactuator. Experiments are ongoing in a custom 1 T pole shoe magnet. The interplay between the degree of crosslinking (i.e. irradiation dose) and cycling of the actuator (i.e. fatigue) are being explored.

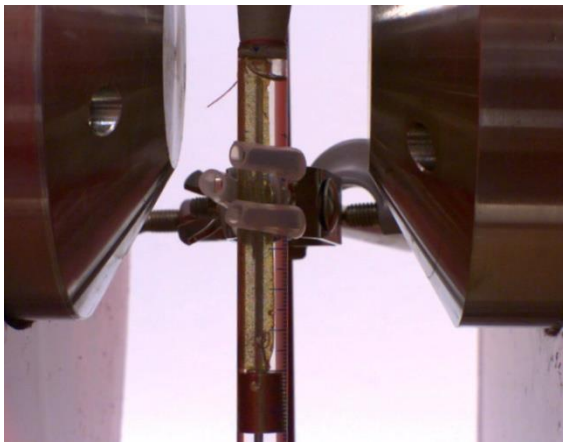

Figure 3: Experimental setup to measure deformation of homogeneously dispersed magnetic particles (20 mg/mL) arrested in 10 wt% gelatin, irradiated with 5 kGy.

Acknowledgments

This research is funded by the German Science Foundation (DFG) Priority Program (SPP) 1681 “Feldgesteuerte Partikel-Matrix-Wechselwirkungen: Er-zeugung, skalenübergreifende Modellierung und Anwendung Materialien” grant number MA 2432/6.

References

[1] Wisotzki, E. I., Eberbeck, D., Kratz, H. and Mayr, S. G. Soft Matter, 12:3908-3918, 2016.

[2] Wisotzki, E. I., Tempesti, P., Fratini, E. and Mayr, S. G. Phys. Chem. Chem. Phys. 19:12064-12074, 2017.

[3] Wisotzki, E. I., et al. J. Mater. Chem. B. 2:4297, 2014.

Stable Suspensions of Magnetic Nanoparticles in Thermotropic Liquid Crystals

M. Hähsler[1], I. Appel[1], A. Eremin[2], R. Stannarius[2], S. Behrens[1]

[1] Institute of Catalysis Research and Technology; Karlsruhe Institute of Technology (KIT), PB 3640, 76021 Karlsruhe; [2] Department of Nonlinear Phenomena, Otto von Guericke University Magdeburg, PB 4120, 39106 Magdeburg

Liquid crystals (LCs) combine properties of both the liquid and crystalline state. The magnetic susceptibility of low-molecular-weight organic LCs is comparably small. Therefore, alignment of such LCs in thin cells requires high magnetic fields. Integration and stabilization of magnetic nanoparticles (MNPs) in LCs can increase the magnetic susceptibility and thereby the response to an applied magnetic field [1]. Chen [2] and Mertelj et al. [3], for example, realized the integration of magnetic NPs in LCs with interesting magneto-optical properties. However, a long-term stabilization of magnetic NPs in LCs is still a challenging task.

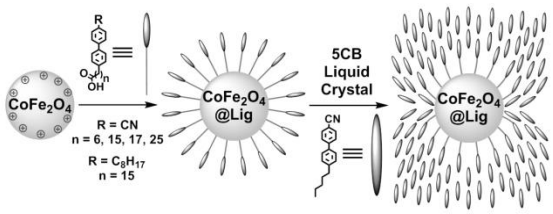

Figure 1**:** Functionalization of magnetic nanoparticles with ligands and integration in a liquid crystal.

The LC anchoring at MNP surfaces, MNP sizes as well as interparticulate interactions are the most important parameters that determine the behavior of ferronematics. In order to modulate the LC-MNP interactions and MNP stability in the LC, a series of (pro-)mesogenic ligands was prepared by systematically varying the chemical nature of the three functional ligand entities, i. e., (1) the MNP binding group and (2) the mesogenic unit both linked via (3) an alkyl chain. Besides loading the electrostatically stabilized MNPs, MNPs functionalized by (pro-)mesogenic ligands were also obtained from oleic-acid stabilized MNPs by using ligand exchange procedures. The behavior of the MNP@Lig nanoparticles was examined in a commercial LC host, 4-pentyl-4‘-cyanobiphenyl (5CB), in the bulk and in thin films in LC test cells. An investigation of the coupling efficiency revealed that carbonic acids lead to the highest ligand loading (TGA of ligand loading: NH_2 (12 wt%), PO_3H_2 (25 wt%) and COOH (50 wt%)) [4]. We have further shown that an increase in length and flexibility of the alkyl linker -$(CH_2)_n$- from n = 6 to 15 result in better stability and increased concentration of MNPs in the LC host.). The further increase of the chain length to n = 17, however, did not significantly improve MNP stability and concentration in the LC, and ligands with a linker length of n > 17 revealed low solubililities in organic solvents and 5CB. Moreover, the endgroup of the (pro-)mesogenic entities (R = CN, C_8H_{17}) significantly influenced the stability of the functionalized MNPs in 5CB (Figure 2).

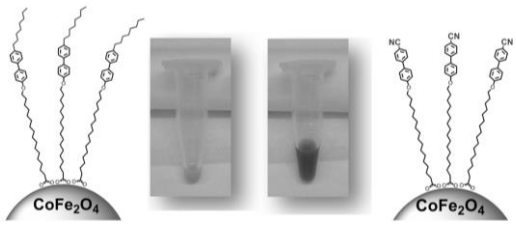

Figure 2**:** Stabilization of MNPs in LCs: CN endgroup leads to better MNP stability and a higher MNP concentration in the LC.

$CoFe_2O_4$@Lig MNPs (size 2.5 nm, R = CN, n = 15) yielded stable colloidal suspensions in 5CB. As compared to undoped 5CB, the $CoFe_2O_4$@Lig-5CB hybrids showed an increased sensitivity to the magnetic field, affecting the Fréedericksz transition. The coupling of the small,

spherical MNPs with the LC director in the magnetic field suggests the formation of LC-induced, anisometric MNP clusters. The interaction of the MNPs with the 5CB host and cluster formation was monitored by SAXS, SANS and by SQUID magnetometer measurements [5].
The understanding of this process supports the preparation of stable colloidal systems with well dispersed MNPs. In view of bigger MNPs, dendric ligands equipped with mesogenic units may minimize the distortion of the ligand sphere (Figure 1) and thus aggregation effects, and offer a promising approach for MNP-LC hybrids, in particular if the dendritic ligand itself exhibits liquid crystalline properties [6, 7].

Acknowledgments

The financial support by the DFG via SPP1681 and the experimental support of Kai Nagel are gratefully acknowledged.

References

[1] F. Brochard; P. G. de Gennes, *Journal de Physique* **1970,** *31* (7), 691-708.
[2] S.-H. Chen; N. Amer, *Physical Review Letters* **1983,** *51* (25), 2298-2301.
[3] A. Mertelj; D. Lisjak; M. Drofenik; M. Copic; *Nature* **2013,** *504* (7479), 237-241.
[4] I. Appel; H. Nadasi; C. Reitz; N. Sebastian; H. Hahn; A. Eremin; R. Stannarius; S. Behrens; Chemical *Phys. Chem. Chem. Phys.*, **2017**, *19*, 12127-12135.
[5] V. Gdovinova; M. Schroer; N. Tomasovicova; I. Appel; S. Behrens; J. Majorosovaa; J. Kovac; D. Svergun; P. Kopcansky, in preparation.
[6] M. Draper; I. M. Saez; S. Cowling; P. Gai; B. Heinrich; B. Donnio; D. Guillon; J. Goodby, Adv. *Funct. Mater.* **2011**, *21*, 1260–1278.
[7] M. F. Prodanov; O. G. Buluy; E. V. Popova; S. A. Gamzaeva; Y. O. Reznikovb; V. V. Vashchenkoa, *Soft Matter* **2016,** *12*, 6601-6609.

Improving the interaction of colloidal particles with a thermotropic nematic phase

M. Kundt,[1] K. Koch,[1] O. Utan,[1] N. Diklić,[2] A. M. Schmidt [1]

[1] *Department Chemie, Institut für Physikalische Chemie, Universität zu Köln, Luxemburger Str. 116, D-50939 Köln, email: Annette.schmidt@uni-koeln.de*
[2] *Faculty of Physical Chemistry, University of Belgrade, Studentski trg 12-16, 11158 Belgrade 118, Serbia*

The spontaneous formation of orientationally ordered, nematic phases in thermotropic liquid crystals and their manipulation by external stimuli is of huge importance for their application, e. g. in optical displays and as sensors.
The control of the orientational order of liquid crystals (LCs) by magnetic fields *via* the magnetic Fréedericksz transition is less common than the use of electric fields, as the relatively small anisotropy of the diamagnetic susceptibility of liquid crystals requires a large threshold magnetic flux of several Tesla to induce a shift of the nematic director in pure LC.
However, as predicted by deGennes and Brochard already in 1970, the incorporation of dipolar particles is expected to result in nematic phases that are readily manipulable at moderate magnetic field strength.[1] One of the main obstacles in that has to be overcome is the aggregation of the dispersed nanoparticles.[2] It is known that the shape and size of the particles are relevant for the degree of anchoring of the mesogens to the particles surface. Due to a comparable shape, elongated particles are shown to better influence the orientation of adjacent molecules of the liquid crystal.[3] The switching of a particle-doped LC with low external fields was successfully realized with small, anisotropic barium hexaferrite particles, but even there agglomeration of the particles could not be completely prevented.[4]

Liquid crystal polymer brush particles

Our new approach toward particle-doped LC phases is based on elongated hematite particles that are decorated with a side-chain LC polymer brush. We couple a polymethylsiloxane (PHMS) with *n*-alkyloxycyanobiphenyl (nOCB)-based mesogenic side chains to a functionalized particle (Figure 1). The approach allows independently the variation of the shell thickness, the mesogen density, and the spacer length. It results in an effective steric stabilization of the particles against agglomeration and offers a high degree of functionalization of the particles with respect to the mesogen. This way, we aim to optimize the coupling energy *W* between the particle surface and the resulting particle-matrix compatibility.

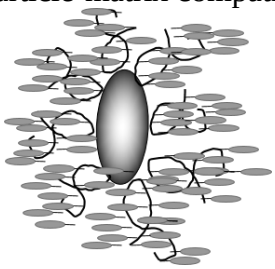

Figure 1. Scheme of LC polymer brush particle

As a model system for the interaction between particle surface and the surrounding matrix, the compatibility of the functionalized polymer with the LC phase is probed by exploring the phase diagram of the LC polymer in a common mesogen (*p*-pentylcyanobiphenyl, 5CB). A stable nematic phase at low polymer content and the formation of a smectic phase at higher polymer fraction is observed, proving the good coupling between the two components.
nOCB-PHMS is grafted onto spherical SiO_2 particles of varying size, magnetically blocked $CoFe_2O_4$ particle as well as spindle-like α-Fe_2O_3 particle. Depending on the particle size, up to 1 m% of particle can be dispersed without formation of agglomerates. The formation of the nematic phase is not disturbed by the particles.

Investigations on the order parameter *S* of the dispersions in 5CB showed that *S* is decreasing for 5CB doped with SiO_2, but is constant or slightly increasing for dispersions of magnetic particles in 5CB.

Optical switching in external magnetic fields

In a setup combining polarization microscopy with magnetic coils, the influence of an external magnetic field on particle doped 5CB is investigated. A magnetic flux of 150 mT is sufficient to change the orientation in non-preoriented sample. Depending on the position of the polarizers the orientation leads to an increase or decrease in transmitted light (Figure 2).

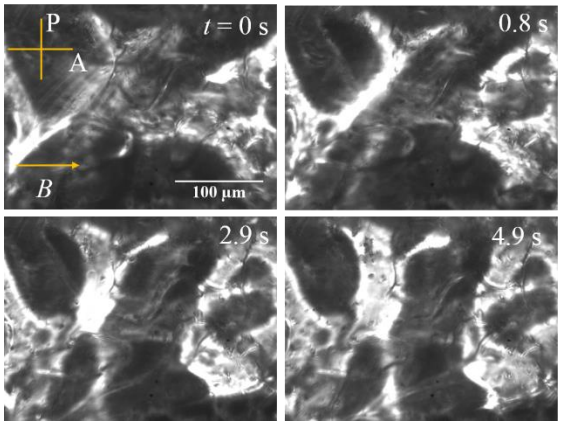

Figure 2. Images from polarization micrscopy woth crossed polarizers of 9OCB-PHMS@Fe_2O_3 in 5CB (0.015 m% magnetic content) at different times *t* after application of a homogenous magnetic field (*B* = 150 mT).

The transfer of the alignment of the anisotropic α-Fe_2O_3 in the applied field to the matrix orientation confirms the coupling between the magnetic particles and the surrounding LC matrix.

Acknowledgments

Financial support is acknowledged from DFG-SPP 1681 “Feldgesteuerte Partikel-Matrix-Wechselwirkungen” (2013 - 2017).

References

[1] F. Brochard, P. P. G. de Gennes, *J. Phys.* **1970**, *31*, 691–708.

[2] O. Buluy, S. Nepijko, V. Reshetnyak, E. Ouskova, V. Zadorozhnii, A. Leonhardt, M. Ritschel, G. Schönhense, Y. Reznikov, *Soft Matter* **2011**, *7*, 644–649.

[3] P. Kopčanský, N. Tomašovičová, N. Iber, K. Fodor-Csorba, T. Tóth-Katona *et al.*, *Phys. Rev. E* **2008**, *78*, 11702.

[4] A. Mertelj, D. Lisjak, M. Drofenik, M. Copič, *Nature* **2013**, *504*, 237–41.

Fundamental eigenmodes and rheological properties of a ferromagnetic nematic liquid crystal

T. Potisk[1,2], D. Svenšek[2], H. Pleiner[3], H. R. Brand[1]

[1] *Theoretische Physik III, University of Bayreuth, 95440 Bayreuth, Germany*
[2] *Faculty of Mathematics and Physics Ljubljana, University of Ljubljana, 1000 Ljubljana, Slovenia*
[3] *Max Planck Institute for Polymer Research, 55021 Mainz, Germany*

Ferromagnetism is a phenomenon well known in solids. An old idea to generate a liquid ferromagnet was that by introduction of ferromagnetic nanoparticles in a nematic liquid crystal one could induce a ferromagnetic liquid crystal phase [1]. Only recently this phase was successfully experimentally realized [2]. The ordering in a ferromagnetic nematic liquid crystal can be described by two fields: the director field **n**, which describes an average orientation of the molecules of the liquid crystal and the magnetization field **M**, describing an average orientation of the magnetic moments of the magnetic particles. Unlike for usual nematics, the ferromagnetic phase is sensitive to very small magnetic fields [3] and could be used in various magneto-optic devices.

Light scattering

Nematic liquid crystals strongly scatter light, which is caused by fluctuations of the director field [4]. Relaxation rates of the fundamental eigenmodes are easy to observe experimentally and are used to determine the viscoelastic properties of the system [5].
In ferromagnetic nematic liquid crystals one has as an additional variable the magnetization, which increases the number of fundamental eigenmodes by two (assuming fixed magnetization modulus). We find that using standard experimental techniques one cannot measure a single fluctuation mode but in general a complicated mixture of at least two. We furthermore derive basic expressions for the dependence of the relaxation rates of the fundamental eigenmodes on the applied magnetic field.

Rheology

To understand the complete dynamic behavior of a ferromagnetic nematic liquid crystal one needs to measure rheological properties of the system. A shear flow in a nematic liquid crystal influences the orientation of the molecules, which in turn influences the measured viscosity. To circumvent the dependence of this coefficient on the shear rate, simple experiments were proposed in [6], where the orientation of the molecules is fixed by an external electric or a strong magnetic field. This way, one can introduce in an ordinary nematic liquid crystal three different Miesowicz viscosities.
In a ferromagnetic nematic the presence of the magnetization leads to additional dynamic cross-couplings [7]. As a consequence the three Miesowicz viscosities for an ordinary nematic are replaced in a ferromagnetic nematic by nine viscosities.

Acknowledgments

We thank the Deutsche Forschungsgemeinschaft for partial support through the Priority program 1681.

References

[1] F. Brochard and P. G. de Gennes, "Theory of magnetic suspensions in liquid crystals", Journal de Physique **31**, 691 (1970).
[2] A. Mertelj, D. Lisjak, M. Drofenik and M. Čopič, "Ferromagnetism in suspensions of magnetic platelets in liquid crystal", Nature **504**, 237 (2013).
[3] A. Mertelj, N. Osterman, D. Lisjak and M. Čopič, "Magneto-optic and converse magnetoelectric effects in a fer-

romagnetic liquid crystal", Soft Matter **10**, 9065 (2014).
[4] P. G. de Gennes and J. Prost, "The physics of liquid crystals", (Clarendon Press, Oxford, 1995).
[5] M. Čopič, M. Vilfan and A. Mertelj, "Flow and anchoring effects on nematic fluctuations in confined geometry", Liquid Crystals **40**, 1646 (2013).
[6] M. Miesowicz, "Influence of a magnetic field on the viscosity of para-azoxyanisol', Nature **136**, 261 (1935); "The 3 coefficients of viscosity of anisotropic liquid", Nature **158,** 27 (1946).
[7] E. Jarkova, H. Pleiner, H.-W. Mueller and H.R. Brand, "Macroscopic dynamics of ferronematics", J. Chem. Phys. **118**, 2422 (2003). '

Immobilization of magnetic nanoparticles – a comparison of different procedures

C. Balceris[1], F. Ludwig[1]

[1] *Institut für Elektrische Messtechnik und Grundlagen der Elektrotechnik, TU Braunschweig, Braunschweig*

The dynamics of magnetic nanoparticles (MNP) are determined by the interplay of the well known Brownian and Néel mechanisms. In order to assess the anisotropy energy KV_c of blocked MNP in dynamic magnetic measurements, such as magnetorelaxometry (MRX) or ac susceptibility (ACS), the Brownian mechanism must be suppressed by immobilization of the MNP. At the same time it must be guaranteed that particle interactions are not altered by the immobilization process, since many models assume non-interacting MNP. The systematic evaluation of immobilization techniques is crucial to further refine existing models and to investigate the anisotropic behavior of MNP by exposing them to a static magnetic field during the immobilization process. Just recently the influence of intra-potential-well contribution on the ac susceptibility spectrum was experimentally verified by immobilizing MNP in presence of a static magnetic field resulting in differently aligned easy axes [1]. In literature a broad variety of different techniques are suggested and used, such as epoxy resin [2], frozen silicone oil, gypsum, freeze-drying and cotton wool, but we found that only few are suitable in terms of general purpose.

Techniques

We systematically compared different techniques on the well understood MNP system FeraSpin R from nanoPET Pharma GmbH with MRX, ACS and magnetic particle spectroscopy (MPS) measurements.
The magnetite/maghemite MNP are coated with a carboxyldextrane shell. The ferrofluid has a Fe concentration of 5 mg/ml which is suitable to neglect concentration dependent particle interactions since the volume susceptibility spectra scale well with applied dilution.
We investigated on heated agarose solution, drenched and air-dried cotton wool strings, two component epoxy glue blended with the MNP solution and air-dried, freeze-drying with mannitol, pure gypsum air-dried, heated egg-white protein and original suspension as Brownian dominated reference sample.
On this basis, MNP in different concentrations have been exposed to both permanent magnets and electromagnets with different field strengths during the freeze-drying process.
FEMM simulations and measurements with a Hall-magnetometer revealed homogeneous fields for all setups with deviations of field strengths <1% within the sample volume of 150 µl.

Evaluation of immobilization techniques

Fig. 1 depicts the normalized ACS spectra measured on all prepared samples. For the reference sample, i.e., suspended MNP, a pronounced Brownian maximum in the imaginary part is observable at around 1.4 kHz corresponding to a mean hydrodynamic diameter of 68 nm, which is in good agreement with the Z-average of 65 nm obtained from DLS measurements. In comparison, the freeze-drying shows a linear decay of the real part over ln(f) while the imaginary part is constant over the whole frequency range which is to be expected for a Néel dominated MNP system with a broad distribution of anisotropy energies [1]. Samples prepared with agarose and cotton wool basically behave like the suspension, i.e., a distinct maximum in the out-of-phase signal is discernable though slightly shifted towards lower frequencies

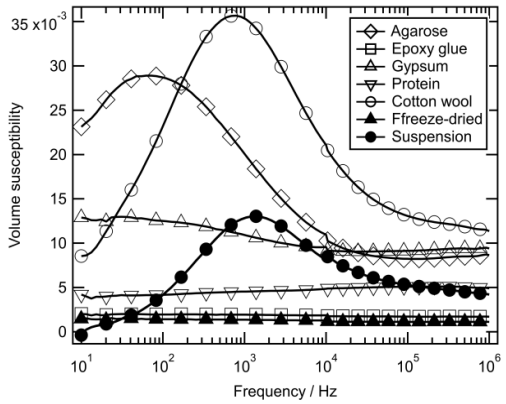

Fig. 1: ACS imaginary parts of immobilized MNP and reference suspension.

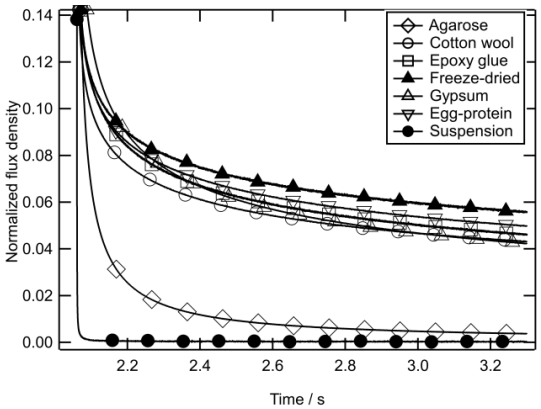

Fig. 2: Normalized MRX relaxation curves of immobilized MNP and reference suspension.

in case of the drenched cotton wool. This might originate from agglomeration due to higher local density of particles, as the MNP are not evenly distributed inside the volume but attached to the cotton wool strings. Only the sample prepared with epoxy glue shows the same performance as the freeze-dried sample which indicates ideal immobilization. Gypsum and cotton wool prepared samples seem to undergo only partial immobilization as features of both Brownian and Néel relaxation are present, like a subtle maximum in the imaginary part and slight deviations from the linear decay of the real part, especially towards higher frequencies. Possible explanations would be an increase of (local) dynamic viscosity or in liquid encapsulated particles which due to decreased mean distance form agglomerates and therefore effectively larger hydrodynamic objects.

The normalized step response of the MRX measurements for all samples is depicted in **Fehler! Verweisquelle konnte nicht gefunden werden.**. After applying an external field of 2 mT for 2 s, the flux density of the decaying stray field is recorded. While the suspension's signal is decaying very quickly as a significant portion of the MNP relaxes via the Brownian mechanism, immobilized MNP only relax via the Néel mechanism which is in case of thermally blocked MNP therefore slower. Here again the sample prepared with agarose shows a very similar behavior as the suspended MNP, while the epoxy glue sample only has minor deviations from the signal of the freeze-dried sample. The signal of the gypsum sample crosses the freeze-dried sample's curve, which can be interpreted that only a portion of the MNP are actually immobilized while the rest remains mobile.

Conclusion

Our research suggests that freeze-drying seems to be the most reliable and robust technique to immobilize MNP as it provides optimal performance, i.e., presumably total immobilization, while not altering the MNP system and being able to control iron content and sample volume.

Applying external fields by means of electro- or permanent magnets up to 300 mT during the freeze-drying process allows one to derive valuable information about magnetic properties of the MNP, such as the effective anisotropy constant and to develop more sophisticated models.

Further investigation of the immobilization of various MNP systems with e.g. different coatings or sizes is in progress.

Acknowledgment

This work was supported by the European Commission Framework Programme 7 under the NanoMag project (grant agreement no: 604448).

References

[1] F. Ludwig et al., IEEE Trans. Magn. (in press)

[2] T. Yoshida et al., J. Magn. Magn. Mater. **427**, 162 (2016)

Aggregation and Hydrodynamics of Superparamagnetic particles in Mag-Guider systems

O. Baun[1], P. Blümler[1], F. Schmid[1], M. Klünker[2],
P. Daniel[2], W. Tremel[2], E. S. Asmolov[3], O. I. Vinogradova[3]

[1] *Institute of Physics, University of Mainz, 55099 Mainz, Germany*
[2] *Institute of Inorganic Chemistry, University of Mainz, 55099 Mainz, Germany*
[3] *A.N.Frumkin Institute of Physical Chemistry and Electrochemistry, Russian Academy of Sciences, 119071 Moscow Russia*

Recently we developed a permanent magnet system to guide and image superparamagnetic particles (SPP) by simple rotation of Halbach cylinders [1]. This instrument was nicknamed Mag-Guider (**Ma**gnetic **Guid**e and Imag**er**).

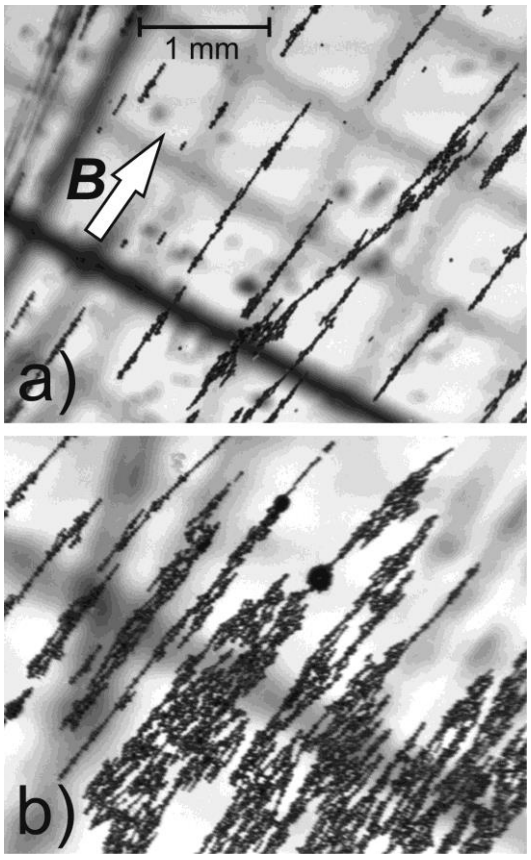

Fig. 1: Micrographs of SP-iron oxide particles with an average diameter of 30 µm in the Mag-Guider system. a) Initially the particles form long chains or strings. b) A few seconds later lateral growth sets in resulting in carpet- or raft-like structures.

The velocity of various SPPs was studied with this system. Although the size of the SPPs varied from some 10 nm to several µm this was not reflected in the measured velocities, which were all several magnitudes bigger than calculated for the single particles.

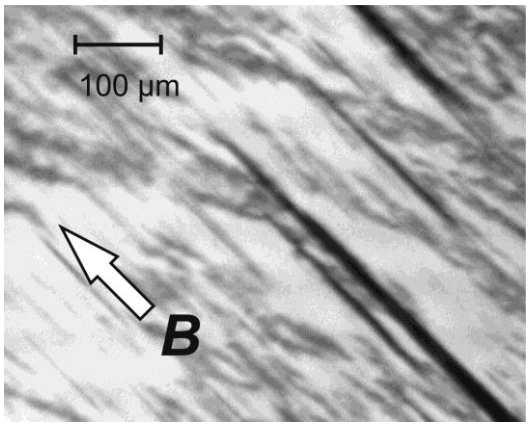

Fig. 2: Micrographs of cobalt ferrite particles with an average size of 70 nm at higher resolution showing big clusters with a needle or lentil shape.

This behavior is explained by the formation of long chains and lentil shaped agglomerates of the particles due to strong and homogeneous magnetic field in the device (cf. Fig. 1). This field orients and magnetizes the SPPs so that they form long chains. Beyond a critical length of such chains particles can not only attach at the poles of such chains but also at their sides, causing lentil shaped forms (cf. Fig. 2).
The experimental data were reproduced by simulations and an analytical hydrodynamics model is suggested and compared with the measurements.

References

[1] O. Baun, P. Blümler, J. Magn. Magn. Mater. **439** (2017) 294-304

Influence of the particles morphology on the properties of magnetorheological elastomers with a magnetically hard filler

D. Borin[1], G. Stepanov[2], S. Odenbach[1]

[1] *TU-Dresden, Chair of Magnetofluiddynamics, Measuring and Automation Technology, Dresden, Germany*
2 State Research Center GNIICHTEOS, Moscow, Russia

Magnetorheological elastomers (MREs) are composites of a rubber or gel-like matrix in which magnetic powder is distributed [1,2]. They belong to the group of controllable materials whose properties can be reversibly changed under the influence of an externally applied magnetic field. One of the most prominent properties of MREs is a field dependent change in viscoelasticity, i.e. an influence of the applied magnetic field on the storage and loss moduli of a specimen at different deformations and loading frequencies. In this contribution we report on the effect of the magnetic powder morphology on the moduli of MREs. Our experimental study is focused on the MRE samples filled with hard magnetic powder (NdFeB-alloy). Samples were characterized in their initial state and subsequently were magnetized prior to the testing procedure in order to tune their initial state by means of remanence magnetization.

Experimental characterization of all samples is performed using dynamic axial loading. The results indicate that different physical processes can be responsible for the obtained material behavior: rotation of particles in the matrix and formation of particle aggregates. Furthermore, a correlation between the powder morphology and viscoelastic response of the MREs is observed.

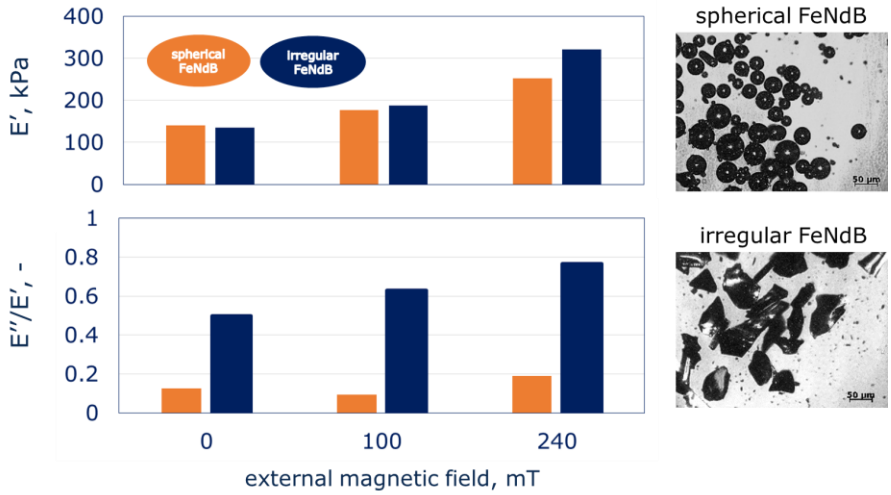

Figure 1: Storage modulus (E') and loss factor (E''/E') of MREs containing particles with different morphologies in an external magnetic field at loading frequency of 0.1Hz and deformation of ~5%.

Acknowledgments

Financial support by Deutsche Forschungsgemeinschaft (DFG) under Grant Bo 3343/1-1 and Od18/24-1 within PAK 907 providing the basis for our investigations is gratefully acknowledged. G.S. would like to acknowledge the support of RFBR under Grant 16-53-12009.

References

[1] M. Jolly et al., J. Intell. Mater. Sys. Struct. 7 (1996)
[2] M. Kalio, VTT Publications (2005) (2009).

Experimentally based finite element simulation of magnetorheological fluids with field dependent anisotropy

E. Dohmen[1,2]

[1] *Institute for lightweight engineering and polymer technology, Technische Universität Dresden, 01062 Dresden*
[2] *Institute for fluid dynamics, Technische Universität Dresden, 01062 Dresden*

The adaptability of the properties of magnetic materials such as magnetorheological (MR) fluids, MR elastomers and magnetic hybrid materials (MHM) drives scientific activities worldwide, trying to broaden the fields of application of such materials. Main focus of most works is the characterization and theoretical description of this material group. Only a few works try to combine experimental results with praxis-oriented and easy to use design and simulation methods. In the work presented the anisotropic magneto-mechanical properties of a MR fluid are experimentally determined to generate an adapted anisotropic material model for finite element (FE) simulations. Utilizing this model the field-dependent anisotropic behavior of this MR fluid and of a MHM are simulated and opposed to experimental results showing potential for improvements and potential of the presented methodology.

Testing methodology

For the experimental determination of the anisotropic magnetomechanical properties of a MR fluid MRF-140CG by Lord Corporation the custom made Magnetic Field Angle Testing Device (MFATD) is used [1]. Experimental tests were performed in presence and absence of a magnetic field for shear and compression under different magnetic field orientations. As for MR fluids field orientation equals a main orientation of internal particle superstructures, this direction was defined as 1-direction for FE simulations.

Results

The experimentally determined anisotropic results are for FE simulations theoretically described via a scaled exponential approach as exemplary shown in figure 1 for shear at different magnetic field directions.

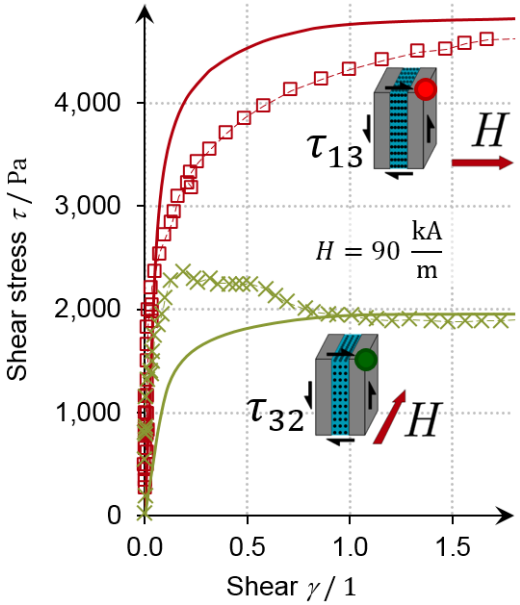

Figure 1: Comparison of theoretical approximation and experimental results for shear under two magnetic field directions

Conclusions

The results indicate that under the influence of a magnetic field and for the considered cases an abstracted simulation of MR fluids as solids is in good accordance with experimental data. The used methodology enables a practice oriented, fast and simplified simulation of magnetic hybrid materials as well as complex assemblies based on MR fluids.

Acknowledgments

This project is supported by the European Union and the Free State of Saxony.

References

[1] Dohmen, E.; Modler, N.; Gude, M. (2017) *Journal of Magnetism and Magnetic Materials* **431**.

Multiparametric Magnetic Particle Spectroscopy

S. Draack[1], T. Viereck[1], M. Schilling[1]

[1] *Institut für Elektrische Messtechnik und Grundlagen der Elektrotechnik, Technische Universität Braunschweig*

Introduction

Magnetic Particle Spectroscopy (MPS) is an increasingly important characterization method for magnetic nanoparticles (MNPs). MPS provides both a powerful tool to examine the suitability of MNP for Magnetic Particle Imaging (MPI) and a wide range of applications to investigate particle characteristics in suspensions or matrices. Multiparametric MPS measurements of selected particle systems make it possible to investigate physical relationships and to derive mathematical descriptions.

Methods

Magnetic Particle Spectroscopy utilizes the non-linear magnetization curve of magnetic nanoparticles. A sinusoidal magnetic excitation field drives the magnetization of the particles periodically into the saturation region. Thus, the magnetization response includes higher harmonics, which provide sensitive information about the particle dynamics and their binding state.
Ocean NanoTech SHP25 is a Fe_3O_4 single-core nanoparticle system with a mean core diameter of approximately 25 nm. Its narrow core size distribution suggests SHP25 as a model system to clarify MPS and MPI signal generation including particle dynamics by mathematical models. For low excitation frequencies, the dynamics of the particles in Newtonian liquids are dominated by the Brownian relaxation process. Therefore, the spectra in MPS measurements significantly modulate with varying matrix properties. To investigate spectral changes depending on the viscosity of the suspension, a series of viscosities with different DI water / glycerol ratios was prepared. Furthermore, a freeze-dried (mannitol) reference sample was prepared to compare spectral viscosity dependencies with the immobilized state. Viscosity-dependent MPS measurements on the series were performed with a custom-built MPS setup using a drive field peak amplitude of 25 mT and an excitation frequency of 1 kHz.
The viscosity and the magnetization dynamics of MNP are very sensitive to the sample temperature. For this reason, temperature influences must be considered. A new temperature-controlled MPS setup was built to additionally investigate temperature dependencies in a temperature range of at least -14°C to +114°C [1].

Results

Fig. 1 shows the spectral magnitude of the odd higher harmonics for different glycerol mixtures.

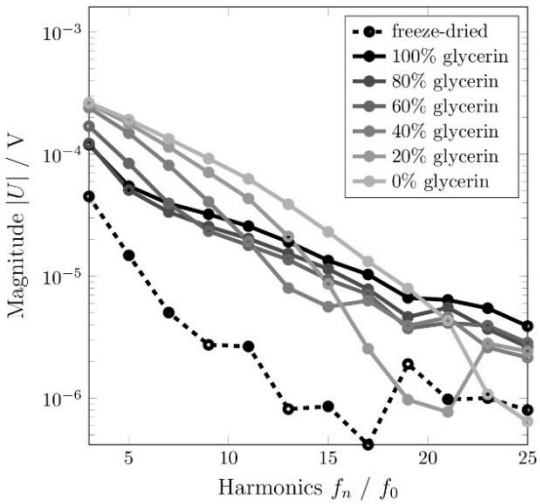

Fig. 1: Spectral magnitude of odd higher harmonics of Ocean NanoTech SHP25 for different glycerol mixtures and a freeze-dried (mannitol) reference sample, acquired in a MPS measurement at $\mu_0 \hat{H} =$ 25 mT and $f_0 = 1$ kHz.

The MPS spectra exhibit a decrease of the lower harmonics for increasing viscosities while the magnitude of higher harmonics increases. This leads to a crossing of the series of curves, which seems difficult to explain at first. A different illustration of the low-order odd harmonics ($3f_0$ – $11f_0$) is shown in Fig. 2. Real and imaginary parts of the acquired data are plotted over the dynamic viscosity η of the Newtonian fluid suspension matrix.

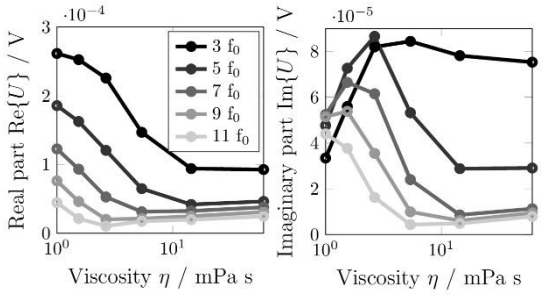

Fig. 2. Real and imaginary parts of the odd higher harmonics depending on the dynamic viscosity of the suspension matrix.

For increasing viscosities, the real part curves of the higher harmonics converge and the amplitude of the real part drops by trend. The imaginary parts feature a maximum, which is near the inflection point of the real part curve for the corresponding higher harmonic. This relationship is well-known from ACS measurements for the fundamental frequency and can be described by the Debye model.

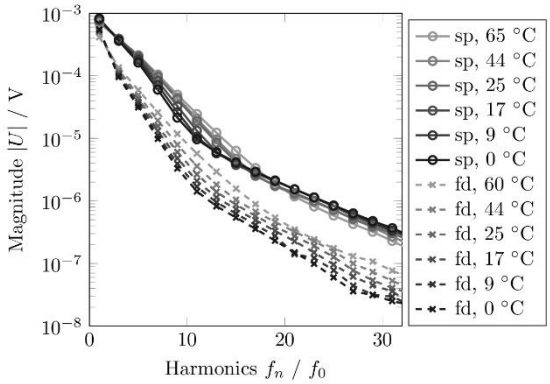

Fig. 3. Spectral magnitude of the odd higher harmonics of Ocean NanoTech SHP25 for different temperatures for a suspension (sp) and a freeze-dried (fd) sample, acquired in a MPS measurement at $\mu_0\widehat{H} = 25$ mT and $f_0 = 5$ kHz.

The explanation of the complex susceptibility in ACS measurements can be extended to MPS by an advanced generalized Debye model which also covers the higher harmonics [2].
Fig. 3 shows MPS spectra for different sample temperatures using Ocean NanoTech SHP25 as suspension (sp) and freeze-dried (fd) sample. In the spectra of the suspension, crossings can be observed due to changing particle dynamics which result from a superposition of altered matrix properties and internal magnetization dynamics.

Conclusion

Magnetic Particle Spectroscopy provides a powerful characterization tool for magnetic nanoparticles, which is very sensitive to particle dynamics. Since the dynamics are directly related to matrix properties, multiparametric MPS measurements allow complex investigations on field-controlled particle-matrix interactions. On the basis of measurement results, mathematical models can be derived and evaluated to describe physical relationships, which are particularly relevant in biomedical applications due to the analogy of MPS and MPI. A comparison of different particle models and a software fitting environment for the derivation of particle properties from measurements are in progress.

Acknowledgments

Financial support by the German Research Foundation, DFG Priority Program 1681 is acknowledged (SCHI383/2-1).

References

[1] S. Draack et al., “Temperature-dependent MPS measurements”, IJMPI, Vol. 3, No. 1, 2365-9033 (2017)
[2] T. Wawrzik et al., “Debye-Based Frequency-Domain Magnetization Model for Magnetic Nanoparticles in Magnetic Particle Spectroscopy”, IEEE Trans. Magn. 51, 5300404 (2015)

Rotational Dynamics of Ni Nanorods in Polymer Solutions

M. Gratz, A. Tschöpe

Universität des Saarlandes, Experimentalphysik, Campus D2 2, 66123 Saarbrücken

Intoduction

Some important properties of complex soft matter, such as the transport of small objects like viruses or nanosized drug carriers through biological barriers, are governed by their structural heterogeneity on the sub-micrometer scale. Investigations of nanoparticle dynamics in such systems contribute to the basic understanding of the involved processes.

The present study focused on the rotational dynamics of ferromagnetic nanorods in polymer solutions. The molecular weight and concentration of the macromolecules provide two control parameters which enable access to a wide spectrum of length and time scales. We present the results of a study on polyethylenglycol (PEG, PEO) solutions for a series of ten different molar masses (PEG-x denotes $M_v = x\,\mathrm{g/mol}$). The concentration was fixed at $c = 1\,\mathrm{wt.\,\%}$ so that the correlation length ξ and the Edwards tube diameter a were nearly constant whereas the radius of gyration R_g varied from 3 nm (PEG-4k) to 100 nm (PEO-2M). With increasing molar mass, the various solutions pass through the major concentration regimes, i.e. dilute, semi-dilute unentangled, and semi-dilute entangled, each with characteristic relaxation properties at different length scales [1].

Methods

Ni nanorods ($l = 234 \pm 4\,\mathrm{nm},\ d = 23.6 \pm 0.3\,nm$) were synthesized by the AAO-template method and processed to a stable colloidal dispersion. The basic physical properties of the nanorods were determined by transmission electron microscopy (TEM) and static field-dependent optical transmission [2]. PEG (PEO) of different molar mass were purchased from Sigma-Aldrich, dissolved in bidistilled water at ≈pH 8 and gently mixed in a rotator for at least 48 h. Nanorod colloid was added to a total volume fraction $\phi_v \approx 10^{-6}$ and mixed for 1 h.

The rotational dynamics of the nanorods was characterized by measuring the optical transmission of linear polarized light in oscillating magnetic field as function of the oscillation frequency [3]. The obtained response function was analyzed using model functions for Newtonian liquids or the generalized linear viscoelastic liquid model with a small number (n=3-6) of Maxwell elements. From the obtained parameters, the zero shear viscosity, dynamical modulus and complex viscosity were calculated. Macrorheological reference measurements were performed using an Anton-Paar DAM4100 M rolling ball viscosimeter and an Anton Paar MCR702 dual drive rheometer.

Results

The OF-OT response function is determined by a particle shape factor K, representing the hydrodynamic size and magnetic moment of the nanorod (determined by a calibration measurement) and the viscoelastic properties of the environment. For Newtonian fluids, the OF-OT response is well described by a Debye relaxation, convoluted with a moderate distribution of K. This behavior was found for the low molar mass samples PEG-4k, PEG-8k, and PEG-35k. The retrieved local viscosities were nearly identical to the macroscopic reference values, Fig.1, indicating that all relevant length scales of the polymer solutions are smaller than the size of the nanorods.

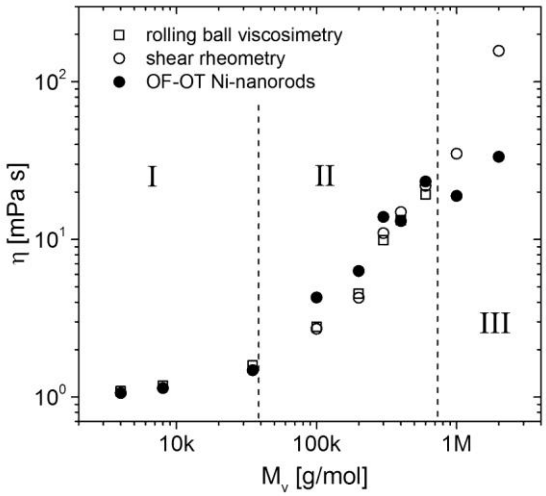

Figure 1: Macroscopic (open symbols) and local viscosity (OF-OT) of 1 wt. % PEG solutions as function of molar mass. The dashed lines separate the dilute (I) from the semi-dilute unentangled (II) and semi-dilute entangled regime (III).

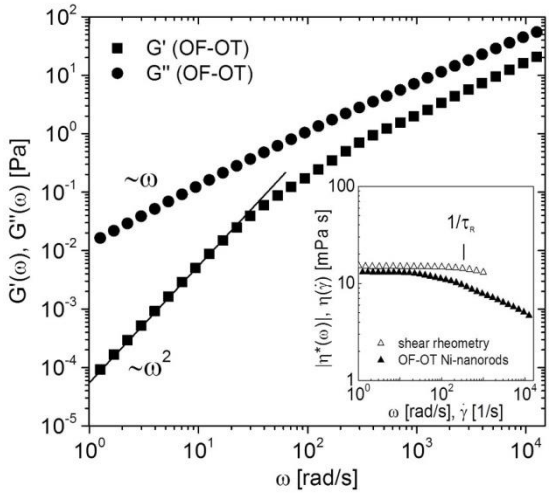

Figure 2: Dynamic modulus obtained from the linear viscoelastic model analysis of an OF-OT measurement of the PEG-400k solution. The derived local complex viscosity decreases at lower frequencies as compared to the onset of macroscopic shear thinning.

By contrast, the OF-OT spectra for higher molar mass PEGs revealed increasing elastic contributions in the particle-polymer interaction. The spectra were fitted using model functions derived for the generalized linear viscoelastic liquid model with a small number (n=3-6) of Maxwell elements. The dynamic modulus calculated using the retrieved model parameters is clearly divided into the terminal region, where $G' \sim \omega^2$ and $G'' \sim \omega$, and a high frequency region, in which $G' \sim G'' \sim \omega^{\approx 0.85}$, Fig.2. In the semi-dilute unentangled regime, polymer stress relaxation is expected to follow the Rouse model ($G' = G'' \sim \omega^{0.5}$) at length scales larger than the hydrodynamic screening length ($\xi_h \approx \xi \approx 40$ nm) with a transition to Zimm-like behavior ($G' = G''/\sqrt{3} \sim \omega^{2/3}$) at smaller length scales, i.e. higher frequencies [1]. The results of the OF-OT measurements show systematic differences, such as the high power law exponent ($\sim\omega^{0.85}$), a larger difference between G' and G'' and a higher terminal relaxation time than expected. The latter difference is also apparent if we assume the Cox-Merz rule to hold for PEG solutions and compare the calculated complex viscosity with the macroscopic shear viscosity, Fig.2. At present, we may only speculate whether size effects or the non-affine deformation of the polymers is the major reason for the observed differences.

The two solutions with the highest molar mass are expected to be in the semi-dilute entangled regime where relaxations at length scales larger than the Edwards tube diameter a are controlled by the reptation time constant τ_{rep}. For these solutions, OF-OT measurements revealed considerably lower local viscosities as compared to the macroscopic values. This difference may be related to the size of the nanorods being smaller or close to the tube diameter $a = 135$ nm so that the rotation dynamics of the nanorods remains controlled by Rouse relaxation.

Acknowledgments

We acknowledge financial support by the DFG, priority program 1681 (TS62/4-2).

References

[1] M. Rubinstein and R. H. Colby, *Polymer Physics* (OUP, New York, 2003).
[2] F. Krämer, M. Gratz, and A. Tschöpe, *J. Appl. Phys.* **120** (2016) 044301.
[3] A. Tschöpe, K. Birster, B. Trapp, P. Bender, and R. Birringer, *J. Appl. Phys.* **116** (2014) 134305.

Microstructural investigations of magnetorheological elastomers (MRE) related to magnetic hysteresis

T. Gundermann[1], S. Odenbach[1]

[1] *TU-Dresden, Chair of Magnetofluiddynamics, Measuring and Automation Technology, 01062 Dresden, thomas.gundermann@tu-dresden.de*

Introduction

By mixing magnetically controllable particles into a soft elastic matrix, a composite material with tunable physical properties can be developed. By applying a magnetic field, the particles inside the elastomeric matrix try to aggregate due to the interaction force of the particles influenced by the external magnetic field. There different physical properties of the particles do have an important influence on the property changes of the MREs, e.g. by using magnetically soft, magnetically hard, or a mixture of both types of particles, different effects could be found. [1]
The primary focus of this work was to combine magnetic and microstructural investigations to enable a complex description of the behavior of MREs under the influence of a magnetic field.

Setup

The magnetic measurements were performed by using a vibrating sample magnetometer (VSM) to carry out hysteresis loops and first-order reversal curves (FORC).
The microstructure was investigated by using micro-computer-tomography (X-µCT) with a magnetic setup consisting of two permanent magnets to generate a magnetic field up to B = 400 mT [2].
Samples with a mixture of NdFeB particles (magnetically hard) and carbonyliron particles (magnetically soft) in a ratio of 1:1 were produced. The particle content has been set to 5 vol.%, as matrix material we used the soft silicon rubber Elastosil RT 623 A/B by Wacker Silicones Germany.
The mechanic behavior of the samples has been tested by strain-stress test measurements and results in an elastic modulus of the sample of E ≈ 80 kPA.

Experimental

Using the CT setup and edit the CT-scans by using image processing it was possible to analyze the particles in the MRE (fig.1) and separate them based on their geometrical properties. Fig. 2 shows the particle size distribution of the MRE, which clearly shows that already the size of the particles allows separation between the NdFeB -particles which are represented by the broad lognormal distribution and the small carbonyliron particles which provide the peek at 5 µm particle diameter.

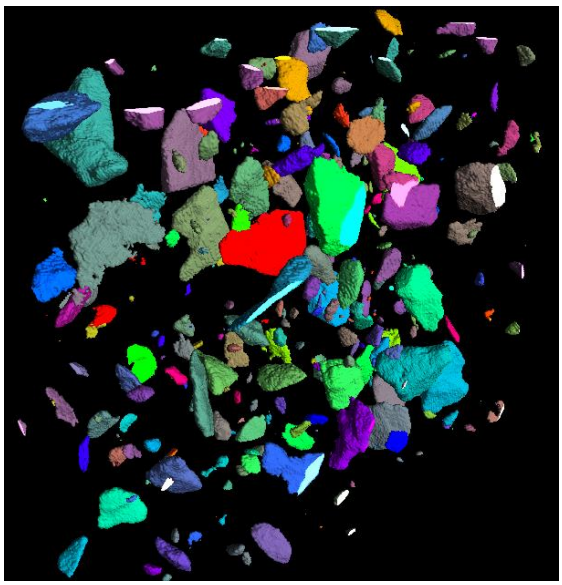

Fig. 1: Separated particles in a CT-scan of a mixed magnetic hybrid material. One can already visually clearly distinguish between the large flake like NdFeB particles and the small carbonyl iron particles.

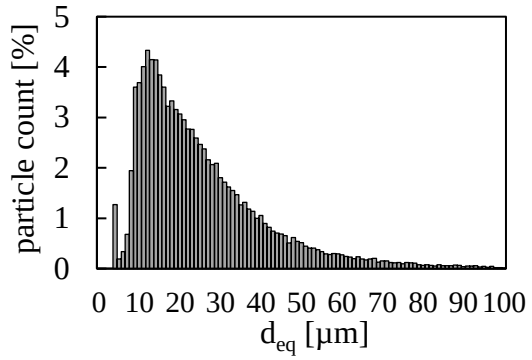

Fig. 2: Size distribution of the separated particles in the MRE sample obtained from a CT-scan.

The magnetic properties of the sample are shown in fig. 3 and suggest that the first hysteresis loop differs from the following loops. To explain this effect CT scans at different points of magnetization of the sample has been performed (exemplarily shown in fig. 4) and the rotation of the NdFeB particles have been evaluated.

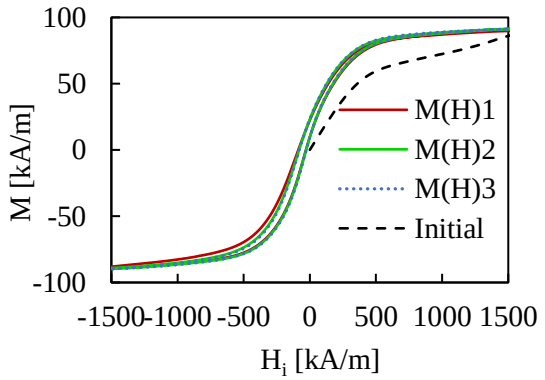

Fig. 3: Three hysteresis loops of the MRE sample. It is clearly seen, that the first loop M(H)1 differs significantly from the subsequent hysteresis cycles.

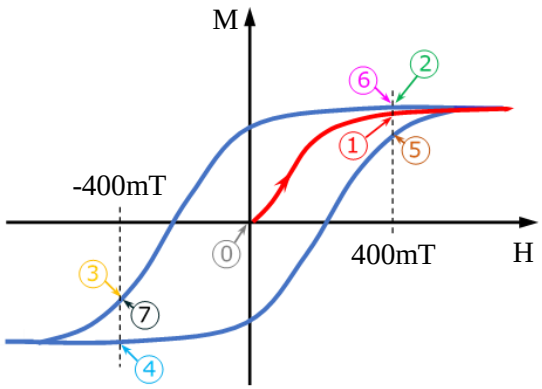

Fig. 4: Schematic representation of the different stages in which tomographic investigations of the sample have been undertaken.

The particle rotation was analyzed approximating the particles with an ellipsoid and measuring the angle between the direction of the magnetic field and the major axis of the particles. The results are shown in fig. 5 and point to an irreversible rotation of the particles comparing the first and the second hysteresis loop (point 2 differs from 6 and point 3 differs from 7) This irreversible rotation respectively the destroying of the matrix locally could be the reason for the disappearance of the asymmetric behavior of the hysteresis loop. These results don't take the influence of the carbonyliron particles into account. Further measurements should be done to evaluate the interaction between the carbonyliron particles and the NdFeB particles.

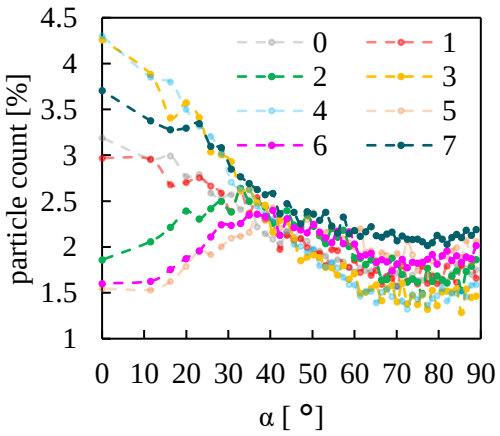

Fig. 5: Distribution of the angles between the major axis of the flake like NdFeB particles and the magnetic field direction for the different magnetisation states showed in fig. 4

Acknowledgments

The financial support by the DFG within SPP1681 under grant no. OD18/21 and PAK 907 under grant no. OD18 is gratefully acknowledged.

References

[1] Linke J M, Borin D Yu, Odenbach S (2016), RSC Adv., 6, 100407-100416

[2] Gundermann T, Odenbach S, (2014) Smart Mater. Struct., Bd. 23, Nr. 105013,

Size Effects on Magnetic Particle Nanorheology in Complex Fluids

M. Hermes[1], E. Roeben[1], A. M. Schmidt[1]

[1] *Department Chemie, Institut für Physikalische Chemie, Universität zu Köln, Luxemburger Str. 116, D-50939 Köln, email: annette.schmidt@uni-koeln.de*

Motivation

Rheological measurements, including static and dynamic rheology, allow to access information on the macroscopic (quasi-)continuous properties of bulk materials. In contrast to that, the interesting properties of microstructured materials (e. g. complex fluids) can be studied further by means of rheological measurements on the micro- or nanoscale. By employing magnetic particles as probes in soft hybrid systems, the possibility to investigate the self-assembly and dynamic interactions systematically by means of dynamic susceptibility, is given. When the size of the probe particles is in the same range as the characteristic length scales within the material, we expect stringent deviations from the rheological performance as obtained by conventional methods. De Gennes postulated, that the viscosity η of a polymer solution depends on the ratio of probe size d to the size of the correlation length ξ.[1] While for large probes ($d >> \xi$), the behavior reaches the (quasi-)continuous case, small probes ($d << \xi$) are dominated by the solvent viscosity.

In this study, we perform nanorheological experiments using the method of Magnetic Particle Nanorheology[2,3] and systematically vary the size of the tracer particles. The experiments are analyzed by paying pronounced attention to the ratio of structural length scales within the investigated material and the probe size.

Method

As merromagnetic $CoFe_2O_4$ (CF) nanoparticles (d_{TEM} = 17.3 nm ± 14 %) are used as magnetic cores and are additionally systematically coated with a silica (SiO_2) shell to obtain tracer particles with variable hydrodynamic size. The Brownian relaxation of the tracer particles in complex fluid is investigated by means of AC susceptometry in the range of 1 Hz – 250 kHz and the use of theoretical models[2,3] gives access to frequency dependent rheological properties.

Results and Discussion

To obtain monodisperse magnetic core-shell nanoparticles with tunable shell thickness and defined hydrodynamic properties, a variant of the classical Stöber method is used.[4] For this reason the reaction conditions are changed systematically and parameters like the reaction time, the amount of precursor, the dropping rate or the amount of the base are screened. Finally, adjusting the right reaction parameters and varying the base concentration lead to an increased particle size with increasing amount of base (see Fig. 1).

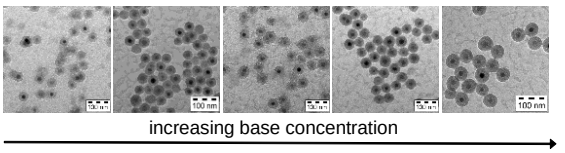

Fig. 1: TEM images of CF@SiO_2 nanoparticles with increasing shell thickness due to an increased amount of base during the reaction process.

The AC susceptometry spectra of the core-shell particles in water indicate defined hydrodynamic properties of the particles and variable particle size, which is indicated by a shift of susceptibility spectra to lower frequencies (see Fig. 2a). These results are confirmed by the determination of the particle sizes using different analytical methods (see Fig. 2b).

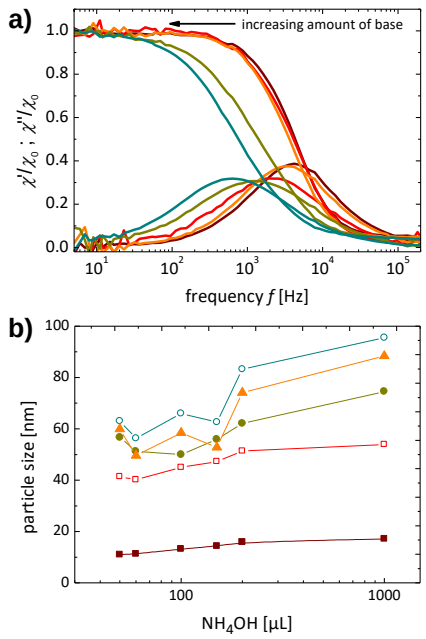

Fig. 2: a) AC susceptometry spectra for CF@SiO_2 nanoparticles with different hydrodynamic size in water. b) Sizes of the probe particles in dependence on the amount of base: filled squares: $d_{\text{layer, TEM}}$; empty squares: $d_{\text{g, TEM}}$; filled circles: $d_{\text{n, DLS}}$; empty circles: $d_{\text{v, DLS}}$; triangles: $d_{\text{h, ACS}}$.

First experiments with CF@SiO_2 (d_h = 58.5 nm) in PEG solutions were performed and compared to the results obtained by using only the magnetic CF core as tracers. The frequency dependent viscosity, storage and loss moduli and diffusion properties are analyzed. The results show systematic differences in the higher frequency range that are caused by the different hydrodynamic properties of the tracer particles (see Fig. 3).
The size-dependent particle diffusion is evaluated further considering the scaling theory of the Gennes and by comparison to the theoretical predictions.[5]

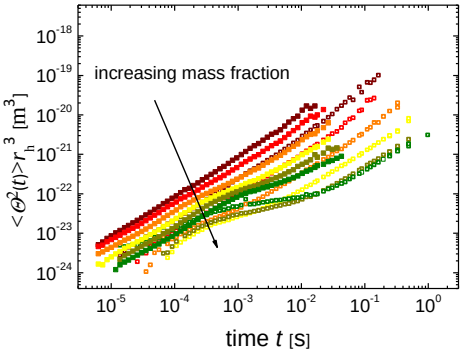

Fig. 3: Time dependence of the product of the mean-square displacement $<\Theta^2(t)>$ and the particle size r_h^3 for PEG (M = 35000 g·mol^{-1}) for CF (filled squares) and CF@SiO_2 (empty squares) probe particles with increasing polymer mass fraction (2 m% - 25 m%).

Acknowledgment

Financial support is acknowledged from DFG-SPP 1681 “Feldgesteuerte Partikel-Matrix-Wechselwirkungen”. (SCHM1747/10-1)
Melissa Hermes acknowledges support by the International Helmholtz Research School of Biophysics and Soft Matter (IHRS BioSoft).

References

[1] P.-G. De Gennes, *Scaling Concepts in Polymer Physics*, Cornell University Press, **1979**.
[2] E. Roeben, L. Roeder, S. Teusch, M. Effertz, U. Deiters, A. Schmidt, *Colloid Polym. Sci. Sci.* **2014**, *292*, 2013–2023.
[3] M. Hermes, E. Roeben, L. Kibkalo, A. M. Schmidt, *Annu. Trans. Nord. Rheol. Soc.* **2017**, *25*, 97–105.
[4] W. Stöber, A. Fink, E. Bohn, *J. Colloid Interface Sci.* **1968**, *26*, 62–69.
[5] L.-H. Cai, S. Panyukov, M. Rubinstein, *Macromolecules* **2011**, *44*, 7853–7863.

Nanorheological Studies on the Scale-Dependent Particle-Matrix Interaction in Magnetically Functionalized Hybrid Materials

M. Hermes,[1] M. Gratz,[2] H. Remmer,[3] S. Webers,[4] J. Landers,[4] S. Huang,[5] D. Borin,[6] A. Tschöpe,[2] F. Ludwig,[3] H. Wende,[4] G. K. Auernhammer,[5] S. Odenbach,[6] A. M. Schmidt[1]

[1] *Institute of Physical Chemistry, Universität zu Köln (UzK)*
[2] *Experimentalphysik, Universität des Saarlandes (UdS)*
[3] *Institute of Electrical Measurement and Fundamental Electrical Engineering, TU Braunschweig (TUBS)*
[4] *Faculty of Physics and CENIDE, University of Duisburg-Essen (UDE)*
[5] *Max Planck Institute for Polymer Research, Mainz (MPI)*
[6] *Institute of Fluid Mechanics, TU Dresden (TUD)*

Introduction

Doping microstructured complex fluids and soft matter with magnetic nanoparticles enables external control of the mechanical properties. In this respect, a detailed understanding of the coupling conditions between the magnetic particles and the matrix phase, being determined by a variety of interactions, becomes important. By using a diversity of rheological approaches ranging from the macro- to the nanoscopic scale, information on scale-dependent particle-matrix interactions are accessible. Deviations from the macroscopic rheological behavior are expected when the size of the probe particles is in the same size range as the characteristic length scales present in a microstructured system.[1,2]

Materials and Methods

Spherical magnetically blocked single domain $CoFe_2O_4$ (CF, d_g = 17.3 nm) and uniaxial ferromagnetic Ni nanorods (l = 234 nm, d = 23.6 nm) are used as nanoscopic tracer particles. We test their frequency-dependent dynamic behavior in aqueous solutions of polyethylene glycol (PEG) as model system for complex fluids using various methods and setups. These solutions are analyzed regarding their rheological properties using various analytical methods which are comparatively employed. Besides macro- and microrheological methods, AC susceptometry, oscillating-field optical transmission and Mößbauer spectroscopy measurements are performed (Fig. 1).

The polymeric aqueous solutions of polyethylene glycol were prepared to have the same macroscopic viscosity of η = 29 mPa·s: the molar masses amount to 33.6 m% for PEG 4k g·mol^{-1}, 11.2 m% for PEG 35k g·mol^{-1} and 2.1 m% for PEG 300k g·mol^{-1}) and with this different characteristic length scales within the fluids are present. The fluids are prepared at UzK and distributed among the partners to assure best comparison.

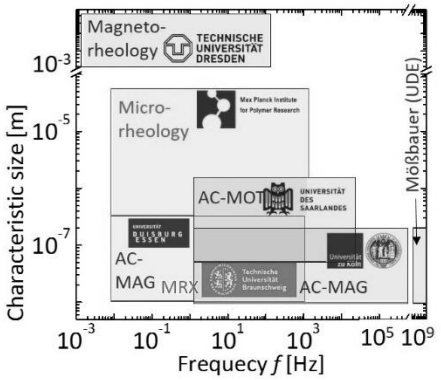

Fig. 1: Probe ize-frequency correlation of the rheological methods compared in this study.

Results

For the small CF particles the different AC susceptometry methods are compared, and the spectra are in good correspondence (Fig. 2). The spectrum for PEG4k can readily be fitted based on a single Debye relaxation, in agreement with the predominant Newtonian behavior of the non-entangled fluid, with length scales (radius of gyration R_g, correlation length ξ) well below the particle diameter d_p).

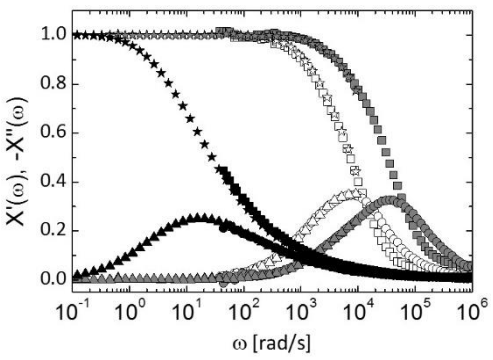

Fig. 2: AC-MAG spectra for aqueous solutions of PEG4k (white), PEG35k (grey) and PEG300k (black) with a macroscopic viscosity of 29 mPa·s. UzK: squares, circles, UDE: stars, triangles.

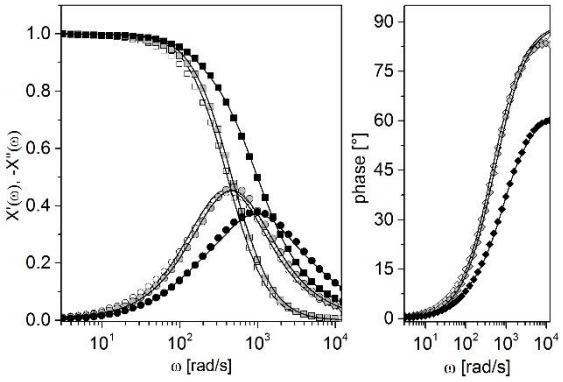

Fig. 3: OF-OT spectra and phase shift for aqueous solutions of PEG 4k (white), PEG 35k (grey) and PEG 300k (black) with a macroscopic viscosity of 29 mPa·s. Black lines: fits for a Newtonian liquid model for PEG 4k / 35k, and a generalized linear viscoelastic liquid model for PEG 300k.

For the PEG35k solution, well above the entanglement molar mass and concentration of PEG in water, deviations from this behavior are observed, and indications for a bimodal distribution of relaxation times can be found. This is in accordance with an intermediate probe size. Even stronger deviations from the macroscopic behavior is observed for PEG300k at the given viscosity. The results are interpreted on base of the empirical Havriliak-Negami and the Gemant-Bishop-diMarzio model.

For Ni nanorods, the comparison of the OF-OT relaxation spectra (Fig. 2) of the doped PEG solutions under investigation shows that for the low molecular weight PEG 4k and 35k solutions, in terms of the relaxation peak profile and the increase of the phase angle to 90°, confirm the Newtonian relaxation behavior of the particles in the investigated frequency range. The values for the local viscosity are close to the macroscopically determined results as expected for nanorods larger than the characteristic length scales of the polymer solutions.

In contrast, the PEG 300k solution revealed a reduced peak amplitude and a plateau of the phase angle at 60° which indicates an elastic contribution in the interaction between the nanorods and the polymer matrix and can be analyzed using the generalized linear viscoelastic liquid model.

The results are complemented by frequency-dependent rheological data available from micro- and macrorheology. The onset of shear thinning was observed for the PEG 300k solution but not for the lower molecular weight polymers.

Conclusions and Outlook

The different methods employed in this study are in good agreement especially when focusing on the frequency regions where the different techniques overlap. This provides the possibility to analyze the hybrid systems in a very large frequency range of more than seven orders of magnitude as seen in Fig. 2. The measurements show the validity of the nanorheological methods for the lower molecular mass range. For higher molar mass, the results show a dependence on the particle size, in agreement with theoretical predictions.

In future experiments, the impact of the particle concentration and of a superimposed DC magnetic field on particle-particle and particle-matrix interactions will be studied.

Acknowledgment

This work was supported by the DFG priority programme SPP 1681.

References

[1] L.-H. Cai, S. Panyukov, M. Rubinstein, *Macromolecules* **2011**, *44*, 7853–7863.

[2] R. Holyst, A. Bielejewska, J. Szymański, A. Wilk, A. Patkowski, J. Gapiński, A. Żywociński, T. Kalwarczyk, E. Kalwarczyk, M. Tabaka, *Phys. Chem. Chem. Phys.* **2009**, *11*, 9025–9032.

Flow control in magnetic fluids

T. Ilzig[1], S. Odenbach[1]

[1] *Technische Universtät Dresden, chair of Magnetofluiddynamics, Measuring and Automation Technology*

Motivation and Aim

The flow behavior of ferrofluids under the impression of external electromagnetic fields is driven by complex mechanisms. In a flow field the rotational axis of a magnetic particle in a ferrofluid is perpendicular to the flow direction, rotational axis of the particle and vorticity of the flow field are thus parallel. Under the impression of a magnetic field, the particles tend to align with this magnetic field. If the orientation of flow field and magnetic field is not parallel, a magnetic torque acts on the particles and thus the viscosity of the fluid apparently increases. Flow field and magnetic field mutually affect each other [1]. The aim of this work is the experimental investigation of the influence of axial electromagnetic fields on flow regimes in a ferrofluid in a hydrodynamic model system, a Taylor-Couette-System.

Materials and Methods

The Taylor-Couette-System consists of two coaxial cylinders of radii r_1 and r_2 and length L which can rotate independently with angular velocity ω_1 and ω_2 respectively. A viscous fluid of kinematic viscosity ν, here the ferrofluid, fills the gap of the width d between the two cylinders. The radius ratio is given by $\eta = r_1/r_2 = 0{,}5$ and the aspect ratio is given by $\Gamma = L/d = 5$. Hence the Reynolds number of each cylinder can be calculated by:

$$\mathrm{Re}_{1/2} = \frac{\omega_{1/2} \cdot \mathrm{d} \cdot \mathrm{r}_{1/2}}{\nu}. \qquad (2.1)$$

The external, homogeneous magnetic field is applied in axial direction with a maximum field strength $H \sim 40\mathrm{kA/m}$. Axial flow profiles are measured by means of ultrasonic Doppler velocimetry.

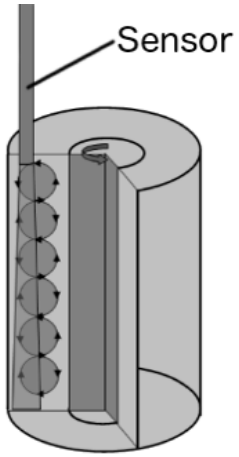

Fig. 1: Schematic sketch of the Taylor-Couette-System and principle arrangement of the ultrasonic transducer [1].

Results and Discussion

In a first step a flow regime of axial propagating, toroidal closed vortices (pV-regime) was established. These flow regimes are currently an active field of research ([2], [3]). Due to the boundary conditions of the experimental setup (rigid top plate, rotating bottom plate) this regime is dominated by an asymmetric propagation of the vortices from top to bottom. The space-time plot in fig. 2 shows clearly three pairs of vortices, one stationary pair at the top plate and two propagating pairs in the bulk region. New vortices are generated between the stationary and the upper propagating pair, the annihilation occurs near the bottom plate. Generation and annihilation are periodic in time with frequency $f_w = 1/t_w$.

By application of an axial homogeneous magnetic field the pV-regime was transferred into an oscillating flow state (oV-regime). The closed toroidal vortex structure retained, but the propagation of the mid pair transferred into an oscillation. The downward propagation of the bottom pair

was superimposed by an additional downward stream. The oscillatory movement was mainly driven by the annihilation and generation of new vortices and periodic in time. Furthermore, the frequency f_w strongly depended on the magnitude of H and decreased with increasing magnetic field strength.

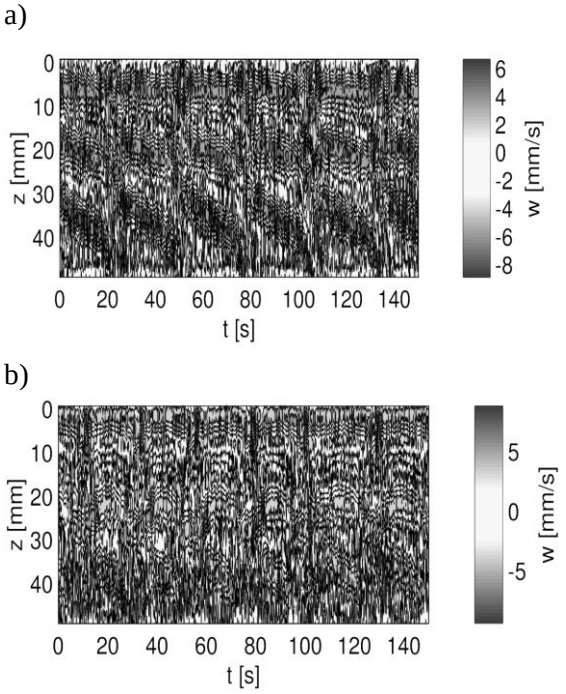

Fig. 2: Space-time plots of the pV-regime (a) and the oV-regime (b). $Re_1 = -189{,}8 \pm 2{,}4$, $Re_2 = 129{,}8 \pm 1{,}6$.

Conclusions and Outlook

In this work the influence of homogeneous axial magnetic fields on axial propagating, toroidal closed vortices in a ferrofluid contained in a Taylor-Couette-System was experimentally investigated. The flow state changed from a propagating state to an oscillating state whilst the magnetic field was applied. Both states were periodically in time with t_w. t_w strongly depended on the magnitude of the magnetic field.

Up to date, the stability and bifurcation behavior of the pV-regime are unknown. Further investigations shall be carried out, to classify the described flow state in the context of the parameter range of the Taylor-Couette-System.

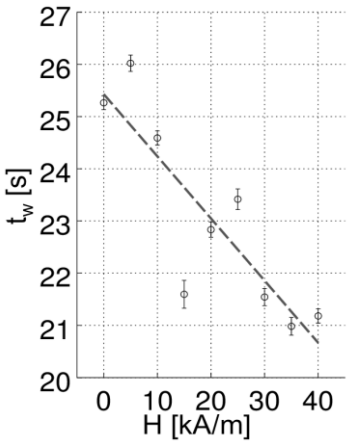

Fig. 3: Dependence of the periodic time t_w on the magnitude of H.

References

[1] M. Reindl, Strömungskontrolle in magnetischen Kolloiden, Dissertation, Technische Universität Dresden, 2011

[2] A. Schulz: Verzweigungen und Strukturen in der Strömung zwischen unabhängig rotierenden Zylindern, Dissertation, CAU Kiel, 2006

[3] C. Hoffmann, S. Altmeyer, M. Heise, J. Abshagen, G. Pfister: Axisymmetric propagating vortices in centrifugally stable Taylor-Couette flow, Journal of Fluid Mechanics, 2013

Mössbauer spectroscopy as an instrument for simultaneous determination of particle mobility and orientation

J. Landers[1], S. Salamon[1], H. Remmer[2], F. Ludwig[2], H. Wende[1]

[1] *Faculty of Physics and Center for Nanointegration Duisburg-Essen (CENIDE), University of Duisburg-Essen*
[2]*Institute of Electrical Measurement and Fundamental Electrical Engineering, TU Braunschweig*

Introduction

Composite materials of magnetic nanoparticles embedded in soft matter matrices exhibit unique magnetic properties, which can be described primarily by two essential parameters: The rate of Brownian particle motion and the particle orientation as a response to external magnetic fields. Using ferrofluids as a simple model system, representing more sophisticated soft matter composite materials, we demonstrate that orientation as well as mobility of the particles can be studied simultaneously and independently by Mössbauer spectroscopy.

Setup & materials

To study particle mobility and orientation, Mössbauer spectra were recorded at temperatures of 230–270K using a Mössbauer setup with integrated Peltier cooling elements [1]. During the experiments, external magnetic fields of up to 200mT were applied parallel and perpendicular to the γ-ray propagation direction, respectively, using either electromagnet or permanent ring magnet setups.
The studied ferrofluids contained maghemite/magnetite nanoparticles of ca. 15 to 25nm core diameter in 70vol% glycerol solution [2].

Results

Exemplary Mössbauer spectra of the 15nm particles in glycerol solution are shown in figure 1, which were recorded at 243K and 252K, respectively, and external magnetic fields up to 122mT along the γ-ray propagation direction. The spectra display a considerable change in the ratio of line intensities, being directly coupled to the relative

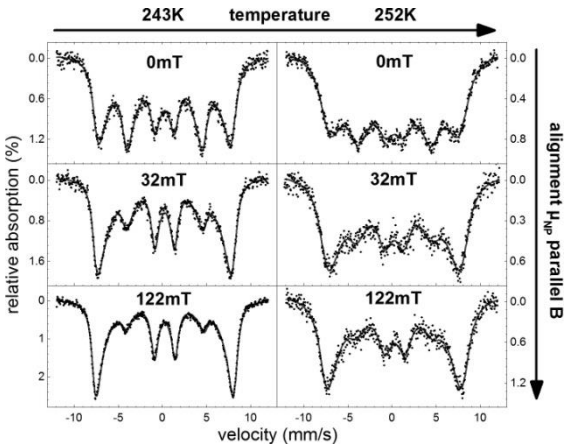

Fig. 1: Mössbauer spectra of 15nm particles in glycerol solution recorded at 243-252K in magnetic fields up to 122mT parallel to the γ-ray direction.

misalignment (canting) angle between spin and magnetic field direction (γ-ray direction). As an absence of lines 2 and 5 corresponds to complete spin alignment coaxial to the magnetic field, we are able to examine the gradual, time-averaged alignment of the particles in the fluid. This is clearly visible in the field dependence of the intensity ratio of line 2 and 3 (measured for parallel and perpendicular field geometry) shown in figure 2, where a fast increase in spin alignment is visible up to about 50mT. Upon further increase in magnetic field, an almost static line intensity ratio is detected, indicative for the complete alignment of particle superspins, whereby the remaning misalignment is bound to be caused by surface spin canting, which is less dependent on the external magnetic field.
At the same time, the broadening of the Mössbauer absorption lines due to the Brownian particle motion and optical Doppler effect provides direct access to study the particle mobility. In figure 1, distinct line broadening upon heating to 252K translates to the exponential decrease in

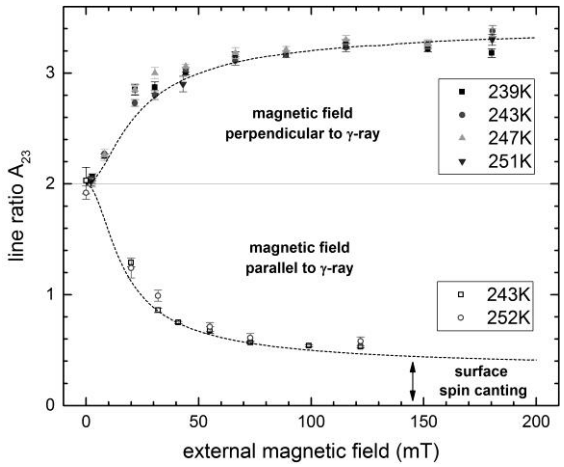

Fig. 2: Intensity ratio of absorption lines 2 and 3 indicating spin orientation relative to the γ-ray direction (parallel/perpendicular to field direction) measured for 15nm particles in glycerol solution.

fluid viscosity. Additional minor asymmetries in lineshape, visible primarily for narrow lines at 243K, are caused by beginning superparamagnetic relaxation and provide information on the Néel type relaxation parameters like the magnetic anisotropy independent of the two aforementioned effects [3]. Parameters of Brownian particle diffusion and Néel relaxation obtained from Mössbauer spectroscopy experiments were crosschecked by means of AC-susceptometry, combining measurements in the high-frequency (ca. 10^2-10^6 Hz) and ultralow frequency (ca. 10^{-2}-10^3 Hz) regime.

In addition to observations described above, a minor reduction in linewidth was detected for the ferrofluid containing 15nm nanoparticles upon rising magnetic field amplitude. As the particles align along the external field direction, this could reflect an increasing suppression of rotational particle motion, whereby the remaining line broadening in higher magnetic fields would correspond to translational particle movement only.

Conclusion

We have successfully demonstrated that mobility, orientation and Néel relaxation of nanoparticles can be studied in ferrofluids individually in one experimental series of Mössbauer spectra. Furthermore, presented experimental results could indicate the ability to resolve rotational and translational modes of motion. Future studies will approach the application of this methodology on soft matter composites, to utilize Mössbauer spectroscopy as a versatile asset for the examination of magnetic particle response behavior in external fields and particle mobility in nanostructured (visco-) elastic media. The analysis of field dependent dynamics shall be compared to magnetic susceptometry experiments in the presence of additional DC magnetic fields performed at the TU Braunschweig.

Acknowledgements

We gratefully acknowledge funding by the DFG through SPP 1681 (grants WE2623/7-2 and LU-800/4-2) and FOR 1509 (grant WE2623/13). The authors are grateful to U. von Hörsten for his expert technical assistance.

References

[1] J. Landers, L. Roeder, S. Salamon, A. M. Schmidt, and H. Wende, J. Phys. Chem. C, **119**, 20642 (2015)

[2] J. Landers, S. Salamon, H. Remmer, F. Ludwig, and H. Wende, Nano Lett., **16**, 1150 (2016)

[3] J. Landers, F. Stromberg, M. Darbandi, C. Schöppner, W. Keune, and H. Wende, Phys.: Condens. Matter, **27**, 026002 (2015)

The anisotropy of the ac susceptibility of magnetic nanoparticle suspensions

F. Ludwig[1], C. Balceris[1]

[1] *Institut für Elektrische Messtechnik und Grundlagen der Elektrotechnik, TU Braunschweig, Braunschweig*

Introduction

AC susceptometry is a widely applied method for the determination of structure parameters of magnetic nanoparticles (MNP). In ac susceptometry, the MNP are exposed to a sinusoidal magnetic field and the voltage induced in a differential detection coil is measured and converted into real and imaginary parts of the ac susceptibility which are displayed as a function of frequency. Custom-built and commercial ac susceptometers cover a frequency range of a few Hz up to several MHz [1,2].

The analysis of the complex susceptibility spectrum is generally performed with the Debye model which is applicable if the ac magnetic field is small enough ($\xi = mB/(k_BT) << 1$) and if all MNP have the same characteristic relaxation time τ. Here the static susceptibility is given by

$$\chi(\omega) = \frac{\chi_0}{1 + i\omega\tau} \qquad (1)$$

with angular frequency ω and static susceptibility

$$\chi_0 = \frac{\mu_0 n m^2}{3 k_B T}. \qquad (2)$$

Here, n is the MNP density, m the magnetic moment of a single MNP, k_BT the thermal energy and μ_0 the vacuum permeability. According to (1), the imaginary part has a maximum at $\omega\tau = 1$ and the real part drops down to zero at high frequencies.

In reality, MNP dispersions exhibit distributions of core and hydrodynamic sizes which can be accounted for by inserting distributions of core and hydrodynamic sizes in the Debye model [3].

Experimentally it is often found that the real part at high frequency does not drop down to zero but levels off at a finite value

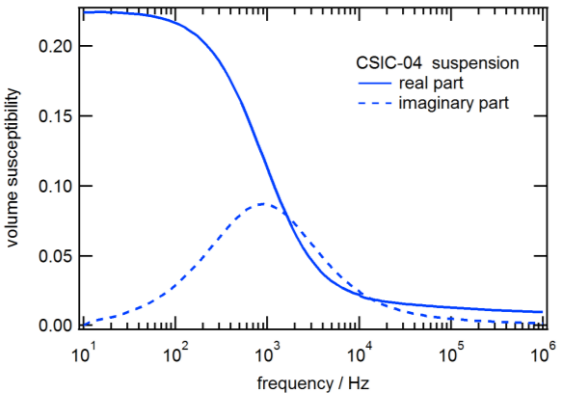

Fig. 1: Complex susceptibility versus frequency of suspension of blocked single-core MNP

(Fig. 1). This is commonly attributed to the presence of some Néel contribution originating from MNP with very short relaxation times ($\tau_N << 1$ µs).

Model

In [4], Shliomis and Stepanov presented a model which accounts for the anisotropic character of the ac susceptibility of suspensions of magnetic nanoparticles with uniaxial anisotropy. Here the complex susceptibility if given by

$$\chi = \frac{1}{3}\left(\frac{\chi_{II}}{1 + i\omega\tau_{II}} + 2\frac{\chi_{\perp}}{1 + i\omega\tau_{\perp}} \right) \qquad (3)$$

where the indices "II" and "⊥" refer to the direction of the applied ac magnetic field either parallel of perpendicular to the MNP easy axis. The characteristic relaxation times of the parallel and perpendicular components are given by

$$\tau_{II}^{-1} = \tau_l^{-1} + \tau_B^{-1} \quad \text{and} \quad \tau_{\perp}^{-1} = \tau_t^{-1} + \tau_B^{-1}$$

where

$\tau_B = \frac{3\eta V_h}{k_B T}$ with viscosity η and hydrodynamic volume V_h. The longitudinal and transversal Néel relaxation times are given by [4]

$$\tau_l = \tau_0 \frac{\sqrt{\pi}}{2\sigma^{3/2}} \exp(\sigma) \text{ (for } \sigma \geq 2) \text{ and}$$

$$\tau_t = 2\tau_0 \frac{1 - \frac{1}{2}\left(3\frac{R'}{R} - 1\right)}{2 + \frac{1}{2}\left(3\frac{R'}{R} - 1\right)}.$$

Since the transversal Néel relaxation time τ_t is of the order of τ_0 (or smaller), $\omega\tau_t << 1$ for frequencies which are accessible in typical ac susceptometers ($f < 10$ MHz). Thus, equation (3) modifies to

$$\chi = \frac{1}{3}\left(\frac{\chi_{II}}{1 + i\omega\tau_{II}} + 2\chi_{\perp}\right). \qquad (4)$$

Experiment and results

To experimentally verify this anisotropic character of the ac susceptibility of MNP suspensions, we immobilized single-core MNP (CSIC-04) so that the characteristic longitudinal and transversal relaxation times are given by the corresponding Néel relaxation times. Immobilization was carried out by freeze-drying the MNP in a mannitol matrix. For the random case (random orientation of easy axes), freeze-drying was done in the absence of a magnetic field, while for the perpendicular and parallel cases a magnetic field of 170 mT was applied during the freeze-drying process, thus aligning the MNP easy axes parallel or perpendicular to the direction of the applied ac magnetic field.

The measured susceptibility spectra are depicted in Fig. 2. Apparently, there is a pronounced anisotropy in the spectra. For the sample with easy axes perpendicular to the ac magnetic field, the real part is constant over the measured frequency range while the imaginary part is zero – in agreement with (4). The spectra of the sample with randomly oriented easy axes are in between the other two scenarios. The observed features are in qualitative agreement with spectra calculated for immobilized MNP for a lognormal-distributed normalized anisotropy energy $\sigma = KV_c/(k_BT)$ with a sufficiently large standard deviation (of the order of 0.6) [5].

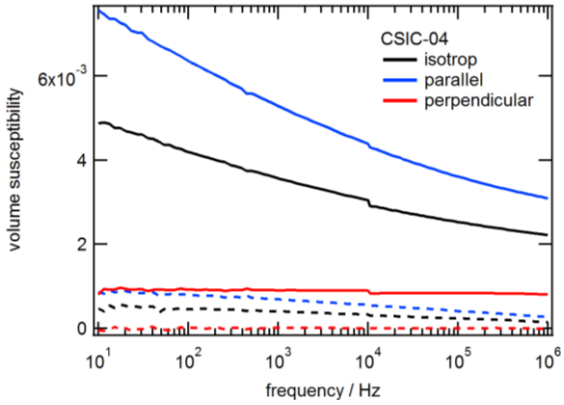

Fig. 2: Measured ac susceptibility spectra for the CSIC-04 samples with random distribution of easy axes as well as with easy axes either parallel or perpendicular to ac magnetic field.

The finite real part at high frequency – caused by intra-potential-well contributions – can also be used to independently determine the effective anisotropy constant. Using (4), one finds $\chi_\infty/\chi_0 = 1/\sigma$. From the data shown in Fig. 1, a value $K = 9000$ J/m^3 is obtained.

The findings also have a strong impact on the phase which is given by $\varphi = \arctan\left(\chi''/\chi'\right)$. If the influence of the intra-potential-well contribution is not corrected for, the phase lag does not converge to 90° for high frequencies but – after an initial rise – drops down to zero.

Acknowledgments

This work was supported by the European Commission Framework Programme 7 under the NanoMag project (grant agreement no: 604448).

References

[1] F. Ahrentorp, et al., AIP Conf. Proc. 1311, 213 (2010).
[2] F. Ludwig, et al., J. Appl. Phys. 108, 033918 (2010).
[3] M. I. Shliomis and V. I. Stepanov, J. Magn. Magn. Mater. 122, 176 (1993).
[4] F. Ludwig, et al., IEEE Trans. Magn. (in press)
[5] F. Ludwig, et al., IEEE Trans. Magn. (in press)

Magnetic field-induced and friction-induced rotation of anisotropic particles in viscoelastic matrices investigated by means of time-resolved Small Angle X-ray Scattering

Annemarie Nack[1], Julian Seifert[2], Christopher Passow[3], Joachim Wagner[1]

[1] *Institut für Chemie, Abteilung Physikalische Chemie, Universität Rostock*
[2] *Department Chemie, Institut für Physikalische Chemie, Universität zu Köln*
[3] *Deutsches Elektronen Synchrotron (DESY), Hamburg*

Rotational motion of anisotropic magnetic particles can either be induced by torques resulting from the interaction with an external magnetic field or by the vorticity of a velocity field in a laminar shear flow even in absence of a magnetic field. In the latter case particles reduce their rotational friction following the angular velocity of the surrounding matrix.

In the case of magnetically induced torques the deformation of the surrounding elastic matrix due to rotation of particles generates restoring torques. When both torques compensate each other, a time-independent orientation of individual particles with respect to the field direction is approached (see *Fig. 1*). Analyzing the canonical average of the orientational distribution function in thermal equilibrium gives insights into the interaction between particles and matrix if both, magnetically induced torques and elastic constants of the matrix are known. As a model system, composites consisting of spindle-shaped hematite particles and poly-N-isopropylacrylamide hydrogels are used.

In absence of a magnetic field, the rotation of particles can be induced in the vorticity of the velocity field in a laminar shear flow. In a first step a prealignment of the particles with their long axes parallel to the shear plane is achieved by compressing drops of isotropic composites between the plates of plate-plate rheometer. A small angle scattering experiment employing a primary beam perpendicular to the shear plane results in a circular symmetric scattering pattern, since the long axes of the particles are statistically aligned within this plane.

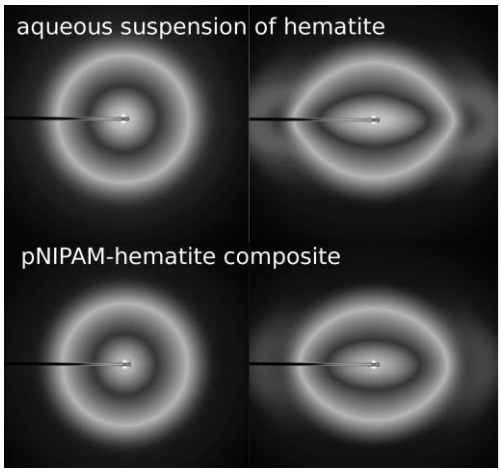

Fig. 1: False color representation of SAXS resulting from aqueous suspension (upper row) and composites (lower row) containing identical number densities of hematite particles at magnetic flux densities B_1= 0 T (left) and B_2 = 1.5 T (right).

In time-resolved scattering experiments during oscillatory shear of the samples, intensity fluctuations in phase with the deformation occur, the frequency of which is twice the frequency of the oscillatory shear (see *Fig. 2*).

The velocity field of a laminar shear flow rotates around an axis in the shear plane. Particles with their long axis parallel to the vorticity rotate around their director. Since the scattering function of axially symmetric particles depends only on the angle between the scattering vector $\mathbf{Q}$ and the particle director $\hat{\mathbf{u}}$, the scattering is not affected by the rotation around the long axis. Particles with

their long axis perpendicular to the vorticity, however, rotate around their short axis out of the shear plane. By this rotational motion, the angle between $\mathbf{Q}$ and $\hat{\mathbf{u}}$ changes and therewith the scattering power of the particle.

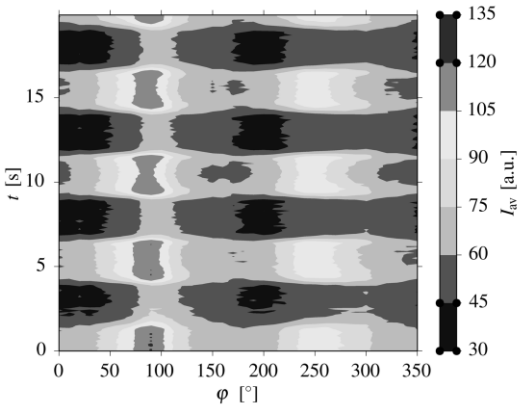

Fig. 2: Contour plots, representing the scattered intensity of a composite in dependence on the time *t* and the angle φ with respect to the direction of the shear flow at shear frequency *f* = 0.1 Hz.

The maximum anisotropy occurs at maximum deformation γ, while in the non-deformed state at $\gamma = 0$ again an isotropic scattering pattern is observed. Since the scattering function depends due to the equatorial mirror plane of the particles on the squared inner product $(\mathbf{Q}.\hat{\mathbf{u}})^2 = (\mathbf{Q}.(-\hat{\mathbf{u}}))^2$, the scattering under the deformation γ is identical to the scattering under the deformation $-\gamma$ which leads to intensity fluctuations with a frequency twice as large as the oscillation frequency (see *Fig. 3*).

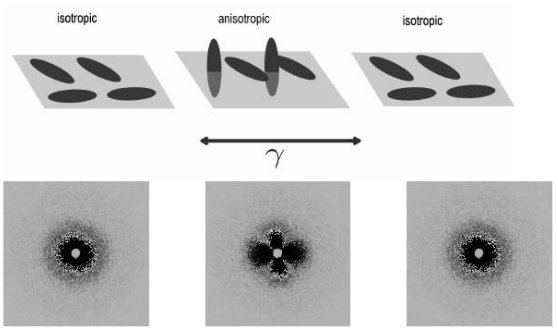

Fig. 3: Differences in scattered intensities under oscillatory shear stress and those of initial configuration without shear stress.

Acknowledgments

We acknowledge the European Synchrotron Radiation Facility (ESRF) and the Deutsches Elektronen Synchrotron (DESY) for providing beamtime at the beamlines ID02 and P10 and the Deutsche Forschungsgemeinschaft for financial support within the priority program SPP 1681.

Comparing the spectra of Magnetic Nanoparticles measured by Magnetic Particle Imaging and Magnetic Particle Spectroscopy

H. Paysen[1], J. Wells[1], O. Kosch[1], N. Loewa[1], U. Steinhoff[1], L. Trahms[1], T. Schaeffter[1] and F. Wiekhorst[1]

[1] *Physikalisch-Technische Bundesanstalt, Berlin, Germany*

Introduction

Quantitative measurements of magnetic nanoparticles (MNP) yield a lot of potential for biomedical applications. Magnetic Particle imaging (MPI) is a new technology with great potential for safe, fast and spatially resolved quantification of MNP distributions in vivo [1]. The technique utilizes spectral analysis of the non-linear dynamic magnetic response of the MNP exposed to a harmonic excitation field. Combined with a static gradient field and a calibration measurement, the measured spectra can be used to reconstruct a quantitative map of the iron amount. However, even the spectra before calibration contain quantitative information about the MNP in the sample. This principle is also used in a magnetic particle spectrometer (MPS), which can be called a "0D-MPI scanner". Here, we present results acquired with an MPI scanner adapted to work as a conventional MPS. The performance is then compared to a commercial MPS and the differences and limitations evaluated.

Methods

Measurements were conducted using a preclinical MPI 25/20 FF scanner (Bruker/ Philipps) and a calibrated magnetic particle spectrometer (MPS-3, Bruker), both operating at an excitation frequency of 25 kHz. Seven samples were measured containing 15 µl Perimag (Mircomod) at different iron concentrations ranging from 8.5 mg/ml to 4.8 ng/ml. MPS measurements were conducted at an amplitude of 12 mT, a receiver bandwidth of 1 MHz and a scan time of 10 s. MPI measurements were executed using only one of the three excitation coils (x-direction) at an amplitude of 12 mT. Initial MPI measurements were done with the gradient system turned off completely, which resulted in additional artefacts in the spectra. A small gradient field of 0.25/0.25/0.5 T/m (*x*/*y*/*z*-direction) was therefore introduced, and the samples were positioned at the center to minimize the effect of the gradient on the spectra. The scan time was also adjusted to 10 s for a fair comparison, and the receiver bandwidth to the maximum value of 1.25 MHz. The response signal was measured using a separate receive coil sensitive in the *x*-direction. The transfer function for the MPI system and the MPS system were used to correct the influence of the receive chain on the measured spectra.
Empty measurements were taken for both techniques subtract time-independent noise. For comparison, all acquired spectra were normalized to the corresponding amplitude of the third harmonic (A_3) measured with the undiluted sample.

Results and Discussion

The amplitudes of the third harmonics are visualized as a function of the iron mass in figure 1. Presented are the data with, and without, background correction. In both cases the signal decreases linearly with decreasing iron mass until a constant signal level (noise) is reached. This noise level is caused by the scanning device and can be used as a definition of the detection limit. For iron masses above 10 µg a good agreement between the measurements of MPI and MPS is observed. However, the noise level of the MPI scanner is reached for an iron mass of about 1 µg, while the MPS device

reaches a value at about 1 ng. The overall sensitivity can be increased by a subtraction of a background measurement. For both measurement techniques the detection limit decreases by a factor of ten.

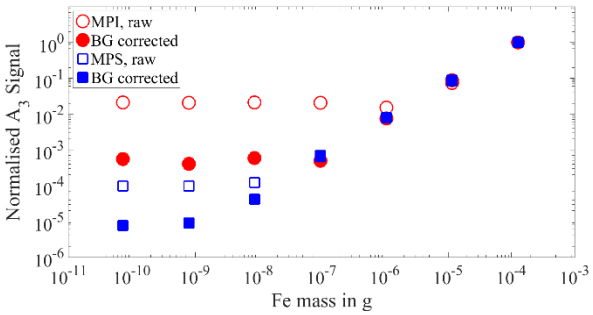

Figure 1: Comparison of normalized A_3 signal amplitudes measured with MPS and MPI as a function of the iron mass. The noise level of the MPI measurements is reached for iron masses of about 1 µg and about 1 ng for the MPI and the MPS scanner without using a background correction. Using a previously measured empty measurement for correction the noise level decreases by a factor of ten.

The difference in sensitivity between the two systems is mainly caused by the different sizes of the receiving coils. The coil of the MPI system has a coil diameter of 72 mm, while the MPS system works with a diameter of 12 mm.

The comparison between the odd and even harmonics of the background-corrected measurements shows similar spectral behavior for MPS and MPI above the detection limits (figure 2). The slightly faster decay of the MPI amplitudes for higher harmonics might be caused by the small gradient, which suppressed parts of the signal. The spectral behavior of the samples, measured with lower iron concentrations, show the same results until the saturation (noise) level of the respective system is reached.

Note that the determined detection limits are only valid if just one of the excitation coils is used. In general, all three excitation coils are used, working with slightly different frequencies. This will generate signal at mixed frequencies, which can be better distinguished from the noise level.

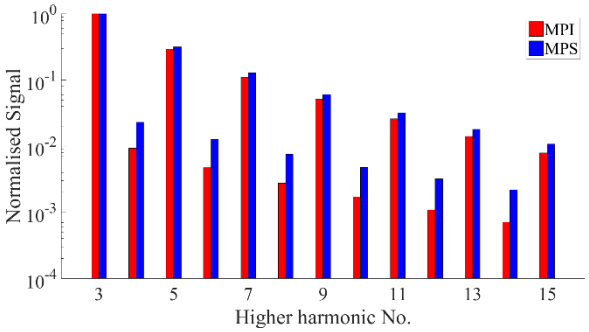

Figure 2: Comparison of the background corrected amplitudes of the odd and even harmonics measured with MPS and MPI. Shown are the data acquired with the biggest iron concentration of 8.5 mg/ml.

Conclusion

We compared the signals of a serial dilution of MNP obtained by an adapted MPI system with MPS measurements. The data are in good agreement with each other, and exhibit a detection limit of the MPS system approximately 100-times lower than the MPI system. This is mainly caused by the smaller coil geometry. Therefore, a first step towards quantitative MPI has been achieved by validating our MPI scanner to a calibrated MPS system.

Acknowledgments

This work was supported by Deutsche Forschungsgemeinschaft (DFG) in the framework of the priority program 1681 (WI4230/1-2, TR408/8-2) and the projects “Aortic Aneurysm MPI” (SCHA 1506/2-1) and “quantMPI” (TR 408/9-1).

References

[1] B. Gleich and J. Weizenecker, “Tomographic imaging using the nonlinear response of magnetic particles,” *Nature*, vol. 435, no. 7046, pp. 1214–1217, 2005.

Self-assembly of nanoparticle magnetic filaments of different topologies

E. Pyanzina[1], E. Novak[1], D. Rozhkov[1], P. A. Sánchez[2], S. Kantorovich[1,2]

[1] *Ural Federal University, Ekaterinburg, Russia*
[2] *Computational Physics: Faculty of Physics, University of Vienna, Vienna, Austria*

Magnetic filaments are semiflexible polymer-like chains of magnetic nanoparticles permanently crosslinked with polymers. The synthesis and control of the properties of these systems has experienced a great progress in recent years thanks to the enhancement of polymer crosslinking techniques. They have been recently pointed as promising building blocks for the creation of sophisticated magnetoresponsive materials [1]. The main application of magnetic filaments today is their use as artificial cilia, driven by a magnetic field, as well as to create micro-swimmers or magnetically controlled devices for drug delivery. Moreover, dispersions of biocompatible magnetic polymers have already been tested as contrast agents for magnetic resonance measurements in biomedicine and give a higher magnetic response than equivalent traditional magnetic fluids. Thus, dispersions of magnetic filaments are promising candidates for the replacement of traditional magnetic fluids in any application that benefits from an increase of magnetorheological response.

Our research addresses the study of magnetic filaments made out of ferromagnetic nanoparticles with different chain conformations - simple open chains, closed rings and branched structures with "X" and "Y" junctions - inspired by the recent findings on the low temperature self-assembly of dipolar hard spheres [2]. The introduction of the polymer crosslinkers to stabilise the structure of such self-assembled nanoparticle aggregates is expected to have an important impact on the properties of the system. Here, using Langevin dynamics simulations, we focus on low-concentration solutions of magnetic filaments, analysing in detail their self-assembly behaviour. Extensive cluster analysis allows us to compare the structures formed by these filament solutions to those observed in conventional magnetic fluids, containing non-crosslinked nanoparticles. Also we investigate initial susceptibility for different parameters (value of magnetic moment, length of filaments). We will show that the topology of the filaments can dramatically change the microstructure and macroscopic response of the solution. These results will pave the way for the development of analytical models and identify the most interesting building block candidates for the design of novel magnetoresponsive materials.

Acknowledgments

This research has been partially supported by the Austrian Research Fund (FWF): START-Projekt Y 627-N27. We gratefully acknowledge research funding from the Ministry of Education and Science of the Russian Federation (Project No. 3.1438.2017/4.6) and RFBR No. 16-52-12008 (DFG Ref.No.: OD 18/24-1). The computational results presented here have been achieved using the Ural Federal University Cluster.

References

[1] Sánchez et al., Faraday Discuss. 186, 241 (2016).
[2] Kantorovich et al., PCCP 17, 25 (2015).

Magnetic Field Dependence of Ni Nanorod Brownian Relaxation in Different Media

H. Remmer[1], M. Gratz[2], A. Tschöpe[2], F. Ludwig[1]

[1] *Institut für Elektrische Messtechnik und Grundlagen der Elektrotechnik, TU Braunschweig, Braunschweig*
[2] *Experimentalphysik, Universität des Saarlandes, Saarbrücken*

Introduction

The dynamics of magnetic nanoparticles (MNP) in large excitation magnetic fields has been subject of numerous theoretical and experimental studies but it is also of interest for biomedical applications like hyperthermia and magnetic particle imaging. In addition, for nanorheological studies of the particle-matrix interaction in applied magnetic fields, which is an important tool to understand the magnetic controllability of hybrid materials, it is important to separate the influence of the magnetic field on the Brownian relaxation time from that on the rheological parameters. While Nowak et al. [1] focused on the magnetorheological effect in a Newtonian fluid, here it is important to extend these studies to non-Newtonian fluids and viscoelastic matrices.

For Langevin parameters $\xi = mB/k_BT >> 1$, the widely known equations for Brownian and Néel relaxation times cannot be applied. In literature several models for field-dependent Brownian relaxation times with $\xi >> 1$ can be found (e.g. [2, 3]).

Here we investigate the dynamics of PAA-coated Ni nanorods in different aqueous polyethylene glycol (PEG) solutions in large ac and dc magnetic fields. The nanorods are uniaxial ferromagnetic single-domain particles with effectively suppressed Néel relaxation because of their high magnetic shape anisotropy energy. With their magnetic moment of the order of a few 10^{-17} A·m^2, the Langevin parameter ξ becomes much larger than unity even for comparably small fields.

The complex ac susceptibility (ACS) measurements are analyzed with different theoretical models for the Brownian relaxation time in the presence of large ac or superimposed dc magnetic fields.

Experiment

The Ni nanorods were prepared by electrodeposition of nickel into anodized aluminium oxide (AAO) templates [4]. This approach results in a narrow size distribution. Determined by TEM, the length of the nanorods amounts to $l = (273 \pm 3)$ nm and the diameter to $d = (20.3 \pm 0.2)$ nm.

The aqueous PEG solutions have a nominal, macrorheologically measured viscosity of 29 mPa·s: PEG 35 k with 11.2 w% 35 kg·mol^{-1} PEG and PEG 300 k with 2.1 w% 300 kg·mol^{-1} PEG.

The ACS spectra presented here are measured with our home-built, fluxgate-based setup which was originally developed for measurements in a rotating field with two orthogonal Helmholtz coils [5]. Because ACS measurements need only one pair, we can use one Helmholtz coil for optional superimposed dc fields. The measurements are performed in a frequency range between 2 Hz and 9 kHz with ac and dc magnetic field amplitudes up to 9 mT.

Results

For the sample with PEG 300 k, the imaginary parts of the ac spectra are shown in Fig. 1 for different magnetic excitation fields. With increasing field, the maxima of the imaginary parts shift towards higher frequencies and the amplitude decreases. A similar behavior can be observed for the sample with PEG 35 k (not shown).

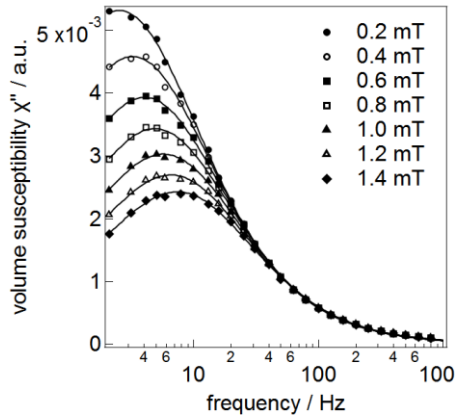

Fig. 1: Imaginary parts of ac susceptibility versus frequency for different ac magnetic field amplitudes.

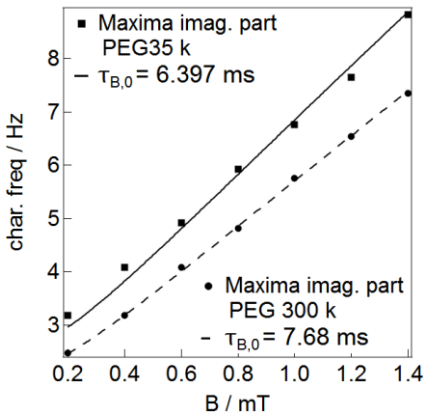

Fig. 2: Extracted characteristic frequencies, maxima for PEG 35 k and PEG 300 k with their corresponding fitting curves.

The experimental data are analyzed with an equation by Yoshida and Enpuku who have solved the Fokker-Planck equation for the Brownian relaxation time of spherical nanoparticles in the non-linear magnetization regime [6]:

$$\tau_B = \frac{\tau_{B,0}}{\sqrt{1+0.126\xi^{1.72}}}. \qquad (1)$$

The characteristic frequencies extracted from the peak positions and their corresponding regression results are mapped in Fig. 2 for the samples with 35 k and 300 k PEG. The data points are well described by the theoretical expression for the Brownian relaxation time. The obtained zero-field Brownian relaxation times $\tau_{B,0}$ can be used for the determination of the viscosity using the Brownian relaxation time of the aqueous nanorod sample. Assuming $\eta_{water} = 0.89$ mPa·s, the received viscosity values are $\eta_{35k} = 23.5$ mPa·s and $\eta_{300k} = 28$ mPa·s. This is in good agreement with the macrorheologically determined zero-shear viscosity of 29 mPa·s. The value of the magnetic moment $m = 4.2 \cdot 10^{-17}$ A·m^2 which is obtained from fitting the characteristic frequencies as a function of applied magnetic field with (1) is also obtained by amplitude dependent measurements on an aqueous nanorod sample [7].

In addition, the ACS measurements are performed with a superimposed dc field up to 9 mT perpendicular to the ac field. In this case the extracted characteristic frequencies are fitted with the expression by Martsenyuk et al. [3]. A good agreement with the ac amplitude dependent results was found.

In summary, the influences of viscosity and ac magnetic field amplitude on the Brownian relaxation time are apparently multiplicative effects. The measured curves can be fitted very well with the expressions of Yoshida and Enpuku respectively Martsenyuk et al.. Thus, based on these measurement results, there is no measurable magnetoviscous effect in the studied magnetic field range applying ACS measurements.

Acknowledgments

Financial support by the Deutsche Forschungsgemeinschaft, DFG Priority Program 1681 (LU800/4-2, TS62/4-2) is gratefully acknowledged.

References

[1] T. Nowak et al., J. Magn. Magn. Mater. 354, 98 (2014).
[2] T. Yoshida and K. Enpuku, Jpn. J. Appl. Phys. Part 1 48, 127002 (2009).
[3] M. A. Martsenyuk, Yu. L. Raikher, and M. I. Shliomis, Sov. Phys. – JETP 38, 413 (1974).
[4] P. Bender et al., J. Magn. Magn. Mater 323, 2055 (2011).
[5] J. Dieckhoff et al., Appl. Phys. Lett. 99, 112501-1-3 (2011).
[6] F. Ludwig et al., Biomed. Engin. 58, 535 (2013).
[7] H. Remmer et al., IEEE Trans. Magn. (accepted).

Interaction of magnetic chains in soft gels

Henrik Schmidt[1], Günter K. Auernhammer[1]

[1] *Max Planck Institute for Polymer Research, Ackermannweg 10, 55128 Mainz, Germany*

At the Max-Planck-Institute for Polymer Research in Mainz, in recent years we focused on the interaction between magnetic particles in magnetic hybrid materials. In 3D and 2D systems we investigated the reaction of the magnetic particles and the surrounding matrix on applied magnetic fields [1-5]. In the 3D systems, superparamagnetic particles were dispersed into reactive polymer in the sol state. The composition was carefully adjusted to be just above the percolation threshold. Thus, soft gels with an elastic modulus lower than 10 Pa were fabricated. When the cross-linking was performed in the presence of an external magnetic field the magnetic particle in the polymer rearranged to chains. After cross-linking, the structure of the magnetic chains deformed when the magnetic field orientation was different to the frozen-in orientation in the soft magnetic gel. Images, taken with confocal microscopy, showed buckling chains. The buckling morphology depends on the length of the chain, orientation of the magnetic field respectively to the chain and the gels modulus.

Here, we investigate the interaction between magnetic chains and their buckling instabilities. Whereas in previous studies, the behavior of single well separate chains were in the focus, now the coupling of the buckling instability between neighboring chains will be studied. By simply increasing the concentration of the magnetic particle, the concentration of the magnetic chains can be tuned in a certain range. However, the distribution of the chains will be random in space. We will explore the chain interaction in such configurations. Furthermore, we want to extract the deformation of the gel and aim for the ability to change the magnetic interactions through deforming the polymer. From these data we want to extract models for an effective tuning of internal deformations in soft magnetic hybrid materials.

Figures

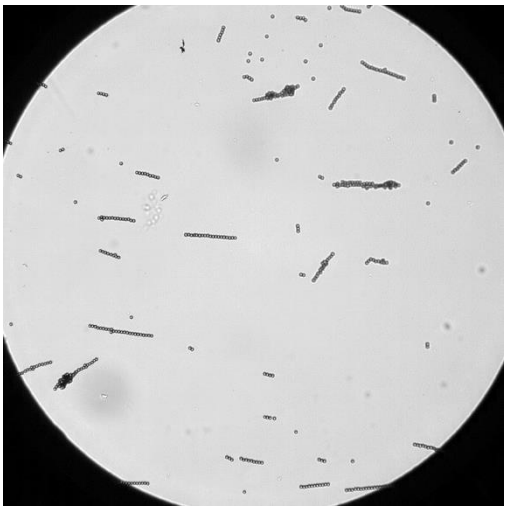

Acknowledgments

The authors thank for support by the Deutsche Forschungsgemeinschaft (DFG) through the SPP 1681.

References

[1] Collin, D., et al., *Frozen-in magnetic order in uniaxial magnetic gels: preparation and physical properties.* Macromol. Rapid Commun., 2003. **24**: p. 737 - 741.

[2] Huang, S., et al., *Microgels at the Water/Oil Interface: In Situ Observation of Structural Aging*

and Two-Dimensional Magnetic Bead Microrheology. Langmuir, 2016. **32**(3): p. 712-722.

[3] Huang, S., et al., *Buckling of paramagnetic chains in soft gels.* Soft Matter, 2016. **12**(1): p. 228-237.

[4] Puljiz, M., et al., *Forces on Rigid Inclusions in Elastic Media and Resulting Matrix-Mediated Interactions.* Physical Review Letters, 2016. **117**(23): p. 238003.

[5] Huang, S., et al., *Structure and Rheology of Microgel Monolayers at the Water/Oil Interface.* Macromolecules, 2017.

Torque-driven deformation of Ni-nanorod/PAM-hydrogel nanocomposites

C. Schopphoven, K. Birster, R. Schweitzer, A. Tschöpe

Universität des Saarlandes, Experimentalphysik, Campus D2 2, 66123 Saarbrücken

Introduction

Magnetic anisotropic polymer composites can be used as active components in soft actuators with remote and independent control of forces and torques. Complex and multidimensional motions are achieved by tailoring the local density and the orientation distribution of the anisotropy axes of the magnetic particles in combination with suitable external magnetic fields [1].
The present study focuses on nanocomposites which consist of homogeneously dispersed and parallel aligned ferromagnetic Ni nanorods in polyacrylamide (PAM) hydrogels. The high compliance of the matrix enables considerable elastic deformations as result of an applied torque in a transversal magnetic field. The local rotation of the individual nanorods was investigated by optical transmission measurements at low particle volume fraction ($\phi_v \approx 10^{-6}$) making use of the optical anisotropy of the nanorods. The macroscopic torsion of a textured hydrogel cylinder with nanorod volume fraction of $\phi_v \approx 10^{-4}$ was studied experimentally and compared with a continuum model based on the microscopic properties of the nanorods and the geometry and shear modulus of the torsion cylinder.

Methods

Ni nanorods were prepared by the AAO-template method and processed to stable aqueous colloidal dispersions [2]. The nanorods were surface-functionalized with polyacrylic acid and mixed at the desired concentration with a degassed solution of 27.3 wt% acrylamide and 0.363 wt% bis-acrylamid. The suspension was polymerized in a homogeneous magnetic field of ≈ 20 mT by addition of a 1 wt% TEMED and 1 wt% APS solution which provided textured hydrogels with parallel alignment of the nanorods.
Basic physical properties of the Ni nanorods were obtained by transmission electron microscopy (TEM), magnetization measurements (VSM, vector-VSM), static (DC-OT) [3] and oscillating field (OF-OT) [4] optical transmission measurements.

Results

The Ni nanorods used in this study are uniaxial ferromagnetic single-domain particles. Their magnetization properties can be described by the Stoner-Wohlfarth model. However, coherent rotation during reversible magnetization changes is restricted to an angular range $\Theta \leq 70°$ between the field- and rod axis as revealed by measurements of the magnetization vector (V-VSM). Within this limited range, the SW-model provides quantitatively consistent values for the magnetic torque $T(\Theta, H)$.
As a result of an applied transversal magnetic field, each Ni nanorod in a soft elastic environment rotates until the magnetic torque is balanced by an elastic counter torque. Taking advantage of their optical anisotropy, this local rotation of the parallel aligned nanorods was determined from the optical transmission of linearly polarized light for different angles Θ as function of magnetic field. When the two experimental variables Θ and H were translated to the corresponding torques by using the SW-model, the various measurements collapse onto a single straight master curve, Fig.1. The slope is given by $(K_v G)^{-1}$, where K_v is a geometry factor representing the hydrodynamic size of the

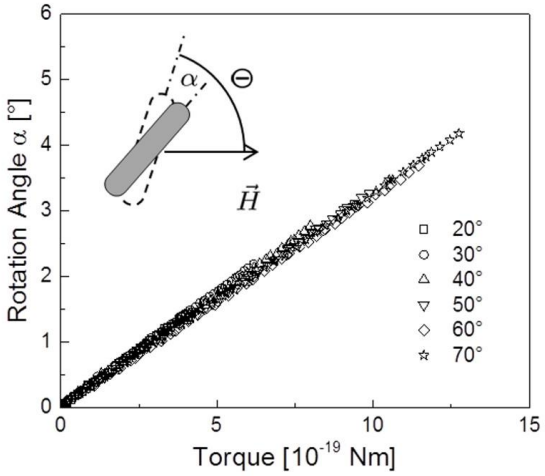

Figure 1: Local rotation angle α of Ni nanorods, measured at different initial orientations Θ, as function of the magnetic torque. The torque was calculated using the SW-model in the limited range of $\Theta \leq 70°$.

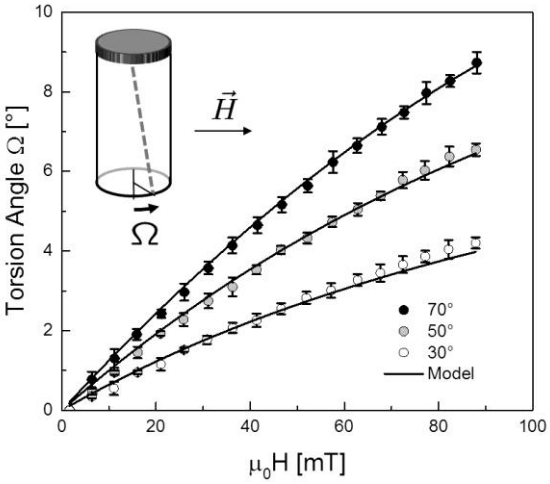

Figure 2: Macroscopic torsion angle Ω of a nanocomposite cylinder measured at different initial orientations of the texture axis as function of magnetic field, and comparison with a continuum model based on the microscopic properties of the Ni nanorods.

nanorods (determined by a calibration measurement) and $G = 260$ Pa is the shear modulus of the hydrogel matrix. This local rotation, measured at a low volume fraction $\phi_v \approx 10^{-6}$, does not cause a macroscopic deformation. However, it decreases the particle orientation angle Θ and consequently leads to a reduction of the magnetic torque which has to be taken into account in the modeling shown below.

Macroscopic deformations were investigated by measuring the torsion of a textured Ni/PAM nanocomposite cylinder ($l = 17$ mm, $d = 2$ mm) in a transversal field. The Ni nanorods at a volume fraction $\phi_v \approx 10^{-4}$ were aligned perpendicular to the cylinder axis. The field-dependent torsion increased with increasing initial orientation angle of the texture axis with respect to the magnetic field direction, Fig.2. The experimental results could be well described by a model based on the magnetic properties of the nanorods (SW-model), their local orientation and the macroscopic torsion of an elastic continuum as a result of distributed body torques, Fig.2.

Conclusion and Outlook

The SW-model predicts a maximum value for the magnetic torque which is achieved for particular combinations of Θ and H only. This indicates a potential strategy to improve the magnetic actuator performance by optimizing the initial distribution of magnetic anisotropy axes.

Acknowledgments

We thank R. D. Shull and C. L. Dennis at the NIST (Gaitherburg, USA) for their cooperation with the V-VSM measurements. We further acknowledge financial support by the Deutsche Forschungsgemeinschaft, DFG Priority Program 1681 (TS62/4-2).

References

[1] G. Z. Lum, Z. Ye, X. Dong, H. Marvi, O. Erin, W. Hu, and M. Sitti, *PNAS* **113** (2016) E6007.

[2] P. Bender, A. Günther, A. Tschöpe, and R. Birringer, *JMMM* **323** (2011) 2055.

[3] F. Krämer, M. Gratz, and A. Tschöpe, *J. Appl. Phys.* **120** (2016) 044301.

[4] A. Tschöpe, K. Birster, B. Trapp, P. Bender, and R. Birringer, *J. Appl. Phys.* **116** (2014) 184305.

In-situ observation of the particle microstructure of magnetorheological elastomers in presence of mechanical strain and magnetic fields

M. Schümann, S. Odenbach

Chair of Magnetofluiddynamics, Measuring and Automation Technology, Technische Universität Dresden, Dresden 01062, Germany

Introduction

Magnetorheological elastomers are a type of smart hybrid material which combines elastic properties of a soft elastomer matrix with magnetic properties of magnetic micro particles. The particle properties and their arrangement in the matrix play a major role in determining the resulting macroscopic magnetorheological effects [1]. In this work the impact of mechanical strain and magnetic fields on the particle structure was observed by means of x-ray microtomography.

Material

40 wt% of Höganäs® ASC200 carbonyl iron particles were combined with silicone polymers by Gelest Inc. to achieve a homogeneous hybrid material with an isotropic particle distribution. Two sizes of cylindrical samples were prepared for tomography (d = 4 mm) and for the mechanical testing (d = 12 mm).

Methods

Stress-strain-tests were performed to evaluate the Young's modulus of the material without and in presence of a 250 mT field. The particle structure was observed via x-ray microtomography. From the reconstructed tomography data, the angle between the longest major axis of individual particles and the cylinder axis of the sample was calculated for 50,000 particles [2]. Furthermore the radial distribution function (RDF) of the particle ensemble was evaluated for each sample state [3].
During the tomography measurements magnetic fields of 0 mT, 10 mT and 250 mT were applied to the sample. In addition to that the sample was compressed to 12 % strain during tomography to recreate the situation during mechanical testing, where the magnetorheological effect occurs. The direction of the magnetic field, the applied strain and the mechanical testing align with the cylinder axis of the samples.

Magnetorheological Effect

The material shows a significant impact of the applied 250 mT magnetic field on the Young's modulus. If the field is removed, the Young's modulus returns to its initial value of 10 mT. An average magnetorheological effect of MRE = 633 % ± 55 % was calculated from the measured moduli.

Distribution of particle angles

The reconstructed tomography data reveal the formation of particle chains if the 250 mT field is applied (Figure 1).

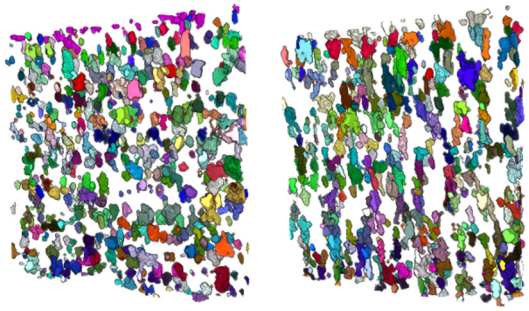

Figure 1: *This excerpts of the reconstructed tomography data (850 µm x 850 µm) show the initial isotropic particle structure (left) and particle chains in presence of the 250 mT field (right).*

The angles as evaluated from the tomography data shown in Figure 1 are depicted in

Figure 2. Different combinations of magnetic fields and mechanical strain lead to significant changes of the particle orientation. The results show a clear impact of the magnetic field on the particle rotation. An impact of the mechanical strain on the particle angles can only be observed for the 10 mT field. The deviation of the initial particle strucutre from a perfectly isotropic distribution of particle angels may be linked to the sample preparation process.

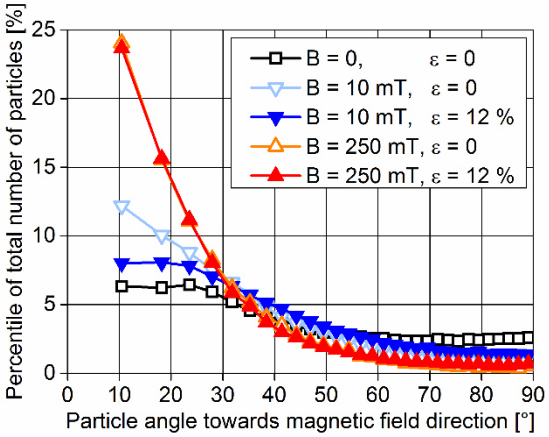

Figure 2: *The increase of the amount of particles featuring a small angle indicates a rotation of the particles tending to align with the magnetic field direction.*

Spatial distribution of the particles

The radial distribution function (RDF) of the particle arrangements were evaluated from the same 3D tomography data sets [3]. The RDF was calculated for every 2D slice and the averaged over the whole sample volume. Figure 3 shows the results for the observed applied fields and strains. As visible in the tomography data, at 250 mT the particles rearrange in chains (Figure 1). This leads to distinct distances of the chains in the 2D slices, in contrast of a 2D random distribution of particles before application of the magnetic field.

This change from a random to a specific particle spacing is reflected in the RDF as occurring extrema. The impact of axial mechanical compression is visible as an increase of the distance of those maxima. This indicates a radial expansion of the particle structure as one would expect with a axially compressed sample. No chain formation was found at 10 mT. Thus, an impact of the strain on the particle structure at 10 mT is not visible due to the isotropic distribution of the particle distances.

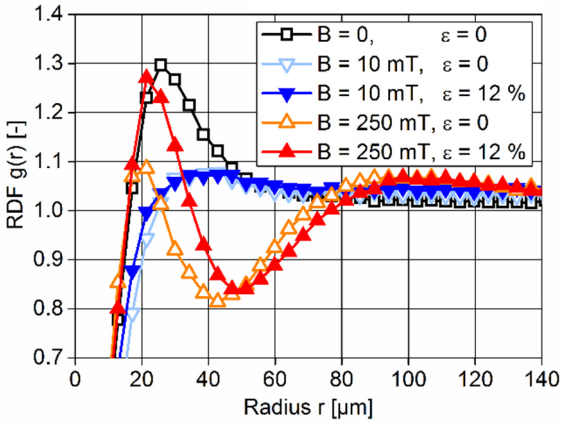

Figure 3: *The results show a transition from a typical RDF indicating an isotropic particle structure to an ordered structure.*

Conclusion

The addition of the evaluation of the RDF to the analysis of the geometrical properties of individual particles offer a more comprehensive characterisatio of the impact of different stimuli on the particle structure in magnetorheological elastomers. A detailed interpretation of the presented data can be found in [4].

Acknowledgments

This work was supported by Deutsche Forschungsgesellschaft (DFG) within the project OD18/21, in the frame of the priority program SPP1681.

References

[1] Filipcsei, G., Csetneki, I., Szilágyi, A., & Zrínyi, M. (2007) *Oligomers-Polymer Composites-Molecular Imprinting, Springer Berlin Heidelberg* pp. 137-189

[2] Gundermann, T., & Odenbach, S. (2014) *Smart Mater. Struct.* **23(10)** 105013

[3] Gundermann, T., Cremer, P., Löwen, H., Menzel, A. M., & Odenbach, S. (2017) *Smart Mater. Struct.* **26(4)** 045012

[4] Schümann, M., & Odenbach, S. (2017) *J. Magn. Magn. Mater* **441**

Remote-Controlled Magnetic Activation of Self-Healing Elastomeric Composites

A. Shaaban[1], N. Hohlbein[1], A. M. Schmidt[1]

[1]*Department Chemie, Institut für Physikalische Chemie, Universität zu Köln, Luxemburger Str. 116, D-50939 Köln, email:* annette.schmidt@uni-koeln.de

The interest in remote-controlled responsive materials and their modelling has increased over the last few decades. In this respect, the combination of magnetic nanoparticles with soft materials offers new possibilities towards smart adaptive materials that can be manipulated by external magnetic fields. In particular, the local heat dissipation by magnetic nanostructures in oscillating electromagnetic fields (OEMF) provides the opportunity to increase the temperature locally and thus stimulate dynamic processes, e.g. for self-healing materials.[1] Designing and modeling the heating procedure in this system allows the fabrication of on-demand tailor-made adaptive materials and an overall control of the procedure.

Ionomers have shown to be promising candidates for self-healing elastomers.[2–4] Polymer of this class contain up to 20 mol% of ionic aggregates that phase-separate and lead to thermoreversible physical crosslinks. The origin of the self-healing behavior of the ionomers is the dynamic viscoelastic nature and the thermal reversibility of the ionic crosslinks. The appearance of an ionic transition temperature T_i is characteristic for the ionic physical clusters.[3]

Results and Discussion

The used ionomer is based on a *n*-butyl acrylate backbone and contains 5 mol% of Zn^{2+}-neutralized acrylic acid units.[3] After a comparative investigation concerning magnetic particles, cube-like Fe_3O_4 particles (FC) with an edge length of $d = (212 \pm 57)$ nm were identified as good candidates due to their energy harvesting efficiency.

Magnetic composites of the FC particles and the self-healing ionomer matrix are obtained by coprecipitation and analyzed with respect to their magnetic, thermal and mechanical properties. It is shown that the thermal transition of the ion clusters is in the desired range (T_i = 339.6 K), and that the viscoelastic behavior changes accordingly at T_i from elastic to viscous at intermediate frequencies for healing capability. Rheological experiments show an increase of the mobility of the matrix by increasing temperature.

Figure 1a shows a typical thermogram for OEMF measurement at f = 250 kHz and $H = 31.5\ \mathrm{kA \cdot m^{-1}}$ for ionomeric composite with 0.05 vol% FC. A steady-state temperature T_{max} is reached due to the remaining heat loss to the environment. It is also noticed that T_{max} as well as the initial heating rate $(\mathrm{d}T/\mathrm{d}t)_{t\to 0}$ increase with increasing particle fraction. The steady-state condition is characterized by equality of the heat flow (Q_{int}) generated by magnetic heating, and the heat transfer from the sample to the environment (Q_{ex}), and thus T_{max} under a given field condition depends on the particle fraction, their specific heat power (*SHP*), and also on the sample dimension, shape, geometry, and contact to its environment.

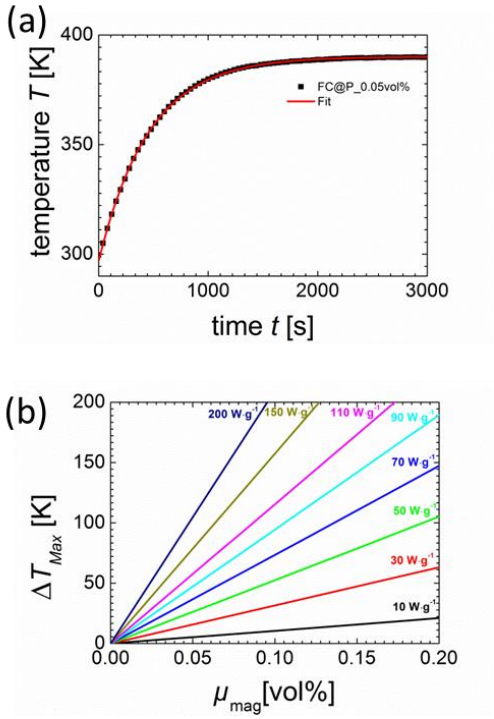

Figure 1: a) OEMF measurements of P@FC with filler fraction of 0.05 vol%, b) Simulated steady-state temperature ΔT_{Max} vs. the magnetic content μ_{mag} at different specific heating powers for a composite with a geometry of (25 x 10 x 2) mm^3.

The heating process can be described by a logarithmic equation, involving τ as the characteristic time constant depending on the heat transfer of the sample to the environment (Q_{ex}) and therefore on the sample geometry. Further the heat transfer coefficient h is accessible. The knowledge of h of a specific interface allows the prediction of T_{max} depending on the heat efficiency of the particle P_M for different sample geometries (figure 1b).

The magnetic field-induced heat development and the resulting temperature profile can effectively be predicted and modelled for various materials on the base of accessible material characteristics and geometry.[5] The heat transfer coefficient is determined and the steady-state temperature and time scale can be forecast by the described method.

Acknowledgments

This work was supported by the DFG priority program SPP 1568 'Design and Generic Principles of Self-healing Materials'. Funding from the European Union Seventh Framework Program (FP7/2007-2013) under grant agreement no. 290308 (Marie Curie ITN SHeMat 'Self-Healing Materials: from Concepts to Market') is gratefully acknowledged.

References

[1] A. Shaaban, A. M. Schmidt, *Smart Mater. Struct.* **2016**, *25*, 1–13.

[2] J. A. Syrett, C. R. Becer, D. M. Haddleton, *Polym. Chem.* **2010**, *1*, 978–987.

[3] N. Hohlbein, A. Shaaban, A. R. Bras, W. Pyckhout-Hintzen, A. M. Schmidt, *Phys. Chem. Chem. Phys.* **2015**, *17*, 21005–21017.

[4] N. Hohlbein, A. Shaaban, A. M. Schmidt, *Polymer (Guildf).* **2015**, 301–309.

[5] I. Levine, R. Ben Zvi, M. Winkler, A. M. Schmidt, M. Gottlieb, *Macromol. Symp.* **2010**, *291–292*, 278–286.

Torque on suspensions of anisotropic pigment particles and magnetic nanoparticles in rotating magnetic field

A. Storozhenko[1], R. Stannarius[2], A. Eremin[2], I. Aref'ev[3]

[1] *Southwest State University, Kursk, Russia*
[2] *Otto von Guericke University, Magdeburg, Germany*
[3] *Ivanovo Power Engineering University, Ivanovo, Russia*

The reorientation dynamics of complex liquids in external magnetic fields is important for their potential application in magneto-mechanical and magneto-optical devices, and provides fundamental insights into their structures and internal dynamic mechanisms. The phenomenon that nanostructured magnetic fluids follow a rotating magnetic field is known as the rotational effect [1,2]. We study this effect in mixtures of ferrofluids and colloidal suspensions of anisotropic, plate-shaped pigment particles (Fig.1), by exploring its dependence on the concentration of magnetic nanoparticles (MNP) and rheological properties of the carrier fluid.

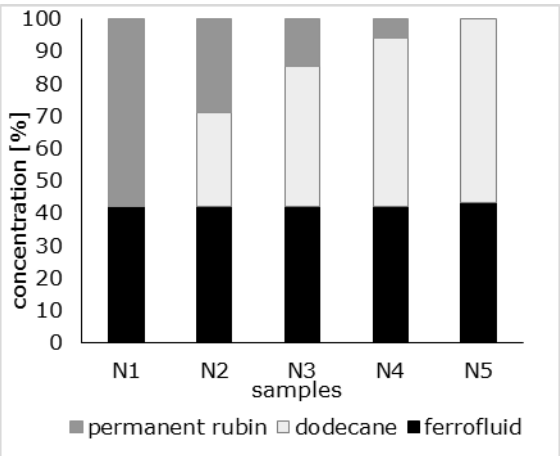

Fig. 1

The detailed description of the setup can be found in Ref. [3]: A spherical glass container completely filled with the suspension is fixed to a thin glass fiber and placed in a rotating magnetic field generated with two pairs of Helmholtz coils. The spherical container geometry provides a uniform demagnetization, and thus a homogeneous inner magnetic field. We determine the magnetic torque density T in dependence on the applied external magnetic induction B and frequency f from the torsion of the glass string (Fig.2).

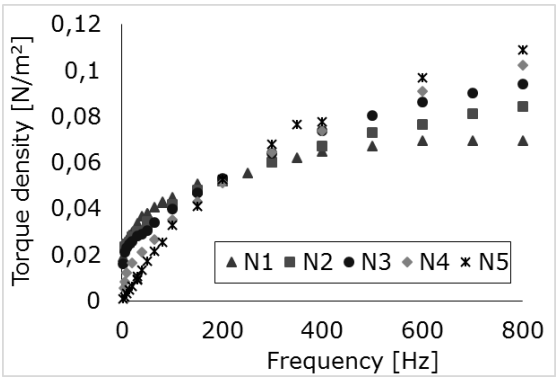

Fig. 2

We demonstrate that the frequency dependence of the torque strongly depends on the rheological character of the carrier fluid. A monotonic increase of the torque with increasing frequency is found in nearly Newtonian carriers with only small concentrations of the plate-shaped particles (N3-N5). A non-Newtonian character of the fluid (shear-thinning) in suspensions with high concentration of the pigment particles (N1-N2) results in a larger slope of the torque $T(f)$ at low frequencies. The saturation of $T(f)$ shifts to the lower frequency range in samples with higher pigment particles concentrations. This reflects an intricate interaction between the flow induced by the rotating MNPs and the plate-shaped pigments. A detailed theoreti-

cal study is in progress to understand this behavior.

Acknowledgments

Support by RFBR, Russia within research project No. 16-52-12035/16, and by DFG, Germany within Topical Program SPP 1681, Project STA 425/36, is acknowledged.

References

[1] A.F. Pshenichnikov, et al., *Magnetohydrodynamics*, **36** (2000) 275-281.

[2] C. Holm, J.-J.Weis, *Current Opinion in Colloid &Interface Science*, **10** (2005) 133.

[3] A.M. Storozhenko, et. al, *J. Magn. Magn. Materials*, **431** (2017) 66-69.

Concentration dependent studies of PEG-solutions with CFO nanoparticles as tracer particles

S. Webers[1], M. Hermes[2], J. Landers[1], A. M. Schmidt[2], H. Wende[1]

[1] *Fakultät für Physik, Center für Nanointegration Duisburg-Essen (CENIDE), Universität Duisburg-Essen, Lotharstraße 1,D- 47057 Duisburg*
[2] *Department Chemie, Institut für Physikalische Chemie, Universität zu Köln, Luxemburger Str. 116, D-50939*

Spherical and monodisperse cobalt ferrite nanoparticles in a polyethylene glycol (PEG) solution display decelerated Brownian motion due to the presence of the PEG chains. The nanoparticles are in the same size of the structural units of the matrix and as a result the relative length scale of the magnetic particles compared to the size of the structural units of the polymer gets relevant. Therefore, the particle mobility is influenced. Similar investigations were performed in a ring survey within the SPP1681 [see Abstract *Nanorheological Studies on the Scale-Dependent Particle-Matrix Interaction in Magnetically Functionalized Hybrid Materials*].

Here we proceed with the study of PEG with different concentrations in an aqueous solution above the critical mass fraction where the PEG chains form entanglements. 1 wt% of cobalt ferrite nanoparticles with a diameter of 17.3 nm are dispersed in x PEG300k solution with x=2.1, 5, 10…25 wt%. With increasing PEG concentration the solution changes, starting as a viscous sample it becomes more and more viscoelastic.

Results

For a pre-characterization cobalt ferrite nanoparticles in water were studied by magnetic AC susceptometry and low temperature in-field Mössbauer spectroscopy to get information about the hydrodynamic radius and the structural properties.

The Brownian rotation frequency of the particles in various PEG solutions was studied by magnetic AC susceptometry at different temperatures mainly from 250 K to 300 K.

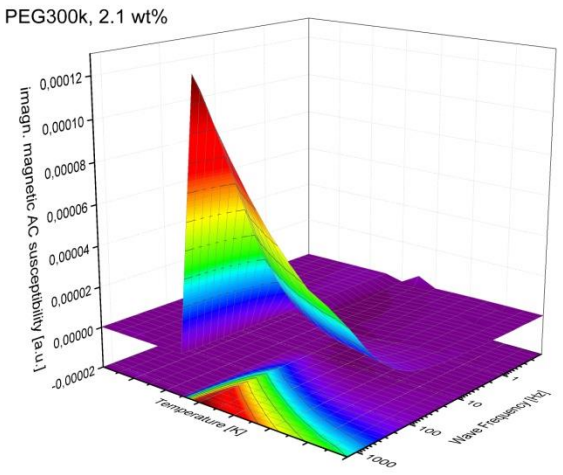

Figure 1: The imaginary part of the magnetic AC susceptibility as a function of temperature and frequency for PEG300k with 2.1 wt%.

With increasing temperature the Debye peak shifts to higher frequencies than expected [1].
Above a certain concentration of PEG a bimodal behavior was found: The real part shows a double step-like behavior and the imaginary part of the magnetic AC susceptibility exhibits two relaxation peaks as displayed in Figure 2.

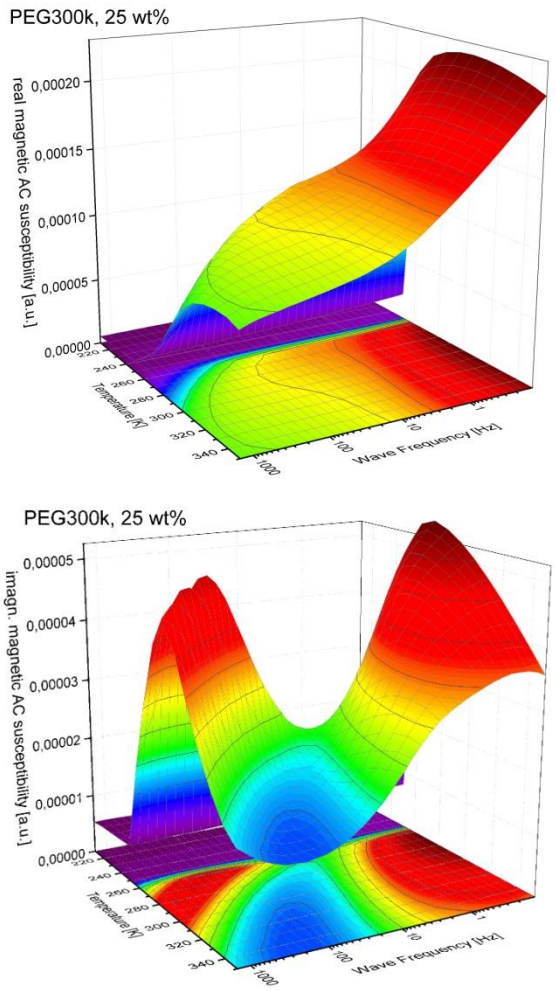

Figure 2: The real part and the imaginary part of the magnetic AC susceptibility as a function of temperature and frequency for PEG300k with 25 wt%.

Acknowledgments

We would like to thank U. von Hörsten for his expert technical assistance. This work is supported by the DFG-Priority Programme SPP1681 (WE2623/7-1).

References

[1] E. Roeben et al. *Colloid Polym Sci* **2014** 292:2013-2023

[2] J. Landers et al. *J. Phys. Chem. C* **2015** 119 (35) 20642-20646

Modeling and finite element simulation of macroporous ferrogels at finite strains

P. Gebhart[1], A. Attaran[1], T. Wallmersperger[1]

[1] *Institute of Solid Mechanics, Technische Universität Dresden, 01062 Dresden, Germany*

Introduction

Ferrogels are magneto-sensitive polymeric materials consisting of a chemically cross-linked network with embedded iron oxide particles, which can absorb and release water. Their fabrication was first reported in the late 90s [1, 2].
Due to their bio-compatibility, ferrogels have a great potential to be applied e.g. in biomedical engineering and medicine. Possible applications comprise remotely controlled drug delivery devices, sensors and actuators.
Ferrogels demonstrate large volumetric deformations up to 100% and more. But, due to their low porosities, the water transport through the gel is restricted.
In [3], macroporous ferrogels with interconnected pores in the micrometer range and porosities up to 80% were synthesized by freezing gels at different temperatures.
These kinds of ferrogels have the ability to respond to applied magnetic fields with fast and dramatic change in shape and volume.
In the present work, a fully coupled magneto-mechanical computational framework is developed in order to investigate the behavior of composite porous ferrogels in reaction to applied magnetic fields.

Modeling

Additionally to the modelling of ferrogels derived by Attaran et al. [5] based on the Theory of Porous Media, in the present work, a model for macroporous ferrogels at finite strains based on the macroscopic consolidation theory of Biot [4] is presented.
In the newly developed model, the authors provide a comprehensive modeling approach to investigate magnetic field induced large deformation and fluid transport in magnetically sensitive porous materials. In this model, unknowns for the mechanical displacement, for the fluid pore pressure and the magnetic scalar potential – in order to satisfy Ampère's law – are chosen as primary field variables.
The developed formulation is discretized by using the finite element method and is implemented in FEniCS [6].

Numerical Simulation

In order to demonstrate the capability of the derived formulation, a three-dimensional composite beam consisting of two different macroporous ferrogels is investigated. The analyzed beam, supported at its left end, has the following dimensions, see Figure 1: $\Omega_0 = \{\boldsymbol{X} \in \mathbb{R}^3 | \boldsymbol{X} \in [0, L] \times [0, B] \times [0, B]\}$ with $L = 40$ mm and $B = 8$ mm. The poromechanical behavior of the top (ferrogel 1) and bottom gel layer (ferrogel 2) is identical, but both ferrogel layers own different magneto-mechanical coupling properties.

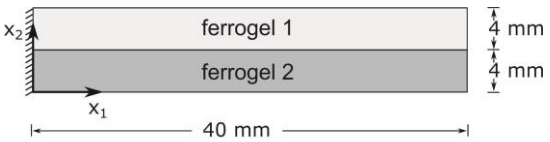

Figure 1: Geometry and mechanical boundary conditions of the composite beam.

A magnetic scalar potential of $\Phi_{\text{left}} = 0$ A at the left side and of $\Phi_{\text{right}} = 9600$ A t/t_0 at the right side – where $t_0 = 15$ s – is prescribed, resulting in a material magnetic

field strength of H_1 = 240 A/mm t/t_0. On the free surfaces a constant fluid pressure is prescribed.

Numerical Results

The total displacement $u_{\mathrm{tot}} = \sqrt{u_1^2 + u_2^2 + u_3^2}$ of the composite beam at t= 0 s, 5 s, 10 s and 15 s is depicted in Figure 2.
Due to the different magneto-mechanical coupling properties of both gel layers, the composite ferrogel bends downwards obtaining its maximal bending at t = 15 s.
In the present example the large-strain theory is essential to model the physical behavior of highly porous ferrogels.

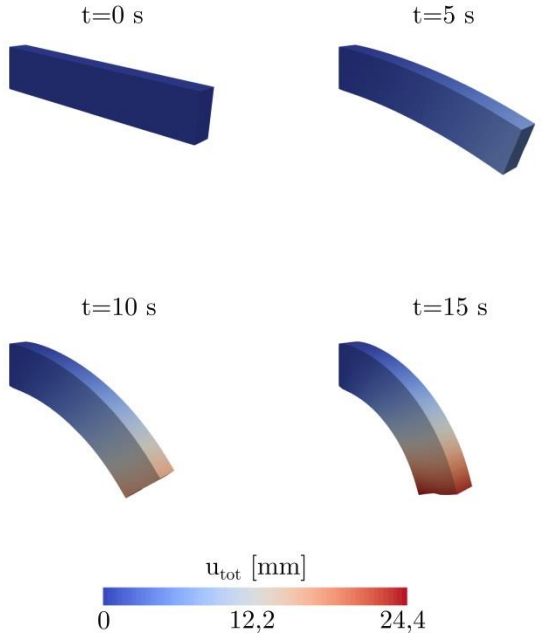

Figure 2: Total displacement u_{tot} of the composite beam at different times.

Conclusion

In the present work, a fully coupled magneto-mechanical computational framework has been developed and discretied by using the FEM in order to investigate the behavior of porous ferrogels in reaction to applied magnetic fields.
It has been shown that the proposed finite strain based framework is well suited for ferrogels which exhibit large deformations.

Acknowledgments

This research has been financially supported by the Deutsche Forschungsgemeinschaft in the framework of the Priority Programme SPP1681.

References

[1] M. Zrínyi, L. Barsi, and A. Büki, “Deformation of ferrogels induced by nonuniform magnetic fields”, The Journal of Chemical Physics, vol. 104, no. 21, p. 8750, 1996.

[2] M. Zrínyi, L. Barsi, and A. Büki, “Ferrogel: a new magneto-controlled elastic medium”, Polymer Gels and Networks, vol. 5, no. 5, pp. 415-427, 1997.

[3] X. Zhao, J. Kim, C. A. Cezar, N. Huebsch, K. Lee, K. Bouhadir, D. J. Mooney, “Active scaffolds for on-demand drug and cell delivery”, Proceedings of the National Academy of Sciences, vol. 108, no. 1, pp. 67-72, 2011.

[4] M. Biot, “Theory of Finite Deformations of Porous Solids”, Indiana University Mathematics Journal, vol. 21, 1972.

[5] A. Attaran, J. Brummund, T. Wallmersperger, “Modeling and finite element simulation of the magneto-mechanical behavior of ferrogels”, Journal of Magnetism and Magnetic Materials, vol. 431, pp. 188-191, 2017.

[6] A. Logg, K.A. Mardal, G. Wells, “Automated Solution of Differential Equations by the Finite Element Method: The FEniCS Book”, Lecture Notes in Computational Science and Engineering, Springer Berlin Heidelberg, 2012.

Equilibrium magnetization and magnetization relaxation of multi-core magnetic nanoparticles from computer simulations

P. Ilg[1]

[1] *School of Mathematical, Physical, and Computational Sciences, University of Reading, Reading, RG6 6AX, United Kingdom*

Motivation

More and more frequently, biomedical and biotechnical applications make use of multi-core magnetic nanoparticles [1, 2]. However, their magnetic properties are less well studied and less well understood than their single-core counterparts. Therefore, several ad-hoc assumptions are often needed in order to interpret experimental results. Previous simulation studies have either focused on the equilibrium magnetization [3] or disregarded the rotational diffusion of the cluster. Here, we present a series of computer simulations of multi-core magnetic nanoparticles were we investigate the effects of magnetic anisotropy and dipolar interactions on the equilibrium magnetization and magnetization relaxation, taking into account Néel relaxation, thermal fluctuations as well as Brownian rotation of the clusters.

Model System

We consider a system of N identical spherical magnetic nanoparticles that each posses a magnetic point dipole of strength m at their centers. The N nanoparticles together form a dense multi-core cluster that we generate by simulating the diffusion-limited cluster aggregation process. Once the cluster is formed, no translations or rotations of the individual nanoparticles relative to each other are allowed, so that we deal with a rigid cluster. Sufficiently large clusters, $N > 50$, are found to be dense and spherical to a good approximation.

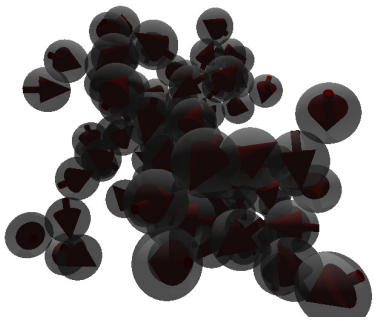

Figure 1: One realization of a multi-core cluster containing $N = 100$ nanoparticles. The magnetic moments of the nanoparticles are indicated by arrows.

The internal Néel relaxation of the magnetic moment of each nanoparticle we model by the stochastic Landau-Lifshitz-Gilbert equation, including the effect of an external magnetic field, the magnetic anisotropy as well as dipolar interactions between the nanoparticles [4].
In order to model rotational diffusion of the cluster as a whole that is suspended in a suitable carrier liquid, we include rotational Brownian motion of the cluster as a rigid body resulting from the angular momentum balance.

Equilibrium Magnetization

In order to study the equilibrium magnetization, we apply a static external field and numerically solve the stochastic Landau-Lifshitz-Gilbert equation together with the rotational Brownian motion of the whole cluster. We record the resulting total magnetic moment of the cluster parallel to the

field direction once the equilibrium state has been reached. Performing time averages as well as averaging over an ensemble of statistically independent clusters, we determine the mean magnetization of the cluster as a function of the strength of the external field. In agreement with earlier results [3], we find that for weak dipolar interactions, the equilibrium magnetization is rather well described by the Langevin function that corresponds to non-interacting particles. Upon increasing dipolar interaction strength, the magnetization is reduced compared to non-interacting case, mainly due to frustrated dipole-dipole interactions.

Magnetization Relaxation

Magnetization relaxation plays an important role in different applications. One example of particular relevance is magnetorelaxometry, where a strong magnetic field is applied initially and the magnetization is measured when the field is suddenly switched off [2]. We perform the corresponding simulations for our model system. The magnetization relaxation is found to proceed in a two-step fashion with a fast initial decay being followed by a long-time relaxation. For moderate dipolar interaction strengths, the latter can be approximated quite well by an exponential decay with rate given by the sum of the relaxation rates in the immobilized state and the Brownian rotation. For strong dipolar interactions, slow non-exponential relaxation is observed.

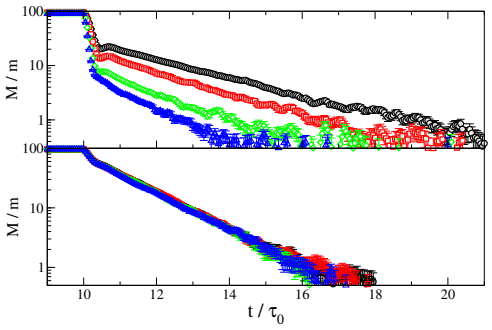

Figure 2: Magnetization relaxation of multi-core clusters each containing $N = 100$ nanoparticles after switching off a strong orienting field. Top panel: Brownian relaxation is slow compared to Néel (dipolar interaction strength increases from top to bottom), bottom panel: Brown and Néel relaxation times are comparable.

Acknowledgments

Valuable discussions with Dietmar Eberbeck and Stefan Wenk are gratefully acknowledged. PI acknowledges support from the German Science Foundation (DFG) within the priority program SPP1681 “Field controlled particle matrix interactions: synthesis multiscale modelling and application of magnetic hybrid materials” under grant no. IL 122/1-1 as well as an EU FP7–MC–CIG Grant No. 631233.

References

[1] M. Colombo, S. Carregal-Romero, M. F. Casula, L. Gutiérrez, M. P. Morales, I. B. Böhm, J. T. Heverhagen, D. Prosperi, and W. J. Parak, Chem. Soc. Rev. **41**, 4306 (2012).

[2] S. Dutz, J. H. Clement, D. Eberbeck, T. Gelbrich, R. Hergt, R. Müller, J. Wotschadlo, and M. Zeisberger, J. Magnet. Magnet. Mater. **321**, 1501 (2009).

[3] V. Schaller, G. Wahnström, A. Sanz-Velasco, P. Enoksson, and C. Johansson, J. Magnet. Magnet. Mater. **321**, 1400 (2009).

[4] W. T. Coffey, P. J. Cregg, and Y. P. Kalmykov, in *Advances in Chemical Physics*, edited by I. Prigogine and S. A. Rice (1993), pp. 263-464.

Concentration-dependent zero-field magnetic dynamic response of polydisperse ferrofluids

A.O. Ivanov[1], S.S. Kantorovich[12], E.A. Elfimova[1], V.S. Zverev[1], A.V. Lebedev[3], A.F. Pshenichnikov[3], P.J. Camp[4]

[1]*Ural Federal University, Lenin Av. 51, Ekaterinburg 620000, Russian Federation*
[2]*University of Vienna, Sensengasse 8, 1090 Vienna, Austria*
[3]*Institute of Continuous Media Mechanics of UB RAS, Ac. Korolev Street, 1, Perm 614013, Russian Federation*
[4]*School of Chemistry, University of Edinburgh, David Brewster Road, Edinburgh EH9 3FJ, Scotland*

In the present contribution we discussed three possible mechanisms, through which particle concentration can affect the dynamic zero-field magnetic response of ferrocolloids. These mechanisms are: (i) linear dependence of the initial dynamic susceptibility on ferroparticle number density, which however cancels out in case of measuring a phase shift; (ii) the growth in the collective relaxation time related to dipolar correlations intensified by the increase in concentration; (iii) the overall slowdown of the particle rotational diffusion due to the concentration growth of the system effective viscosity. We tried to separate the latter highly interweaved mechanisms by analyzing the combination of experimental data for samples obtained on dilution with fixed polydispersity, analytical model based on the perturbation theory and Brownian Dynamics simulations of monodisperse dipolar soft sphere fluids.

We discuss the experimental results obtained for seven ferrofluid samples with the same particle size distribution that differ only in concentration of magnetic material. The dynamic response to a weak linearly-polarized probing AC field is measured for each sample at five different temperatures from 232 K to 237 K. We investigate Cole-Cole diagrams and phase shifts in order to describe the impact of ferroparticle concentration on the initial magnetic susceptibility.

We showed that the strongest impact of the concentration, for the range of parameters studied here, comes through the growing effective viscosity. The latter leads to a complex transformation of the relaxation time spectra and gives rise to the qualitative changes in Cole-Cole diagrams and phase shifts at fixed temperature. In general, if one considers the distribution of relaxation times for a ferrofluid with a given polydispersity, its evolution is defined by the changes in temperature and concentration and related to the redistribution of particles between Ne´el and Brownian mechanisms. The relaxation time spectra, *per se*, as a function of temperature and concentration and its trans formations deserve a separate investigation, which we plan to perform in the future.

Acknowledgments

This research was supported by Russian Science Foundation, Grant No. 15-12-10003.

Modeling and Simulation of Hystereses in MREs filled with NdFeB Particles

K. A. Kalina[1], J. Brummund[1], P. Metsch[1], M. Kästner[1,2]

[1] *Chair of Computational and Experimental Solid Mechanics, TU Dresden, 01062 Dresden, Germany*
[2] *Dresden Center for Computational Materials Science (DCMS), TU Dresden, 01062 Dresden, Germany*

Introduction

Magnetorheological elastomers (MREs) are active composites consisting of magnetizable particles embedded into a polymer matrix. A specific class of these materials are MREs with magnetically hard fillers as NdFeB. These MREs have features as field dependent coercivity and remanent magnetization which are typical for conventional magnetically hard materials. However, as recently published by Linke et al. [1], measured magnetization loops of MREs based on a soft polymer matrix filled with NdFeB differ considerably from the loops of the bulk magnetic component or NdFeB particles fixed in a comparatively stiff matrix as epoxy resin.
To investigate the microstructural causes of the measured macroscopic behavior, a continuum-based modeling approach is presented in this contribution.

Modeling and Simulation

The analyzed MREs are described by a microscopic model, i. e. the heterogeneous microstructure consisting of magnetizable inclusions embedded into a polymer matrix is taken into account explicitly.
The constitutive models for the particles and the matrix are formulated separately. To describe the magnetic behavior of the embedded NdFeB particles, a phenomenological rate independent vector hysteresis model which is based on the work of Bergqvist [3] is used. Experimental data and the least square fit of the hysteresis model are depicted in Figure 1. The matrix material is assumed to be purely elastic.

In order to connect the macroscopic and the microscopic magnetic and mechanical quantities, a suitable computational homogenization scheme [4,5] is used. The governing equations of the coupled magneto-mechanical boundary value problem are solved within a nonlinear finite element (FE) formulation as presented in [2]. Since the local magnetic and mechanical fields are resolved explicitly, the presented approach accounts for particles close to each other.

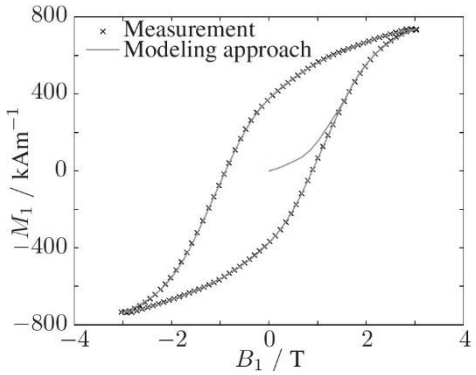

Figure 1: *Magnetization of NdFeB: Least-square fit of the major hysteresis loop.*

Results and Discussion

In order to investigate the behavior of the considered MRE, a homogenization with a representative volume element (RVE) containing monodisperse circular inclusions is examined. In the performed simulations, different random microstructures are evaluated statistically to ensure validity.
These simulations indicate a rotation of the particles within the soft polymer matrix material. Due to this effect the effective hystereses of the MRE are significantly smaller than the hystereses of pure NdFeB, see Figure 2. Furthermore, it has been observed that

the reversion of the effective magnetization occurs due to a combination of the particle rotation and internal domain conversion processes.
The discussed computational results are qualitatively in good agreement with the experiments presented in [1].

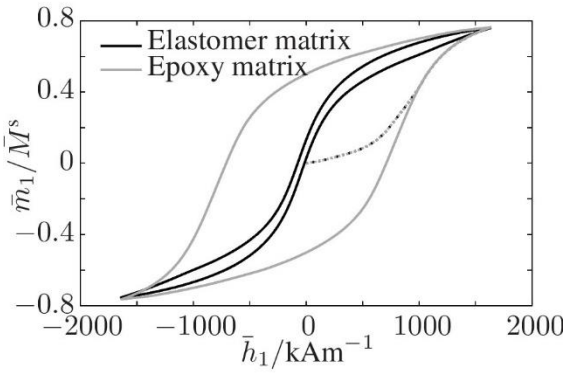

Figure 2: *Predicted effective macroscopic magnetic behavior: initial curves (dotted lines) and second hysteresis loops (solid lines) of an MRE with an elastomer matrix and a composite with an epoxy resin matrix.*

Acknowledgments

The authors would like to thank J. M. Linke, Dr. D. Yu. Borin and Prof. S. Odenbach for providing the experimental data. The present study is funded by the German Research Foundation (DFG), Priority Program 1681, grant KA 3309/2-2.

References

[1] J. M. Linke, D. Yu. Borin and S. Odenbach, RSC Adv., 6, 2016.

[2] K. A. Kalina, P. Metsch and M. Kästner, Int. J. Solids Struct., 102-103, 2016.

[3] A. Bergqvist, Physica B, 233, 1997.

[4] G. Chatzigeorgiou, A. Javili and P. Steinmann, Math. Mech. Solids, 19(2), 2012.

[5] P. Metsch, K. A. Kalina, C. Spieler and M. Kästner, Comput. Mat. Sci., 124, 2016.

Self-assembly of magnetic filament pairs

E. Novak[1], D. Rozhkov[1], E. Pyanzina[1], P. A. Sánchez[2], S. Kantorovich[1,2]

[1] *Ural Federal University, Ekaterinburg, Russia*
[2] *Computational Physics: Faculty of Physics, University of Vienna, Vienna, Austria*

Newly developed experimental techniques allowed combining magnetic particles and polymers and create magnetic filaments. These techniques make it possible to create certain aggregated structures with finely controllable mechanical, magnetic and other properties, using directed self-assembly at nano- and microlevel. We study the self-assembly of pairs of magnetic filaments made out of ferromagnetic nanoparticles with different chain conformations and particle shape. For spheres we use simple open chains, closed rings and branched structures with "X" and "Y" junctions - inspired by the recent findings on the low temperature self-assembly of dipolar hard spheres [1,2]. For ellipsoidal nanoparticles simple open chains and closed rings are used. To the best of our knowledge, there are no other configurations of ellipsoids in the ground state [3]. Using Langevin dynamics simulations, we investigate pairs of magnetic filaments with the same conformations (chain-chain, ring-ring, etc.), analysing in detail their self-assembly behaviour depending on the length of filaments, distance between filaments, particles shape and magnetic moment. On Fig. 1 the comparison between pairs of chains and rings are presented. One can see the different self-assembly. We investigate also average magnetic moment and magnetic energy of filaments pairs for different filament's conformations. We show that all system's parameters can dramatically change self-assembly of magnetic filaments pairs. All these results will form the basis for developing theoretical model for effective pair potential of two filaments and will be the first step for design of novel magnetocontrollable systems.

Figure 1: Pair of chains (top line) and rings (bottom line) for spheres and ellipsoids. The distance between middle particles is 3 and square of magnetic moment is 5.

Acknowledgments

This research has been partially supported by the Austrian Research Fund (FWF): START-Projekt Y 627-N27. We acknowledge research funding from the Ministry of Education and Science of the Russian Federation (Project No. 3.1438.2017/4.6) and RFBR No. 16-52-12008 (DFG Ref.No.: OD 18/24-1). The computational results presented here have been achieved using the Ural Federal University Cluster.

References

[1] Prokop'eva et al, JETP 113, 435 (2011).
[2] Kantorovich et al., PCCP 17, 25 (2015).

[3] Kantorovich et al, Soft Matter 9, 6594 (2013).

Coupled displacements and rotations of magnetic particles in elastic environments in bulk and near rigid substrates

M. Puljiz[1], S. Huang[2], G. K. Auernhammer[2], A. M. Menzel[1]

[1] *Institut für Theoretische Physik II: Weiche Materie, Heinrich-Heine-Universität Düsseldorf, D-40225 Düsseldorf, Germany*
[2] *Max Planck Institute for Polymer Research, Ackermannweg 10, 55128 Mainz, Germany*

Overview

In ferrofluids, magnetic colloidal particles are suspended in a carrier liquid. External magnetic field gradients impose forces on these particles, while the magnetic field itself may induce particle rotations. Similarly, induced magnetic interactions between the particles imply forces and possibly torques on the particles. Since the particles are suspended in the liquid and Reynolds numbers are small on the particle scale, the forces and torques are transmitted to the surrounding fluid. This sets the fluid into motion. Other suspended particles are exposed to these induced fluid flows. Resulting hydrodynamic interactions couple the particle motions, and an analytical theoretical approach is available to describe and quantify this situation [1].
Recently, we have transferred this approach to the case of magnetic gels and elastomers. There, the particles are embedded in a soft elastic, i.e., reversibly deformable environment [2]. In this case, magnetically induced forces or torques on the particles are transmitted to the surrounding elastic matrix. The consequence are long-ranged elastic distortions of the environment. Other embedded particles are exposed to these distortions, which leads to coupled displacements and rotations of the inclusions.
We have explicitly analytically calculated the resulting coupled displacements and rotations for linearly elastic deformations. The role of the elastic matrix is implicitly included in our resulting expressions. It does not need to be calculated separately, e.g., by corresponding simulations. Compressibility of the elastic matrix is readily taken into account.

Coupled displacements under imposed forces

As a first step, we only considered magnetic forces acting on the embedded particles [3]. For simplicity, the elastic matrix is considered as homogeneous, isotropic, and infinitely extended, while the particles are rigid, spherical, and of identical size.
It turns out that the rigidity of the particles leads to effective reflections of the deformation fields induced by other particles. That is, a first particle distorts the elastic matrix. A second particle is exposed to the deformation field and would be deformed itself, if it were soft. However, due to its rigidity, the particle counteracts, which leads to a secondary deformation field in the elastic matrix. The first particle is now itself subject to this secondary deformation field. Also higher-body interactions result in this way. Our approach is an expansion in the inverse separation distance between the particles. The order of this expansion determines, if and how many back-and-forth reflections are taken into account.
We have compared our theoretical approach with experimental data [3]. They were obtained by embedding paramagnetic nickel particles into soft elastic polymeric gel matrices. Applying and rotating an external magnetic field induces and tunes magnetic interactions between the particles. Experimental data points and theoretical results on the resulting coupled particle displacements show very good agreement.

Moreover, in a simplified situation of point-like particles and centrally symmetric particle displacements, we have mapped our description onto an effective dipole-spring model. It serves as an input for a statistical description of magnetic gels [4].

Coupled displacements and rotations under additionally imposed torques

In a second step, we have included additional torques acting on the particles [5]. We have then explicitly calculated the resulting coupled displacements and rotations of the inclusions. In all these calculations, we have assumed no-slip boundary conditions for the elastic matrix on the particle surfaces.
For spherical particles exposed to magnetic fields, torques can arise, if the crystalline structure of the particle material leads to magnetic anisotropy. As an example, we have considered uniaxial magnetic anisotropy in an idealized Stoner-Wohlfarth model. The effect of the additional torques on the resulting particle displacements and rotations were evaluated for simplified example situations.

Influence of a rigid wall

Finally, we have considered the situation close to a rigid wall, e.g., the substrate of a magnetic gel or elastomer [6]. The coupled displacements of magnetically interacting point-like particles were addressed. Results obtained for both, no-slip and free-slip surface conditions on the substrate, were compared to each other and to the bulk behavior. No-slip surface conditions often occur in experimental situations when the polymeric matrix adsorbs to the substrate. Free-slip conditions could possibly be realized by lubrication.
Our results suggest that vanishing slip of the elastic matrix on the substrate surface usually hinders the displacements of the particles within the matrix. In contrast to that, free-slip surfaces can in some situations support the particle displacements when compared to the bulk behavior. We always found larger displacements for free-slip conditions. These results suggest free-slip surface conditions for certain applications, e.g., to achieve larger deformation amplitudes when magnetic gels are used as soft actuators.
Apart from that, we identified a qualitatively inverting effect of the rigid substrate under certain conditions. If magnetic particles attract each other but are additionally subject to an external magnetic field gradient, their mutual attraction can sometimes be reversed into effective repulsion (and vice versa).

Conclusions

In summary, we have derived explicit analytical expressions to calculate the coupled displacements and rotations of magnetic particles embedded in a linearly elastic matrix in bulk and near a rigid substrate. In the future, the formalism shall be used to characterize analytically and quantitatively different practical situations of applications of magnetic gels and elastomers. Yet, we wish to stress that our formalism is not restricted to the situation of magnetic interactions, nor to the polymeric nature of the surrounding matrix. For instance, also certain situations concerning soft biological tissue and living cells can be described analogously.

Acknowledgments

We thank the DFG for support of our work through the SPP 1681.

References

[1] J. K. G. Dhont, *An Introduction to Dynamics of Colloids* (Elsevier, Amsterdam, 1996).
[2] A. M. Menzel, Phys. Rep. **554**, 1 (2015).
[3] M. Puljiz, S. Huang, G. K. Auernhammer, and A. M. Menzel, Phys. Rev. Lett. **117**, 238003 (2016).
[4] P. Cremer, M. Heinen, A. M. Menzel, and H. Löwen, arXiv preprint arXiv:1704.00231 (2017).
[5] M. Puljiz and A. M. Menzel, Phys. Rev. E **95**, 053002 (2017).
[6] A. M. Menzel, Soft Matter **13**, 3373 (2017).

Towards the simulation of dynamic processes in magnetic gels

N. Roth[1], R. Weeber[1], C. Holm[1]

[1] *Institute for Computational Physics, Universität Stuttgart*

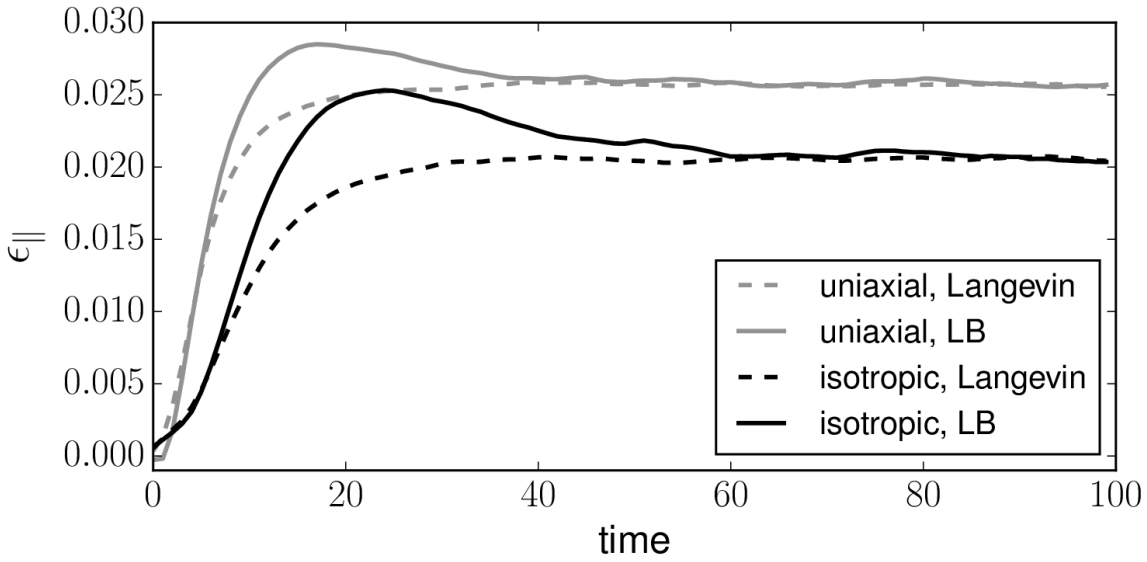

Figure 1: Relaxation of different gel samples, namely isotropic and uniaxial (cross-linked in presence of a magnetic field), when switching on an external magnetic field. The deformation of the gel shape parallel to its longest axis is shown. Dashed lines indicate the relaxation process without hydrodynamic interactions. When lattice Boltzmann hydrodynamics are taken into account, an overshoot due to inertia effects can be observed (solid lines).

We use a particle-based molecular dynamics approach for simulating the magnetic, deformational and elastic response for magnetic gels. So far our focus was gaining an understanding of the deformation mechanisms in ferrogels under the influence of a DC magnetic field. Both, deformations driven by the dipole-dipole interaction and by the nanoparticle-polymer coupling were studied [1, 2, 3, 4], as well as the influence of the particle and network structures [5]. Many experiments are, however, conducted using time-dependent stimuli, in particular AC magnetic fields. Furthermore, oscillatory deformation responses may be of interest for actuation and transport applications.
Hence, in this contribution, we report initial results for the relaxation processes in a magnetic gel. These are studied by applying a jump in the external magnetic field and observing the time-dependent magnetic and deformation responses.
We show that hydrodynamic interactions have a significant influence on the deformational relaxation time. Also, an overshoot and subsequent secondary relaxation behavior can be observed, which we attribute to inertia effects.
Additionally, first results for the magnetic and deformational AC susceptibility will be presented.

Acknowledgments

The authors are grateful for funding by the DFG through the SPP 1681.

References

[1] Weeber, Rudolf and Kantorovich, Sofia and Holm, Christian. “Deformation

mechanisms in 2D magnetic gels studied by computer simulations". Soft Matter 8(9923–9932), 2012.

[2] Weeber, Rudolf and Kantorovich, Sofia and Holm, Christian. "Ferrogels cross-linked by magnetic nanoparticles – Deformation mechanisms in two and three dimensions studied by means of computer simulations". Journal of Magnetism and Magnetic Materials 383(262–266), 2015.

[3] Weeber, Rudolf and Kantorovich, Sofia and Holm, Christian. "Ferrogels cross-linked by magnetic particles: Field-driven deformation and elasticity studied using computer simulations". Journal of Chemical Physics 143(154901), 2015.

[4] Pessot, Giorgio and Weeber, Rudolf and Holm, Christian and Löwen, Hartmut and Menzel, Andreas M. "Towards a scale-bridging description of ferrogels and magnetic elastomers". Journal of Physics: Condensed Matter 27(325105), 2015.

[5] Rudolf Weeber and Christian Holm. "Interplay between particle microstructure, network topology and sample shape in magnetic gels – A molecular dynamics simulation study". arXiv preprint 1704.06578, 2017.

Computer modeling of bidisperse hybrid magnetic elastomers

P. A. Sánchez[1], S. S. Kantorovich[1,2], O. V. Stolbov[3], Y. L. Raikher[3]

[1] *University of Vienna, Vienna, Austria*
[2] *Ural Federal University, Ekaterimburg, Russia*
[3] *Institute of Continuous Media Mechanics, Ural Division of RAS, Perm, Russia*

Among the most recent strategies developed to improve the properties of soft magnetic elastomers, the mixture of different types of magnetic particles filling the polymer matrix is one of the most promising solutions. In recent experimental studies, a new family of magnetic elastomers containing magnetically soft nanoparticles and magnetically hard microparticles was synthesized for the first time [1-2]. Typically, in such hybrid elastomers, one keeps a relatively low volume fraction of magnetically hard colloids—usually ferromagnetic particles with diameters of 3-5 μm—and a high volume fraction of magnetizable particles—in most cases paramagnetic particles with a diameter of around 10nm.

An accurate theoretical characterization of these materials and their magnetic response requires to take into account the complex interplay between the two types of magnetic particles and the external fields, as well as their magneto-elastic coupling with the polymer matrix.

Here, we present a simple bead-spring model of such a hybrid soft magnetic elastomer materials intended to capture the essential interactions in the system. The model takes into account the magnetization of the magnetically soft particles by the presence of the magnetically hard ones, as well as the effect of external magnetic fields on both types of magnetic particles. With this model we performed extensive computer simulations focused on one "elementary cell" of the elastomer microstructure. This cell consists of a central fixed particle with a permanent dipole moment, representing one magnetically hard colloid. This colloid is surrounded by a corona of polymers grafted on its surface, that include the embedded magnetically soft beads. We analyze the magnetic response of this system with the aim to connect our results to experimental results and analytical models based on continuum approaches.

Acknowledgments

Research supported by the DFG grant Ref. No. OD 18/24-1 and FWF START-Projekt Y 627-N27. Computer simulations were performed at the Vienna Scientific Cluster.

References

[1] Stepanov G V, Borin D Y, Raikher Y L, Melenev P V and Perov N S, J. Phys.: Condens. Matter **20**, 204121 (2008).
[2] J. Linke, D. Y. Borin and S. Odenbach, RSC Adv. **6**, 100407 (2016).
[3] M.V. Vaganov, J. Linke, S. Odenbach, Yu.L. Raikher, *J. Mag. Mag. Mat.* 431, 130 (2017).

Minimal modeling of initial inelastic deformations in composite magnetic elastomers

P. A. Sánchez[1], A. Dobroserdova[2], S. S. Kantorovich[1,2], T. Gundermann[3], J. Linke[3], S. Odenbach[3]

[1] *University of Vienna, 1090 Vienna, Austria*
[2] *Ural Federal University, Ekaterimburg, Russia*
[3] *Tesnische Universität Dresden, Dresden, Germany*

In this contribution we report on our recent progress on the theoretical modeling of a novel type of composite magnetic elastomers, created by embedding a mixture of magnetically soft and hard particles into a polymer matrix [1]. In particular, we focus on the characterization of the unconventional magnetic response exhibited by freshly synthesized samples of these materials: for a broad range of synthesis parameters, it has been observed that their initial magnetization loop, obtained when exposed for the first time to external fields, is significantly different from the ones obtained in subsequent measurements. The two main potential reasons suggested to explain this behavior are the interplay between the magnetically soft and hard particles and/or the existence of inelastic deformations in the polymer matrix as a consequence the field-induced rearrangements of the particles. Here, we study if the latter mechanism is enough to produce the experimental behavior. With this goal, we performed extensive computer simulations with a minimal model of the elastomer microstructure that takes into account the mechanical coupling between the magnetic particles and the polymer matrix. This coupling is modeled as elastic rotational and/or translational constrains on the movement of the particles. Our simulations show that the introduction of irreversible relaxations on these constrains during the first magnetization loop reproduces qualitatively the experimental differences between initial and later loops.

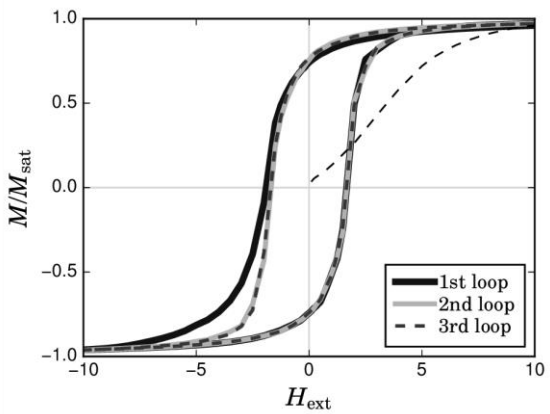

Fig. 1. Example of a sequence of three consecutive magnetization loops obtained for our minimal model of magnetic elastomer with rotational and translational constrains, including irreversible relaxations during the first loop.

Acknowledgments

Research supported by the DFG grant Ref. No. OD 18/24-1 and FWF START-Projekt Y 627-N27. Computer simulations were performed at the Vienna Scientific Cluster and the Ural Federal University computing cluster.

References

[1] J. Linke, D. Y. Borin and S. Odenbach, RSC Adv. **6**, 100407 (2016).

To the theory of shear elasticity of magnetic gels

A. Zubarev, L. Iskakova

Department of Mathematical Physics, Ural Federal University, Ekaterinburg, Russia

One of the interesting and practically important features of magnetic gels is their ability to vary rheological properties and behavior under the action of an external magnetic field. Physical explanation of these phenomena and development of methods of their quantitative description require detailed study of origination of the magentorheological effect on the level of the particles of the magnetic filler. In its turn, solution of this problem requires account of cooperative effects of multiparticle interactions, the particles displacement in the host polymer matrix and large deformations of the matrix as well. In the general case, these problems cannot be solved strictly. Very often they are considered by using heuristic models and simplifications, whose accuracy and even qualitative adequacy a 'priory are unknown.

To achieve deep insight in this problem, it is necessary to develop of mathematically regular, free from any intuitive constructions, methods of analysis of the studied phenomena. One needs to note that the payment for the mathematical regularity is restriction of the models applicability by certain limiting situations (usually - small concentrations of the particles and small deformations of the host matrix). Nevertheless, we believe that the results, obtained with the help of the mathematically strict approaches, can be a reliable basement for development of semi-empirical and intuitive methods of description of the practically interesting highly concentrated and severely deformed composites.

We present results of theoretical study of shear properties of magnetic gels with random and isotropic distribution of non-Brownian magnetic particles in a host elastic matrix. The system undergoes deformation of a simple shear; a uniform magnetic field is applied in the direction of gradient of the sample deformation.

Analysis shows that in the shear deformed composite the total macroscopic shear modulus G can be presented as the sum $G=G_{el}+G_m$. Here G_{el} is the modulus of the composite with the solid inclusions. This term can be estimated by using the known results of classical theory of composite materials (see, for example, [1]). The second term G_m reflects effect of magnetic field and can be presented in the form:

$G_m=0.5\mu_0\varphi M_\perp H/\gamma$

Here μ_0 is the vacuum magnetic permeability; φ is volume concentration of the particles; $M_\perp$ is the component of the sample magnetization, perpendicular to the field H in the sample; γ is the macroscopic shear of the gel. The main problem is to determine the component $M_\perp$.

Three kinds of the composites have been considered.

Ferrogels with magnetically hard spherical particles. We have studied a system of identical spheres with permanent magnetic moment each, randomly distributed in an elastic matrix. The initial orientation of the moments is supposed isotropic. Magnetic moment is "frozen" in the particle body and rotates with the particle. The analysis is based on the equation of rotation of the single particle in an elastic media under the action of an applied field and macroscopic shear of the sample. The component $M_\perp$ is determined from the balance between the magnetic and elastic torques, acting on the particles.

Our results show that magnetic field *increases* the total modulus G (i.e. $G_m>0$); in

the lowest approximation with respect to the particle concentration $G_m \sim \varphi$.

Composites with non spherical magnetizable particles. A system of ellipsoidal, linearly magnetizable particles has been considered. Initial distribution of orientations of the ellipsoids axes is supposed isotropic. Determination of $M_\perp$ again is based on the analysis of the particle rotation under the action field and elastic torques in the sheared composite. The results demonstrate that G_m is positive, i.e. magnetic field *enhances* the composite rigidity; in the low concentrated systems $G_m \sim \varphi$, effect of the particle shape on the total modulus G is estimated.

Materials with spherical linearly magnetizable spheres. In these systems the perpendicular component $M_\perp$ cannot appear in the single-particle approximation; the magnetic interparticle interactions must be taken into account. Analysis shows that macroscopic shear changes the function of relative disposition of the particles, making it asymmetric. Due to this fact, the mutual magnetization of the particles leads to appearance of $M_\perp$. We have studied this effect in the regular pair approximations, taking into account magnetic and elastic (through the matrix deformations) interactions between the particles. The last is considered by using the Batchelor results [2] for the particles hydrodynamic interaction in suspensions as well as the mathematical identity of the hydrodynamic equations and equations of deformations of elastic media [1]. The particles spatial rearrangements, induced by their magnetic interaction, are taken into account. This rearrangement leads to the uniaxial anisotropy of the non sheared composite.

Our results show that, if the field induced structural anisotropy is insignificant, then the modulus G_m is negative, i.e. magnetic field *reduses* the total elastic modulus G. If the induced anisotropy is strong enough, the opposite effect can take place - magnetic field will *increase* the modulus G (G_m will be positive). It should be noted that in the real ferrogels with magnetizable particles effect of the interaction between them can be masked by non spherical shape, at least, part of the particles, as well as by the anisotropic agglomerates, which very often appear in the liquid and polymer magnetic systems on the stage of their synthesis. Both these factors increase the macroscopic shear modulus G. This conclusion must be taken into account at interpretation of experimental results on the magnetomechanic effects in the composite materials.

We have estimated effect of the shear γ on the modulus G and have shown that G always decreases with γ. In the lowest approximation with respect to the particles concentration, $G_m \sim \varphi^2$.

References

[1] R.Cristensen, Mechanics of Composite Materials, New York: Wiley, 1979

[2] G.K.Batchelor, J.T.Green, *J.Fluid Mechanics*, 1972, 56 (3), 4101

.

Mag-Guider: A permanent magnet system to guide and image super-paramagnetic nanoparticles

O. Baun, P. Blümler

Institute of Physics, University Mainz, 55099 Mainz, Germany

A new concept of using permanent magnet systems for guiding superparamagnetic nano-particles (SPP) on arbitrary trajectories over a large volume is presented [1]. The same instrument can also be used for magnetic resonance imaging (MRI) [2] using the inherent contrast of the SPP.
The basic idea is to use one magnet system which provides a strong, homogeneous, dipolar magnetic field (B_0) to magnetize and orient the particles, and a second constantly graded ($dB/dr = G$), quadrupolar field, superimposed on the first, to generate a force on the oriented particles. In this configuration the motion of the particles is driven predominantly by the component of the gradient field which is parallel to the direction of the homogeneous field. As a result, particles are guided with constant force and in a single direction over the entire volume. The direction is simply adjusted by varying the angle between quadrupole and dipole. Since a single gradient is impossible due to Gauß' law, the other gradient component of the quadrupole determines the angular deviation of the force, which is negligible for $B_0 >> Gr$.

A possible realization of this idea is a coaxial arrangement of two Halbach cylinders [3,4]. A dipole to evenly magnetize and orient the particles, and a quadrupole to generate the magnetic force, F_{mag}, on SPPs.

$$\vec{F}_{\mathrm{mag}}(x,y) = \frac{m\,G}{\Xi}\begin{pmatrix} Gx + B_0 \sin 2\alpha \\ Gy + B_0 \cos 2\alpha \end{pmatrix}$$

$$\Xi \equiv \sqrt{B_0^2 + G^2\left(x^2 + y^2\right) + 2B_0 G\left(x \sin 2\alpha + y \cos 2\alpha\right)}$$

where m is the magnetic moment of the SPP and α is the angle between dipole and quadrupole (see Fig. 1).

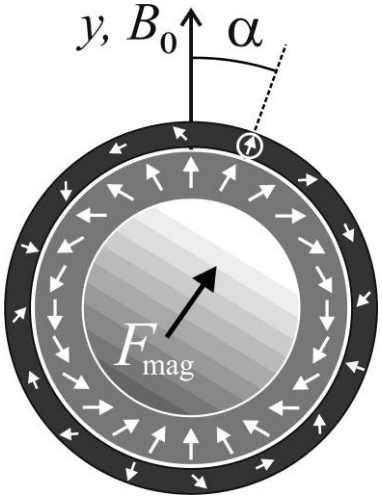

Fig. 1: Schematic drawing of an ideal Halbach dipole (inner ring in lighter gray, white arrows indicate the magnetization of the permanent magnetic material) surrounded by an ideal Halbach quadrupole (darker gray). Since Halbach mutipols have no external (stray)field, the quadrupole can be rotated force free around the dipole by an angle α. The resulting magnetic force points then along 2α.

A simple prototype was constructed to demonstrate the principle in two dimensions on several nano-particles, which were moved along a rough square by manual adjustment of the force angle (see Fig 2).

The observed velocities of SPPs in this prototype were always several orders of magnitude higher than the theoretically expected value. This discrepancy is attributed to the observed formation of long particle chains –like iron filings– as a result of their polarization by the homogeneous field. The magnetic moment of such a chain is then the combination of that of its constituents, while its hydrodynamic radius stays low [5].

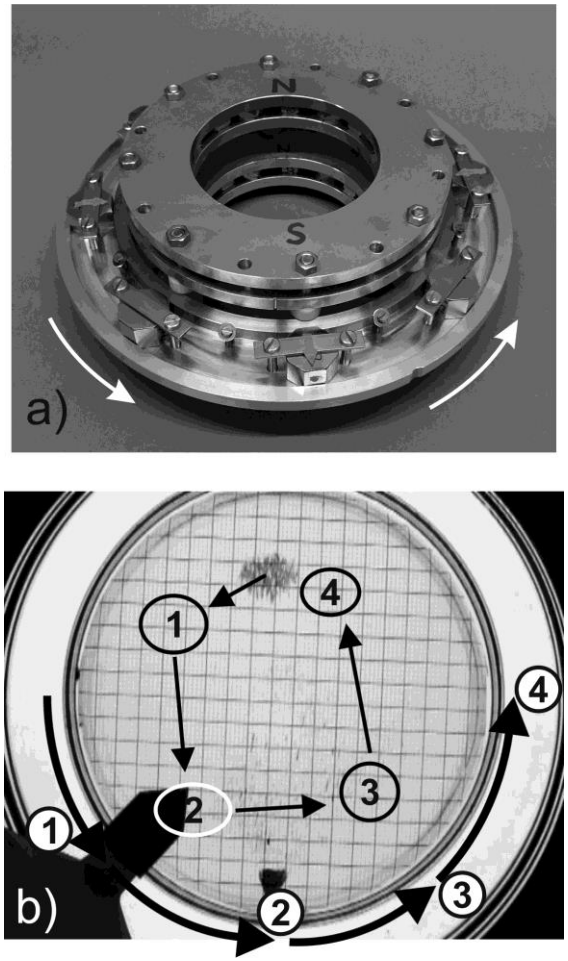

Fig. 2: a) Photograph of a simple prototype. The inner dipole is made from 2 layers of 16 magnets each. The outer quadrupole is made from 8 of the same FeNdB-magnets and can be rotated without a noticeable force. This instrument generated B_0 = 0.1 T and $G \approx 0.2$ T/m. It has an opening of 28 cm in diameter and weights 9.5 kg.
b) Some 30 µm size SPP (dark cloud on top) are moved in a rough square by manual rotation of the quadrupole in four steps of $\alpha = 45°$. The particles wander with a speed of ca. 5 mm/s to positions marked by the numbered circles. (taken from a movie).

A complete system will consist of another quadrupole (third cylinder) to additionally enable scaling of the gradient/force strength by another rotation. In this configuration the device could then also be used as a simple MRI machine to image the particles between movement intervals.
Finally, a concept is proposed by which superparamagnetic particles can be guided in three-dimensional space. In case that SPP agglomeration shall be prevented after guided transport (e.g. in magnetic drug targeting) yet another dipole ring can complete the design so that ideally all magnetic fields can be removed once the SPP reached their destination.

Acknowledgments

The DFG funded Collaborative Research Center *"Nanodimensional polymer therapeutics for tumor therapy"* – SFB 1066 has to be accredited for financial support.

References

[1] O. Baun, P. Blümler, J. Magn. Magn. Mater. (2017) in press. DOI: 10.1016/ j.jmmm.2017.05.001
[2] P. Blümler, Concepts Magn. Reson. B 46 (2016) 41-48. DOI: 10.1002/cmr.b. 21320.
[3] K. Halbach, Nucl. Instr. Methods, 169 (1980) 1-10. DOI: 10.1016/ 0029-554X(80)90094-4.
[4] P. Blümler, F. Casanova, in: M. Johns, et al. Mobile NMR and MRI: Developments and Applications, RSC 2015 DOI: 10.1039/978178 2628095-00133
[5] O. Baun et al. Poster at this conference

Investigations of magneto-sensitive elastomers in context of actuator and sensor applications

T.I. Becker[1], J. Chavez Vega[1], V. Böhm[1], Yu.L. Raikher[2], O.V. Stolbov[2], S. Dutz[3], M. Zhou[4], S. Odenbach[5], K. Zimmermann[1]

[1] *Technische Universität Ilmenau, Technical Mechanics Group, 98684 Ilmenau, Germany*
[2] *Institute of Continuous Media Mechanics, Ural Branch of Russian Academy of Sciences, 614013 Perm, Russia*
[3] *Technische Universität Ilmenau, Institute of Biomedical Engineering & Informatics, 98684 Ilmenau, Germany*
[4] *Friedrich Schiller University of Jena, Institute of Organic Chemistry & Macromolecular Chemistry, 07743 Jena, Germany*
[5] *Technische Universität Dresden, Institute of Fluid Mechanics, 01069 Dresden, Germany*

The main research direction in context of realisation of actuator and sensor systems using magneto-sensitive elastomers (MSEs) focuses on the change of their mechanical properties by applying a static magnetic field. This change corresponds to the interactions between embedded magnetic particles and the elastomer matrix in the microscopic scale. Especially samples with a complex filler, made of large magnetically hard grains and small magnetically soft particles, reveal sophisticated properties.

This work reports investigations of the free vibrational behaviour displayed by MSE cantilevers with magnetically soft particles in the presence of a uniform magnetic field. Such construction may serve as a core element for fabricating sensors of several kinds, e.g., acceleration, force and pressure sensors. The concept to design a system incorporating an MSE sensor element to detect mechanical stimuli of the environment is presented in [1]. According to it, an MSE cantilever with a complex filler shows bending vibrations induced by an external excitation of its base. This response is identified by magnetic field measurements. The key point is that an adaptivity of the MSE sensor element can be realised by means of an external magnetic field, which causes the change of the material properties, above all the mechanical compliance.

An alternative possibility for adjusting the mechanical properties is to use thermoplastic elastomers or compounds consisting of elastomer and thermoplastic as material matrix, instead of just an elastomer. In this case, the change of properties can be mainly affected by variation of properties of the thermoplastic component due to a temperature change in an alternating magnetic field [2]. Hence, the magnetic particles of these MSE materials are used primarily to induce indirectly the resulting properties change in contrast to MSEs based on elastomer matrix. Thus, the technical use of such smart materials is promising due to the possible realisation of their properties changes.

Dynamical properties of MSE cantilevers

The description of the influence of an external magnetic field on the material properties is essential for the development of sensor systems with variable sensitivity ranges. One of the interesting aspects is the eigenfrequency dependence of MSE cantilevers on a magnetic field. Therefore, free vibrational behaviour displayed by a macro MSE beam with one end fixed and the other free in the presence of a uniform magnetic field is investigated experimentally. Isotropic MSE beams of three lengths (40, 60, and 80 mm) and four concentrations (0, 10, 20, and 30 vol%) of magnetically soft particles of carbonyl iron powder (CIP, Ø 6 μm) are used in tests. For each set of these parameters, samples with various rectangular cross-sections are prepared. Based on the deflection measurements, it is found that for the

samples containing CIP, the eigenfrequency dependencies are quadratically increasing with the field strength.
In order to describe this microscale induced system behaviour, the theoretical model is developed. It extends the classical vibrational dynamics of thin rods to allow for the ponderomotive torque induced by magneto-mechanical interactions experienced by an MSE beam in a uniform magnetic field. The expression for this torque is derived from the approximation of the prismatic beam by a magnetisable ellipsoid with the same dimensions of the principle axes. Two adjustable parameters that characterise the geometric configuration of the beam's cross-section and its magnetic material properties are introduced.
The model is applied for interpretation of the measured frequency dependencies. As it turned out from the calculations, the values of these parameters are "universally" valid, i.e., they provide good agreement (percent error below 5.6%) between the theoretical eigenfrequency dependencies with the experimental results for all used MSE beams. Thus, the developed magneto-mechanical model can be reliably used to predict the amplitude-frequency characteristics of a vibrating sensor element made of an MSE with magnetically soft particles.

MSEs with elastomer-thermoplastic matrix

The grade of mechanical properties change of MSE materials based on an elastomer-thermoplastic matrix is essentially dependent on the material design as well as the frequency and magnitude of an applied magnetic field. As a first step of investigations, basic considerations for finding suitable material composition are made. Type of magnetic particles, their concentration and parameters of the magnetic field are varied. Due to the specific activating principle of these materials, the focus of investigations is on the possibility of the temperature change. It is found that by using CIP of 5 wt% in an elastomer matrix under an alternating magnetic field of H_{max} = 20 kA/m, f = 400 kHz (sample volume of 1 cm^3) within 20 s, a temperature change of 30 °C can be induced.
For applications to be developed, small temperature changes of the MSE in comparison to room temperature are preferred. Therefore, thermoplastic materials with low melting points are selected for the preparation of the MSE matrix. First investigations with Dextran Myristic Ester particles (Ø 1 mm, melting point of 42 °C, 0.5…10 wt%) show that a stiffness reduction up to 30% is possible (temperature range is 20…55 °C).
Based on these promising results, upcoming investigations will focus on more detailed experimental considerations and material study regarding the concentration of the MSE components. These investigations will enable the further realisation of sensor and actuator systems based on MSEs with variable mechanical properties.

Acknowledgments

This work is supported by the Deutsche Forschungsgemeinschaft (DFG) and the Russian Foundation for Basic Research (RFBR) within PAK 907, projects PO 2013/1-1 and 16-51-12001, as well as by the DFG priority programme SPP 1681 under the projects DU 1293/4-2, HE 2054/14-1, MU 2382/4-1, OD 18/22-2, and ZI 540/17-2.

References

[1] Volkova T.I., Böhm V., Kaufhold T., Popp J., Becker F., Borin D.Yu., Stepanov G.V., Zimmermann K. Motion behaviour of magneto-sensitive elastomers controlled by an external magnetic field for sensor applications. *J. Magn. Magn. Mater.* **431** (2017) 262-265.

[2] Zimmermann K., Böhm V., Kaufhold T., Chavez Vega J., Becker T., Odenbach S., Gundermann T., Schilling M., Martens M. Investigations and simulations on the mechanical behaviour of magneto-sensitive elastomers in context with soft robotic gripper applications. Int. Scient. J. of IFToMM *Problems of Mechanics* **65**, 4 (2016) 13-25.

Hydrostatic bearing with MR texturing

Stefan G.E. Lampaert[1], Ron A.J. van Ostayen[1]

[1] *Delft University of Technology, Mekelweg 2, 2628 CD Delft, The Netherlands*

Introduction

All systems that contain moving components, have some sort of lubrication involved. One of the biggest problems seen here is wear, which makes lubrication a big issue in industry. The wear is generally caused by contact between the bearing faces resulting in material detaching from the surfaces. In general, it can be said that if you can guarantee that the surfaces are not touching under all operating conditions, you can guarantee that there is no wear in your bearing under all operating conditions.

The scope of this research is on the bearing of rotating equipment, where the failure of these bearings is mainly caused by wear that causes blocking of the rotating shaft. Which consequently results in system failure. This is especially troublesome for rotating equipment in failure sensitive systems like for example emergency power system, chemical plants and nuclear power plants.

The goal is to develop a bearing system that is contactless for all operating conditions. All current solutions, that can be characterized as contactless, are hydrodynamic (HD) bearings (Figure 1) and hydrostatic (HS) bearings (Figure 2). The drawback of the HD bearing is that the system does not have any load carrying capacity at low speeds. A HS bearing does have load carrying capacity for all speeds but it always needs a failure sensitive high pressure supply pump for proper operation.

In this research the properties of MR fluid are used to combine the advantages of both the HD and HS bearing in one design: a bearing concept that is contactless for all operating speeds and relies on pump only at low speeds (Figure 3). The bearing works as a HS bearing at low speeds and a HD bearing at high speeds, something that is normally not efficient since surface texturing, which is desired for maximum efficiency of a HS bearing, reduces the efficiency of a HD bearing.

This work presents the basic working principle of the bearing in the HS working regime. Furthermore, the work demonstrates the effect of control on the bearing performance as is shown in [1].

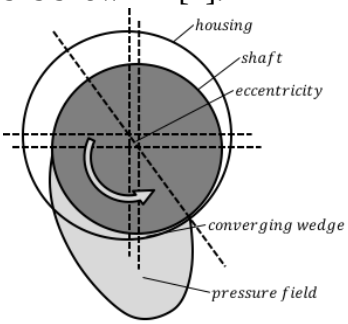

Figure 1: Example of a hydrodynamic bearing(HD). The inner cylinder moves counter clockwise while the outer cylinder stays static. The eccentricity between the two cylinders causes a converging wedge that results in a local pressure field.

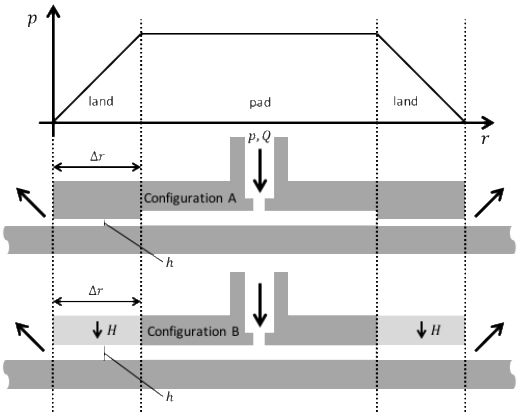

Figure 2: Configuration A presents a hydrostatic bearing that works by actively pumping lubricant in-between the two bearing faces to create a load carrying capacity. The pad area has close to constant pressure since the flow has little resistance there, the land area has a declining pressure due to the high resistance caused by the small fly height h. Configuration B presents a hydrostatic bearing with MR texturing that works by actively pumping MR lubricant in-between the two bearing faces to create a load carrying capacity. A land and pad configuration is created by respectively activating and not activating the MR fluid.

Figure 3: A schematic overview of a hybrid bearing with MR texturing. The bearing works as a MR textured hydrostatic bearing at low speeds and as a conventional HD bearing at high speeds(see Figure 1).

Bearing model

The load carrying characteristic of a hydrostatic bearing is defined by the potential divider presented in Figure 4. A basic model of the HS bearing with MR texturing is derived by deriving a relation for the resistance of the bearing $R_{bearing}$.

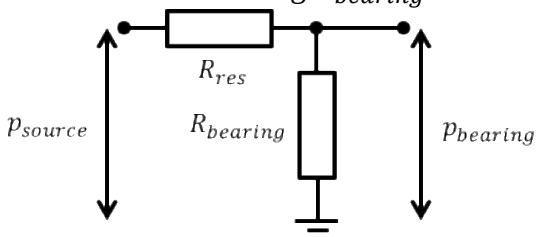

Figure 4: The pressure in the bearing is defined by a potential divider of the restrictor resistance R_{res} and the bearing resistance $R_{bearing}$.

With the following relations a 2D model is derived that has as main assumption a low Reynolds number flow and a Bingham plastic fluid model.

$$p_{bearing} = \frac{R_{bearing}}{R_{bearing} + R_{res}} p_{source} \quad (1)$$

$$R_{bearing} = \frac{24\eta\Delta r}{Lh^3(2 - 3\Re + \Re^3)} \quad (2)$$

$$\Re = \frac{2\tau\Delta r}{hp_{bearing}} \quad (3)$$

The relations use η as viscosity, Δr as the distance over which the pressure drop $p_{bearing}$ acts, L as the length of the bearing, h as the spacing between the bearing surfaces and τ as the yield stress of the fluid.

The bearing pressure can be obtained by solving relation (1). From relation (3) it can be seen that the bearing is actually a function of the same bearing pressure. Still the relation can be solved analytically by rewriting it to a 3rd degree polynomial that has one physically correct solution.

Results

The bearing pressure as a function of the fly height is given in Figure 5. The graph shows that the bearing pressure at low fly height is equal to the feeding pressure. For higher fly heights, the bearing pressure follows either a -3 slope or a -1 slope. The -3 slope is followed where the MR effects are small ($\Re \sim 0$) and a -1 slope is followed where the MR effects are big ($\Re \sim 1$).

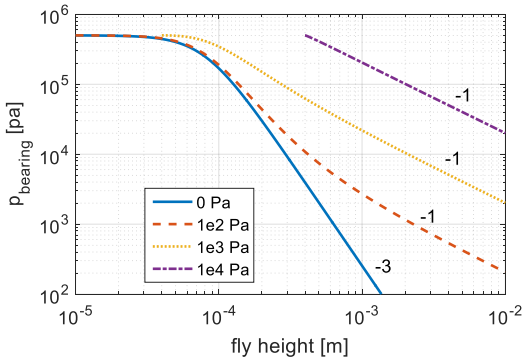

Figure 5: Bearing pressure in function of fly height for different yield strengths.

Conclusion

A basic model for the load and stiffness of a hydrostatic bearing with MR texturing is derived. The model furthermore shows how the load characteristic is changing with changing yield stress in the fluid.

Acknowledgments

This research has been supported by the Dutch TKI maritime funding program.

References

[1] J. M. Guldbakke, C. Abel-Keilhack, and J. Hesselbach, "Magnetofluidic Bearings and Dampers J.M.," in *Colloidal magnetic fluids : basics, development and application of ferrofluids*, 2009.

Differentially charged SPIONs interfere with inflammation response during interaction with tumor cells

J. Demut[1], P. Scheerer[1], C. Grüttner[2], C. Bergemann[3], F. Müller[4], P. Czerney[5], A. Hochhaus[1], J.H. Clement[1]

[1] *Klinik für Innere Medizin II, Abt. Hämatologie & Internistische Onkologie, Universitätsklinikum Jena, Am Klinikum 1, D-07747 Jena, Germany; mail to: johanna.demut@med.uni-jena.de*
[2] *Micromod Partikeltechnologie GmbH, Friedrich-Barnewitz-Straße 4, 18119 Rostock, Germany*
[3] *Chemicell GmbH, Eresburgstraße 22-23, 12103 Berlin, Germany*
[4] *Otto-Schott-Institut für Materialforschung, Professur für Oberflächen- und Grenzflächentechnologie, Löbdergraben 32, 07743 Jena, Germany*
[5] *Dyomics GmbH, Otto-Schott-Straße 15, 07745 Jena, Germany*

Introduction

Nanoparticles are very versatile not only in their composition but also in their application. They are increasingly used for biomedical approaches as for diagnostic analysis or therapy. Especially superparamagnetic iron-oxide nanoparticles (SPIONs) are suitable for this purpose. Their long-term effects are of particular interest since they may remain in the human body, e.g. in the liver or in other organs. Thereby an inflammatory response may be induced, which has to be considered evaluating the biocompatibility of newly designed nanoparticles. Therefore we intend to analyse the effect of different nanoparticles on the expression levels of inflammation associated genes in more detail in hypopharyngeal squamous cell carcinoma cells (FaDu).

Materials & Methods

FaDu cells were incubated for 3h and 24h with different SPIONs (starch-coated fluidMAG-D - neutral, glucuronic acid-coated fluidMAG-ARA – anionic, polyethyleneimine-coated PEI-M - cationic, polyethylene-glycol-coated PEG-5kDa – neutral, silica-iron oxide composite SiliFe42 - neutral). The physical interaction of the particles with the cells was analysed with laser-scanning-microscopy. Their influence on the viability of the cells was investigated via PrestoBlue Viability Assay. For gene expression analysis RNA was isolated from incubated FaDu cells using the innuPREP RNA Mini Kit (Analytik Jena) and mRNA was transcribed into cDNA utilising Reverse Transcriptase. Quantitative real-time PCR was performed to determine the expression level of selected inflammation-associated genes (*c-fos, icam1, cyp1a1, pdgfb*). Results were evaluated according to Pfaffl (2001).

Results

At first we confirmed biocompatibility of the selected SPIONs (up to 100 µg/cm^2) with the exception of PEI-coated nanoparticles, as expected. Depending on the coating of the SPIONs a unique interaction pattern with the cells was observed by laser scanning microscopy. Positively charged PEI-M particles formed large aggregates and exhibited a strong interaction with the cells already after a 3h incubation. Neutrally charged fluidMAG-D showed a slight agglomeration and cell interaction behavior after 3h, which was more pronounced after 24h. Negatively charged fluidMAG-ARA and neutrally charged PEG-5kDa particles interacted only weakly with FaDu cells even after a 24h incubation. In addition, fluidMAG-ARA showed a high stability in the cell culture medium with almost no visible agglomeration.
The expression of *c-fos, icam1, cyp1a1* and *pdgfb* was not significantly altered after a 3h incubation with 25 µg/cm^2 fluidMAG-D, fluidMAG-ARA, PEI-M or SiliFe42 each as compared to controls.

Conclusion

Short-term application of neutrally and negatively charged SPIONs neither interferes with cell viability and cellular uptake, nor alters expression of inflammation-associated genes.
Future work will focus on long-term application of SPIONs and its consequences on cellular metabolism.

Acknowledgements

This work was supported in part by the BMBF joint project NanoBEL (grant 03XP0003).

References

Pfaffl, M. A new mathematical model for relative quantification in real-time RT-PCR. Nuc Acids Res. **2001**, 29(9), e45

Interaction of iron oxide nanoparticles with breast cancer cells

R. P. Friedrich[1], J. Poller[1], J. Zaloga[1], E. Schreiber[1], H. Unterweger[1], C. Janko[1], P. Radon[2], D. Eberbeck[2], L. Trahms[2], C. Alexiou[1]

[1]*Department of Otorhinolaryngology, Head and Neck Surgery, Section for Experimental Oncology and Nanomedicine (SEON), Else Kröner-Fresenius-Stiftung-Professorship, Universitätsklinikum Erlangen, Germany*
[2]*Physikalisch-Technische Bundesanstalt Berlin, Berlin, Germany*

Introduction

Superparamagnetic iron oxide nanoparticles (SPIONs) have gained increasing importance as promising new tools for biomedical applications. In this investigation, we studied the influence of physicochemical properties like particle size, Zeta potential and coating of various SPIONs on particle uptake, cell proliferation and viability of various human breast cancer cell lines [1]. To address the heterogeneity of nanoparticles and cells, we synthesized 3 different, precisely characterized SPIONs (lauric acid-coated SPIONs [SPION^{LA}], lauric acid and human serum albumin-coated SPIONs [SPION$^{LA\text{-}HSA}$] and dextran-coated SPIONs [SPION^{Dex}]). We investigated their effects on 4 breast cancer cell lines (T-47D, BT-474, MCF7 and MDA-MB-231) belonging to different subtypes, as defined by receptor expression and proliferation rates. As a tumor-unrelated control, we used human umbilical vein endothelial cells (HUVECs). We analyzed cellular SPION uptake, magnetic properties, cell proliferation and toxicity using atomic emission spectroscopy, magnetic susceptometry, flow cytometry and microscopy.

Results and Summary

We found that the particle internalization by cells is strongly related to the SPION-surface coating. Moreover, our studies demonstrated a cell type-dependent SPION uptake and toxicity (Fig. 1 and 2). SPION^{LA} are relatively non-toxic to breast cancer cells and could easily be functionalized to target these cells, but they are harmful to HUVECs and possibly also to other healthy cells. Due to this fact, there is a risk of enhanced toxicity, which excludes their clinical use. SPION^{Dex}, shows high

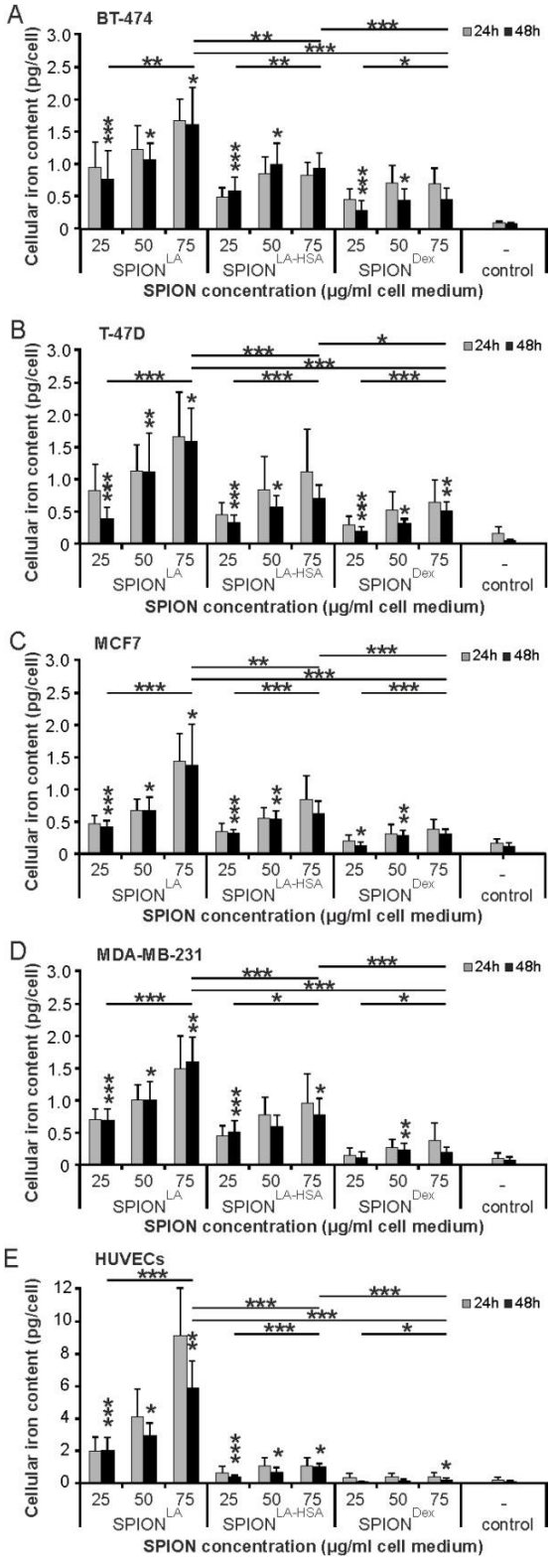

stability, extremely low toxicity and barely detectable cell uptake. SPION$^{LA\text{-}HSA}$ displayed good magnetic properties, adequate stability and low toxicity. Future experiments addressing the underlying biological and chemical reasons for this heterogenic response might reveal essential principles for the interaction between cells and SPIONs.

Figure 1 Quantification of the cellular nanoparticle load via MP-AES.
Cells were incubated for 24 and 48 h with 0–75 µgFe/mL SPION^{LA}, SPION$^{LA\text{-}HSA}$ and SPION^{Dex}, and cell lysates were investigated by MP-AES. The cellular iron content (pg/cell) is shown for (A) BT-474, (B) T-47D, (C) MCF7, (D) MDA-MB-231 and (E) HUVECs. n=4 with technical triplicates. *P,0.05, **P,0.001 and ***P,0.0001. Asterisks on bars indicate dose-dependent significance to the next lower SPION concentration. Asterisks over the lines indicate dose-dependent significance between lowest and highest SPION concentrations and between the highest SPION concentrations of different SPIONs.

Figure 2 Viability of different cells after SPION treatment.
Cells were incubated for 48 h with increasing amounts of SPION^{LA}, SPION$^{LA\text{-}HSA}$ and SPION^{Dex}. Cell viability was determined by annexin A5-FITC/PI staining and analyzed by flow cytometry. The amount of viable (Ax-PI-), apoptotic (Ax+PI-) and necrotic (PI+) cells are shown for (A) BT-474, (B) T-47D, (C) MCF7, (D) MDA-MB-231 and (E) HUVEC cells. Positive controls contain 2% DMSO. n=4 with technical triplicates. *P,0.05, **P,0.001 and ***P,0.0001. Asterisks indicate dose-dependent significance between lowest and highest SPION concentrations on necrosis (light grey asterisks), apoptosis (white asterisks) and viability (dark grey asterisks).

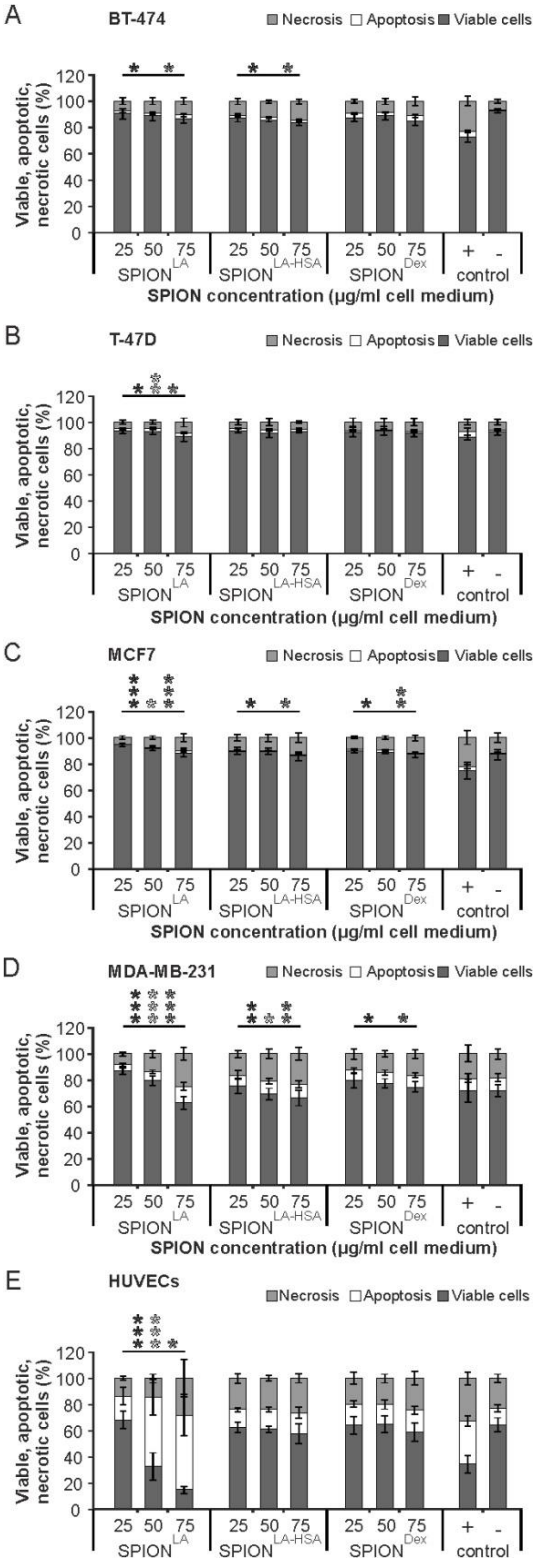

Acknowledgments

DFG SPP1681 [AL552/5-2, TR408/8, WI4230/1]

References

[1] Poller JM, Zaloga J, Schreiber E, Unterweger H, Janko C, Radon P, Eberbeck D, Trahms L, Alexiou C, Friedrich RP: Selection of potential iron oxide nanoparticles for breast cancer treatment based on in vitro cytotoxicity and cellular uptake. Int. J. of Nanomedicine. 2017;12:3207-3220.

Protein corona dependent passage of SPIONs through cellular barriers

P. Globig[1], C. Gräfe[1], E. Schreiber[2], R. P. Friedrich[2], C. Alexiou[2], A. Hochhaus[1], J. H. Clement[1]

[1] *Klinik für Innere Medizin II, Abt. Hämatologie & Internistische Onkologie, Universitätsklinikum Jena, Am Klinikum 1, D-07747 Jena, Germany; mail to: christine.graefe@med.uni-jena.de*
[2] *Hals-Nasen-Ohren-Klinik, Kopf und Halschirurgie, Sektion für Experimentelle Onkologie und Nanomedizin (SEON), Universitätsklinikum Erlangen, Glückstraße 10a, D-91054 Erlangen, Germany*

Introduction

Superparamagnetic iron oxide nanoparticles (SPIONs) are highly promising in the field of biomedicine due to their outstanding physiochemical and magnetic properties [1]. Entering a biological system, especially blood circulation, nanoparticles interact with the environment and are often provided with a protein corona consisting of an adsorptive layer formed by soluble proteins on the particle surface. The formation of this corona does not only depend on the nanoparticle properties, but also on parameters like temperature, incubation conditions and time [2]. Thus, the nanoparticle is provided with a new biological identity, which might affect its interaction with cellular structures [3] or passage through biological barriers, respectively.
The aim of our project is to investigate the influence of such a protein corona of SPIONs on established cell culture-based barrier models (blood-brain barrier (BBB) and blood-placenta barrier). This includes the analysis of the interaction of SPIONs with barrier-forming cells in a short- and long-term observation, as well as the passage through cell layers and subsequent characterization of the protein corona.

Materials and Methods

Lauric acid-coated SEON particles, additionally covered with bovine serum albumin (BSA) or human serum albumin (HSA) respectively, were used as nanoparticle systems [4, 5]. To investigate interaction with biological barriers, BBB representing human microvascular endothelial cells (HBMEC, 5 days cultivation in RPMI +10 % FCS) were used. For short-term observance of cell viability, cells were exposed to 5 to 100 µg/cm^2 of SPIONs and analyzed by the PrestoBlue Assay. Long-term investigations were performed using the xCELLigence-based real time cell analysis (RTCA). Therefore, cells were incubated with 100 µg/cm^2 SPIONs under serum-reduced conditions (i.e. cell culture medium supplemented with 2 % fetal calf serum (FCS)). Additionally, the interaction of these SPIONs with the aforementioned cells was investigated using Prussian Blue staining. Cell barrier integrity was verified by trans-endothelial electrical resistance (TEER) measurements and molecular permeability assays using sodium fluorescein as small molecular dye. To simulate the formation of a protein corona the SEON particles were incubated in human serum for 12 min at 37 °C, magnetically washed and resuspended in *aqua bidest*. All following cellular experiments were performed under serum-reduced conditions (2 % human serum). SEON particles were added to the HBMEC-based BBB model and incubated for 24h [6]. Subsequently, iron content of upper and lower compartment as well as their separating membrane/cell layer were quantified using atomic absorption spectroscopy (AAS).

Results and Discussion

For the native SEON particles it was demonstrated that SEON BSA show a time-dependent cytotoxic effect, whereas SEON HSA particles do not affect the cell viability during long-term observation for up to 72h (Figure 1). Prussian Blue stain-

ing revealed a higher interaction with cells for SEON BSA than for SEON HSA particles.

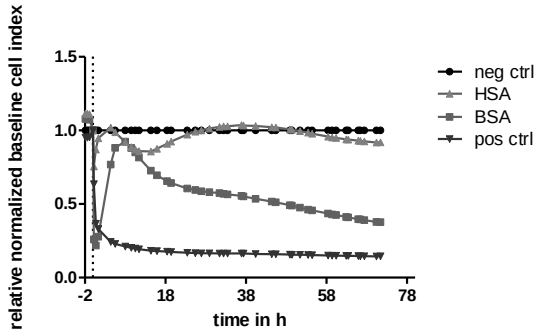

Figure 1: Cell viability measured by RTCA. HBMEC cells were incubated with 100 µg/cm^2 of either SEON BSA or HSA in 2 % FCS.

In order to analyze the corona-associated effects on the cellular particle interaction, SEON particles were additionally equipped with a protein corona by incubation in human plasma. Since the formed protein corona needed to be preserved and a corona formation on the surface of reference particles is not intended, the presence of serum as cell culture medium supplement is critical. In order to compromise this requirement for cell culture experiments, the effect of different serum media supplements on both cell viability and barrier integrity were tested.

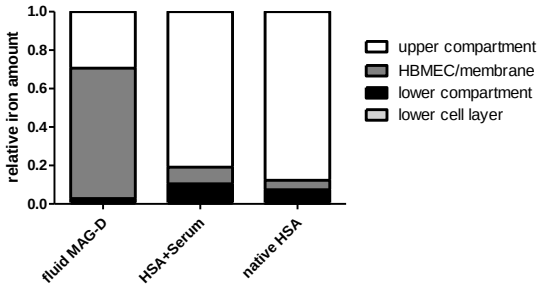

Figure 2: Iron content quantification by AAS. HBMEC cells were incubated with 100 µg/cm^2 of serum-incubated HSA, native HSA particles or reference particles (fluid MAG-D).

Both, TEER measurements and molecular permeability assays confirmed that medium supplemented with 2 % human serum is sufficient for following tests. Thus, cell barrier integrity appears reasonable and the protein corona on the particle surface mostly unaffected. Determination of iron quantification by AAS revealed that passage of coated SEON particles through cell layers is facilitated compared to neutral starch-coated reference particles (fluid MAG-D), as indicated by the relative iron amount in the lower compartment. Furthermore, the presence of a protein corona favors this passage even more (Figure 2).

Conclusion

The presented work emphasizes the importance of a protein corona affecting the interactions of SPIONs with cells or cell layer models. Hence, the study account for the understanding of nanoparticle passage through biological barriers highlighting the role of the protein corona on the particle surface.
Future parts of this study will focus on the blood-placenta barrier and the composition of the protein corona in detail.

Acknowledgement

This work was supported by Deutsche Forschungsgemeinschaft (DFG) in the framework of the priority program 1681 (FKZ: CL202/3-2, AL552/5-2).

References

[1] S. Dutz, J. H. Clement, D. Eberbeck, et al. *J Magn Magn Mater*. **2009**, *321, 1501-1504*

[2] T. Cedervall, I. Lynch, S. Lindman, et al., *Proc Natl Acad Sci USA*. **2007**, *104, 2050-2055*

[3] C. Gräfe, A. Weidner, M. von der Lühe, et al. *Int J Biochem Cell Biol.* **2016**, *75, 196-202*

[4] J. Zaloga, C. Janko, J. Nowak, et al., *Int. J. Nanomedicine*. **2014**, *9, 4847–4866*

[5] J. Zaloga, M. Pöttler, G. Leitinger, et al., *Eur J Pharm Biopharm*, **2016**, *101, 152–162*

[6] C. Gräfe, I. Slabu, F, Wiekhorst, et. al., *Phys Med Biol*. **2016**, *61: 3986-4000*

The passage of SPIONs through an *in vitro* blood-brain barrier is dependent on the SPIONs' surface charge

C. Gräfe[1], I. Slabu[2], A. Weidner[3], E. Schreiber[4], R.P. Friedrich[4], F. Wiekhorst[2], C. Alexiou[4], S. Dutz[3], A. Hochhaus[1], J. H. Clement[1]

[1] *Klinik für Innere Medizin II, Abt. Hämatologie & Internistische Onkologie, Universitätsklinikum Jena Am Klinikum 1, D-07747 Jena, Germany; mail to: christine.graefe@med.uni-jena.de*
[2] *Physikalisch-Technische Bundesanstalt, Abbestrasse 2–12, D-10587 Berlin, Germany*
[3] *Institut für Biomedizinische Technik und Informatik, Technische Universität Ilmenau, Gustav-Kirchhoff-Straße 2, D-98693 Ilmenau, Germany*
[4] *Sektion für Experimentelle Onkologie und Nanomedizin, Universitätsklinikum Erlangen, Glückstraße 10a, D-91054 Erlangen, Germany*

Introduction

Biological barriers such as the blood-brain barrier constitute highly specialized and selective semipermeable membrane tissues. On the one hand its integrity should not accidentally be affected. On the other hand they act as obstacle for numerous drugs making sufficient and targeted drug delivery a mayor challenge. Thus, dedicated strategies and drug delivery systems specially designed for the definite application are developed. Based on their huge diversity and functionalization capacity superparamagnetic iron oxide nanoparticles (SPIONs) are highly attractive candidates for accomplishing not only drug delivery but also utilizing them as contrast-enhancing agents in magnet-based imaging techniques and in hyperthermia cancer therapy [1]. However, for a successful implementation, a detailed knowledge concerning their interaction with cellular interfaces and their effect on barrier integrity are of essential importance. In order to study these aspects we establish a standardized *in vitro* test system to investigate and understand the passage of coated SPIONs through cell layers driven by magnetic forces.

Methods

Previously, we have demonstrated that dependent on the particle type SPIONs can penetrate into three-dimensional cellular structures such as spheroids [2]. In order to analyze the ability of SPIONs to passage distinct cellular layers, we now generated an *in vitro* cell culture model representing the human blood-brain barrier [3]. Human brain microvascular endothelial cells (HBMEC) were seeded on PET transwell membranes (3µm pore size) and cultivated for five days. As reporter cells the breast cancer cell line MCF-7 was seeded on the bottom of the lower compartment. Neutral starch-coated or anionic bovine serum albumin (BSA)-coated SPIONs were added and incubated on top of a block magnet for 30 min before further particle incubation was carried out without the application of the magnetic field. First, we studied the SPION passage through the cellular barrier by quantifying nanoparticle amounts found in the basolateral compartment. This was done by means of highly sensitive measurements via magnetic particle spectroscopy and atomic absorption spectroscopy. Additionally, we analyzed the SPION-induced effect on barrier integrity by performing transendothelial electrical resistance measurements, molecular permeability assays, fluorescence microscopy, and histological cross-sections.

Results and Discussion

We show that both neutral starch-coated and anionic BSA-coated SPIONs can clearly pass our mono-layered blood-brain barrier model. The accumulation of BSA-

coated SPIONs in the barrier cell layer after 3 h as well as after 24 h incubation was approximately 10- and 3-fold higher than that of neutral SPIONs, respectively. Interestingly the content of both SPION types in the lower compartment as well as in the reporter cell layer was nearly the same. However, we found that the SPION type crucially determines the route of SPION passage through the cellular barrier. As the time- and concentration dependent passage of neutral starch-coated SPIONs is accompanied by the maintenance of barrier integrity, the passaging process points towards distinct transcellular routes through the barrier-forming cells. In contrast, anionic BSA-coated SPIONs disrupt the cellular barrier in a time-dependent manner indicating that they overcome the cellular barrier by their barrier-interfering nature (Fig. 1).

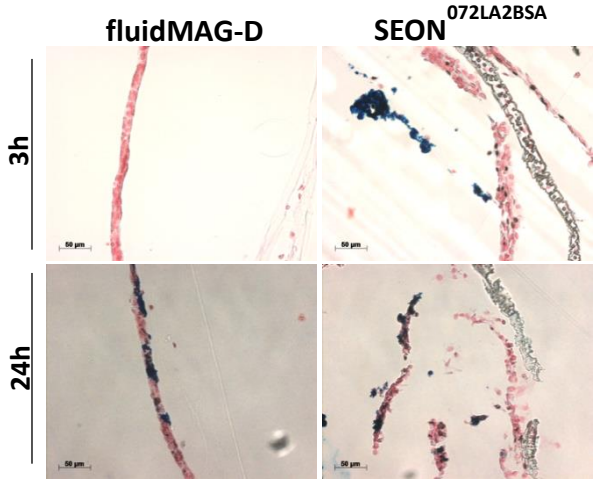

Figure 1: Histological cross section of blood-brain barrier-representing transwell layers. Cell barriers were incubated with 100µg/cm² neutral fluidMAG-D or anionic SEON^{072LA2BSA} particles for indicated durations. Cells and particles of 12µm cross sections were stained using Nuclear Fast Red and Prussian blue, respectively.

Conclusion

Based on the presented *in vitro* system and the highly sensitive SPION detection methods we could establish a valuable tool for the detailed analysis of particle interaction and penetration through such cellular barriers. Thus, our approach considerably contributes to the understanding of tissue penetration mechanism and, in consequence, delivers valuable information for the development of tailored SPION configurations to successfully realize intended biomedical applications.

Acknowledgement

The technical assistance of Cornelia Jörke is highly acknowledged. This work was supported by Deutsche Forschungsgemeinschaft (DFG) in the framework of the priority program 1681 (FKZ: CL202/3-2, TR408/8-1, DU 1293/4-2, WI30/1-2, AL552/5-2) Clinical Research Group KFO213 (TR408/4-3).

References

[1] B. Pelaz, C. Alexiou, R.A. Alvarez-Puebla *et al.*, *ACS Nano.* **2017**, 11: *2313-2381*.

[2] A. Theumer, C. Gräfe, F. Bähring, *et al.*, *JMMM.* **2014**, *380*, *27-33*

[3] C. Gräfe, I. Slabu, F, Wiekhorst, *et. al.*, *Phys Med Biol.* **2016**, 61: 3986-4000

[4] C. Gräfe, A. Weidner, M. von der Lühe, *et al. Int J Biochem Cell Biol*. **2016,** 75:196-202

[5] F. Wiekhorst, U. Steinhoff, D. Eberbeck, L. Trahms, *Pharm. Res*. **2012** 5, *1189-1202*

How to speed up magnetorelaxometry tomography

M. Liebl[1], D. Baumgarten[2], U. Steinhoff[1], L. Trahms[1] and F. Wiekhorst[1]

[1] *Physikalisch-Technische Bundesanstalt, Berlin, Germany*
[2] *University of Health Sciences, Hall in Tirol, Austria*

Introduction

Novel cancer therapies based on magnetic nanoparticles (MNP) share the need for a quantitative MNP imaging operating within tolerable measurement times.
Magnetorelaxometry tomography (MRXT) has proven its feasibility for quantitative MNP imaging in phantom studies [1]. In MRXT, different regions of a spatial MNP distribution are consecutively magnetized and their magnetization decay is recorded by a sensor array. These magnetizing fields are generated by a number of small excitation coils placed around the body. In conventional MRXT (cMRXT), each coil is used one by one to magnetize the MNP distribution. Hence, the total measurement duration is determined by the total number of coils used. Here, we present experimental results of a simultaneous excitation approach "sMRXT" where multiple excitation coils are simultaneously applied for regional magnetization with the aim to reduce the total measurement duration while preserving reconstruction quality.

Methods

In our MRXT setup [1], MRX signals were recorded by the PTB 304 vector magnetometer system. Inside a sample support 15 MNP filled cubes (l=12 mm, X_{MNP}=6.4 mg, each) are assembled to form the letter "P". A total of 30 excitation coils (d=36 mm) with 15 coils above and 15 coils below the support were used to generate the magnetizing fields for cMRXT and sMRXT. An excitation current of I_{mag}=800 mA was used either for magnetizing with one (cMRXT) or multiple coils simultaneously (sMRXT). In each MRX measurement of a MRXT scan the MNP distribution was magnetized for t_{mag}=1 s and MRX signals were recorded for t_{meas}=2 s at a 250 Hz sampling frequency. A settling time between two MRX measurements needed for the multiplexer was set to 500 ms. Hence, the total measurement duration for the N_{MRX}=30 individual MRX measurements in cMRXI summed up to 105 s.

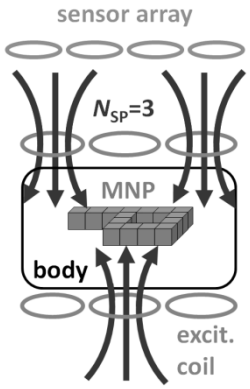

Figure 1: Sketch of a MRXT setup with a sensor array above and excitation coils around a body containing MNP. In this case the distribution forms the letter "P". In cMRXT, each excitation coil is used sequentially for magnetizing. In sMRXT, the magnetizing field is simultaneously generated by N_{SP} coils (here N_{SP}=3).

Figure 1 visualizes options of excitation sequences. In this example the magnetizing field is generated by superposition of the field contributions of N_{SP}=3 excitation coils. Compared to cMRXT, the total measurement duration needed to complete the sMRXT scan is reduced by factor 3. In sMRXT, there are P over N_{SP} possible switch combinations for the P=30 excitation coils. Baumgarten et al. [2] suggests a random generator to choose switch combinations with a minimum of correlation between them. We generated excitation sequences for N_{SP}=[2, 3, 4, 5] coils using the Mersenne Twister algorithm [3]. The number N_{SP} was fixed within each sMRXT scan. Hence, N_{MRX}=[15, 10, 8, 6] MRX measurements were needed to switch each coil once in a complete scan, respectively. For each N_{SP}, excitation sequences for 50

individual sMRXT scans were generated and applied to the "P" shaped MNP distribution. This distribution was reconstructed using minimum-norm estimation within a FOV of about 600 cm^3 and a voxel grid of k=($10N_x$×$10N_y$×$5N_z$) with V=1.72 cm^3 individual voxel volume.

Results and Discussion

For a visual comparison between cMRXT and sMRXT the reconstruction results obtained for one of the 50 sMRXT scans for each N_{SP} are depicted in figure 2.

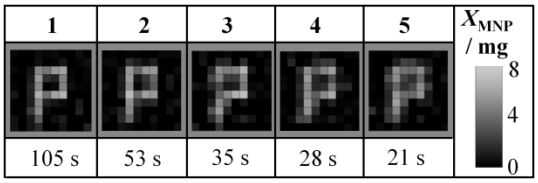

Figure 2: Reconstructed MNP distributions forming the letter "P" for cMRXI (row1) and sMRXI (row2-5). The row number (1-5) indicates the number of excitation coils N_{SP} simultaneously used for magnetizing. The respective total measurement duration is given in the bottom line.

The correlation coefficient R and the total MNP mass deviation X_{diff} between nominal and reconstructed MNP distribution are listed in table 1.

Table 1: Correlation coefficient R and deviation in total MNP amount X_{diff} between reconstruction and nominal MNP distribution for N_{Sp}=1-5.

N_{Sp}	1	2	3	4	5
R	0.92	0.86	0.83	0.80	0.77
X_{diff}	4.4%	-2.0%	3.4%	7.9%	8.6%

A slight decrease in reconstruction quality is visible with increasing N_{SP}. However, even for N_{SP}=4 with a total measurement duration of only 28 s the "P" is clearly visible and X_{diff} is below 10%. For N_{SP}=5 with a total measurement duration of 21 s X_{diff} remains below 10%, but a slight smearing of the "P" is observed. Figure 3 shows a boxplot of the R distribution over the 50 individual sMRXT scans to evaluate the dependence of the choice of switch combinations on the imaging quality. As before, also the average value of R decreases with increasing N_{SP}.

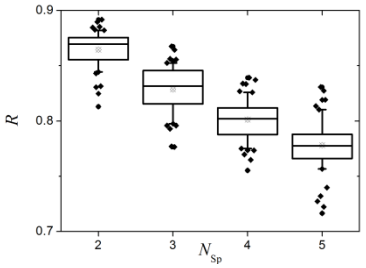

Figure 3: Boxplot of the distribution of the correlation coefficient R in dependence on the number of excitation coils N_{SP} simultaneously used for magnetizing estimated over 50 individual sMRXI scans.

Using N_{SP}=4 on average a well imaging quality with R above 0.8 was obtained. The R distribution for N_{SP}=5 shows large outliners in positive and negative direction, indicating that with increasing N_{SP} the choice of switch combinations has a stronger impact on the imaging quality.

Conclusion

We demonstrated that by simultaneous excitation with multiple excitation coils the total measurement duration of quantitative MRXT can be reduced. For N_{SP}=4 a time reduction from 105 s to 28 s was achieved without visibly deteriorating of the reconstruction quality. Even for N_{SP}=5 (105 s to 21 s) a quantification of the total MNP amount was still possible. Hence, sMRXT enables fast and flexible imaging of large FOVs, what is particularly required for in-vivo imaging. Future work will focus on sensitivity based switch combinations to find optimal excitation sequences for a given MRXT setup.

Acknowledgments

This work was supported by Deutsche Forschungsgemeinschaft (DFG) in the framework of the priority program 1681 (WI4230/1-2, TR408/8-2).

References

[1] M. Liebl, F. Wiekhorst et al. (2015), *Biomed Eng/Biomed Tech*, 60(5):427-43.
[2] D. Baumgarten, J. Haueisen et al. (2013), *EMBS Proc*, 2013:3258-60.
[3] M. Matsumoto & T. Nishimura (1998), *ACM Trans Model Comput Simul*, 8(1):3-3

Multifunctional Nanoclusters for Theranostics in Cancer

Stefan Lyer[1]; Tobias Knopp[2], Franziska Werner[2], Jan Zaloga[1], Ralf Friedrich[1], Lutz Trahms[3], Frank Wiekhorst[3], Tobias Struffert[4], Tobias Engelhorn[4], Arndt Dörfler[4], Tobias Bäuerle[4], Michael Uder[4], Rainer Tietze[1], Christina Janko[1], Christoph Alexiou[1]

[1] *Universitätsklinikum Erlangen, Department of Otorhinolaryngology, Head and Neck Surgery, Section of Experimental Oncology and Nanomedicine (SEON), Else Kröner-Fresenius Stiftung-Professorship, Germany*
[2] *Universitätsklinikum Hamburg-Eppendorf, Diagnostic and Interventional Radiology Department and Clinic*
[3] *Physikalisch Technische Bundesanstalt Berlin, Germany*
[4] *Universitätsklinikum Erlangen, Department of Radiology/Neuroradiology, Germany*

Introduction

Aim of the Section of Experimental Oncology and Nanomedicine (SEON) is to utilize SPIONs for the treatment of cancer and arteriosclerosis by MDT. Therefore, over a period of several years we developed SPIONs optimized for the purpose of magnetic drug delivery. These particles show a very good biocompatibility, are very stable in human and animal blood and can carry a sufficient drug load. Due to their magnetic properties, these particles can be accumulated in a target area by magnetic fields and first results show they can be heated with alternating magnetic fields. These SPIONs were also suitable for MRI-imaging but from the theoretical point of view not optimal for Magnetic Particle Imaging (MPI), because they are clusters of a size between 60 nm and 70 nm with a single core diameter of approximately 7,6 nm. The aim of this study was to show, that multifunctional nanoclusters, which are suitable for magnetic drug targeting, hyperthermia, MR-imaging can also show a signal in MPI.

$SEON^{LA\text{-}BSA}$ - *In vitro* efficiency

The nanoparticle system $SEON^{LA\text{-}BSA}$ has been developed as a platform for delivery of drugs. At the beginning, the chemotherapeutic agent mitoxantrone (MTO) was chosen for cancer treatment.
In various experiments, $SEON^{LA\text{-}BSA*MTO}$ showed an effectiveness comparable to the free drug after 24 h and 48 h in killing cancer cell lines [1]. In 3D-cellculture, spheroids of the tumor cell line HT-29 fluorescence microcopy showed that both free and nanoparticle-loaded MTO infiltrated efficiently into the tumor spheroids. Subsequently, the treated spheroids showed a highly reduced proliferation rate and higher rates of apoptosis and necrosis [2].

$SEON^{LA\text{-}BSA}$ - Biocompatibility

Since, common colorimetry based toxicity assays, show interference of the black iron oxide nanoparticles [3], we used different methods to assess possible toxic effects *in vitro*. $SEON^{LA\text{-}BSA}$ did not show induction of apoptosis or necrosis in Jurkat cells at doses of up to 100 µg/ml after 24 hours or 48 hours measured in flow cytometry [3].
Additionally, $SEON^{LA\text{-}BSA}$ nanoparticles revealed a tremendously improved colloidal stability in blood compared to the precursor particle system $SEON^{LA}$, which only coated with lauric acid for stabilization [1].

$SEON^{LA\text{-}BSA}$ - Heating properties

One option for using SPIONs for the treatment of tumors is magnetic hyperthermia [4]. Therefore, we were interested, if combination of chemotherapeutic treatment with hyperthermia can enhance the outcome of the treatment. Hence, we investigated the heating properties of the $SEON^{LA\text{-}BSA}$ system with alternating mag-

netic fields. It could be shown that these-nanoparticles can be magnetically heated and that this is depended on the iron content, as could be expected [5].

SEON^{LA-BSA} - MPI-Imaging

Magnetic particle imaging (MPI) is a new imaging technique utilizing iron oxide nanoparticles imaging agents. The big advantage of MPI is that it not only generates images but it can also deliver quantitative data about the tracer content in a given volume. Therefore, we were interested, if it is possible to image the SEON^{LA-BSA} nanoparticles with a currently available preclinical MPI-device (Bruker/Philips) at Universitätsklinikum Hamburg-Eppendorf.

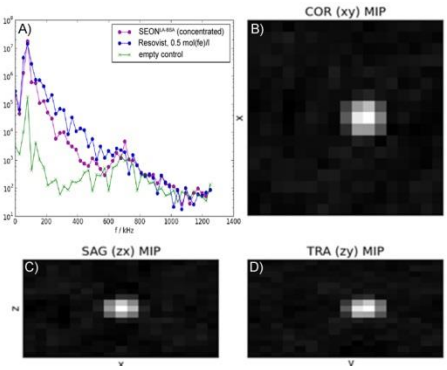

Figure 2: A) Comparison of the MPS signal of SEON^{LA-BSA}-nanoparticles and Resovist® at different frequencies. B) – D) MPI-signal of a point sample of SEON^{LA-BSA}-nanoparticles.

First, we measured a dilution series of these particles Magnetic Particle Spectroscopy (MPS). In comparison to the MPS-signal of Resovist® the signal of the SEON^{LA-BSA}-nanoparticles was weaker at higher frequencies but comparable at frequencies below 100 kHz (Figure 2A). Next, a sample of 20 µl (2 mm * 2 mm * 1 mm) was measured with MPI. Figure 2B to D show that it was possible to get an image of this point sample by MPI.

Conclusion

During the last years SEON developed a multifunctional nanoparticle platform SEON^{LA-BSA}, which is capable of carrying a variety of drugs. We showed that this nanosystem is very biocompatible *in vitro* and has excellent blood compatibility. *In vitro*, mitoxantrone-loaded SEON^{LA-BSA} are very effective in treating cancer cells in 2d, suspension- and 3d-cell-culture, which was similar to the free, unbound drug. Furthermore, it is possible to use alternating magnetic fields for heating this particle system in a concentration depended manner up to ca. 65°C. Additionally and as could be expected, the SEON^{LA-BSA} particles are causing a signal extinction in MRI and is showing a signal in the new imaging modality MPI. Taken this together, the nanoparticle system SEON^{LA-BSA} could be a promising candidate for an effective theranostic approach of cancer and arteriosclerotic diseases.

This preliminary study shows that in principal it is possible to image SEON^{LA-BSA} using MPI. Further experiments will demonstrate how effective and quantitative this imaging is and if modifications on the particle platform or the technical equipment will be able to improve the imaging properties of this system. If this can be realized without impairing therapeutic efficiency, the combination of MDT and MPI could open new doors in the field of theranostics.

Acknowledgments

This study was supported by the German Research Foundation (DFG) (AL552/8-1), the EU project "NanoAthero", FP7-NMP-2012-LARGE-6-309820 the Cluster of Excellence Engineering of Advanced Materials (EAM), and the Manfred Roth Stiftung, Fürth, Germany.

References

[1] Zaloga J, Lee G, Alexiou C et al. Int J Nanomedicine. 2014 Oct 20;9:4847-66. doi: 10.2147/IJN.S68539

[2] Hornung A and Janko C et al.: Treatment Efficiency of Free and Nanoparticle-Loaded Mitoxantrone for Magnetic Drug Targeting in

[3] Monteiro-Riviere NA, Inman AO, Zhang LW. Limitations and relative utility of screening assays to assess engineered nanoparticle toxicity in a human cell line. Toxicology and applied pharmacology 234(2), 222-235 (2009).

[4] Dutz, S. Hergt, R. Magnetic nanoparticle heating and heat transfer on a microscale: Basic principles, realities and physical limitations of hyperthermia for tumour therapy. Int. J. Hyperth. 2013, 29, 790–800.

[5] Zaloga J, Stapf M, Nowak J, et al.; Tangential Flow Ultrafiltration Allows Purification and Concentration of Lauric Acid-/Albumin-Coated Particles for Improved Magnetic Treatment; Int. J. Mol. Sci. 2015, 16, 19291-19307; doi:10.3390/ijms160819291

MRI investigation of biodegradable fibers with incorporated magnetic nanoparticles

B. Mues[1], K.-M. Kossel[2], M. Schümann[3], S. Odenbach[3], S. Jockenhövel[1,2], T. Schmitz-Rode[1], I. Slabu[1]

[1] *Applied Medical Engineering, Helmholtz Institute, RWTH Aachen University, Germany*
[2] *Biohybrid & Medical Textiles at the Institut für Textiltechnik, RWTH Aachen University, Germany*
[3] *Institute of Fluid Mechanics, Chair of Magnetofluiddynamics, Measuring and Automation Technology, Technische Universität Dresden, Germany*

Introduction

Biodegradable implants such as vascular grafts are new promising therapeutic biomedical substitutes to restore the functions of diseased organs [1]. In order to monitor the location as well as the postoperative degradation state using magnetic resonance imaging (MRI), magnetic nanoparticles (MNP) are incorporated in the material of the implants and used as contrast agents. The visualization of the degradation process is linked to the question of how the immobilized MNP in the implant change the MRI signal. For the assessment of the MNP-induced changes of the MRI signal, the behavior of MNP incorporated in polylactic-co-glycolic acid (PLGA) fibers as well as of MNP dispersed in different agarose phantoms are analyzed.

Materials and Methods

The fiber was produced by melt spinning of PLGA pellets mixed with 0.5 wt% freeze-dried MNP. After fabrication, the fibers were stored in physiological cell medium at 37 °C. The mechanical properties were assessed using a DYNA-MESS testing device with and without the application of a 250 mT magnetic field.
In order to mimic the immobilization of MNP in the PLGA implants during the degradation process, various MNP phantoms with up to 2 wt% agarose content were prepared. The MNP had a core diameter of (8.5 ± 2.1) nm and a saturation magnetization of (68.0 ± 1.1) emu/g.
The T2- and T2*- relaxation times of fibers as well as agarose phantoms were investigated with a Philips Achieva 3.0 T MRI scanner.

Results and Discussion

The light microscope image of a PLGA fiber with incorporated MNP shown in **Figure *1*** implies a homogenous distribution of MNP and bigger agglomerates cannot be identified.

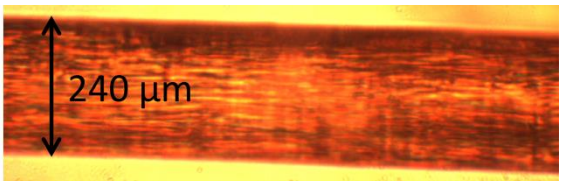

Figure 1: Light microscope image of a PLGA fiber with incorporated MNP (20 fold magnification).

The Young's modulus of the fiber was (7.7 ± 1.5) MPa. First results of stress-strain-tests with and without magnetic field indicate an effect of the field on the elasto-plastic behavior of the fibers. For the verification of this effect, more detailed investigations must be performed using a higher number of fibers with optimized characteristics such as MNP concentration and magnetization.
For the fiber, a r_2 relaxivity value of (0.4 ± 0.1) 1/mM s was calculated.The relaxation times in each pixel in the cross section of the fiber are shown in **Figure *2***. This relaxation time mapping illustrates the induced susceptibility differences by the MNP in the fiber demonstrating the feasibility of quantitative determination of the degradation state of the fiber. However, new data acquisition methods such as sus-

ceptibility gradient mapping must be developed [2, 3].

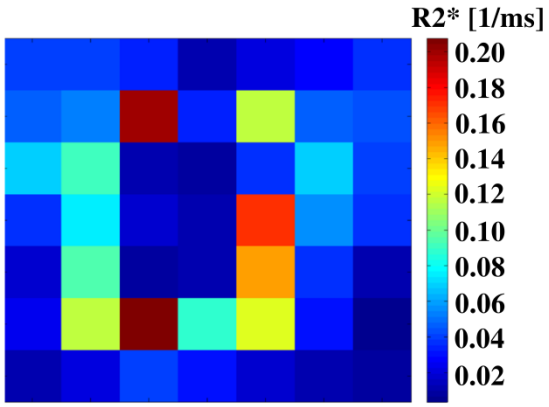

Figure 2: Relaxation time (R2*) map of the cross section of a PLGA fiber loaded with 0.5 wt% MNP.

The increase of the relaxivity with increasing content of agarose in the MNP phantoms shows a clear dependency on the state of immobilization (**Figure *3***). However, the relaxivity values are much higher than those measured for the fiber. This might be due to the low state of MNP immobilization inside agarose compared to that in the fiber. In case of higher immobilization, a drop of the relaxivity value is expected for the agarose phantom.

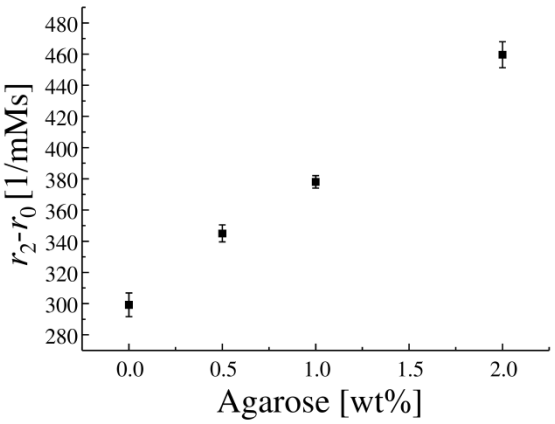

Figure 3: Relaxivity values for different agarose phantoms incorporated with MNP and with an agarose loading of up to 2.0 wt% (r_0 denotes the relaxivity value of the agarose phantom without MNP).

Conclusions

To conclude, the relaxation times of both phantoms and fibers showed a clear dependency on MNP state of immobilization. These results demonstrate the feasibility of quantitative imaging of the degradation state of implants with MRI. Further investigations on PLGA fibers with incorporated MNP and on phantoms must be performed in order to understand the mechanisms responsible for the induced changes of the MR signal and develop new analytical algorithms.

References

[1] E. Benrashid, C. C. McCoy, L. M. Youngwirth, J. Kim, R. J. Manson, J. C. Otto, and J. H. Lawson, "Tissue engineered vascular grafts: Origins, development, and current strategies for clinical application", *Methods*, vol. 99, pp. 13-19, 2016.

[2] H. Dahnke, W. Liu, D. Herzka, J. A. Frank, and T. Schaeffter, "Susceptibility Gradient Mapping (SGM): A New Postprocessing Method for Positive Contrast Generation Applied to Superparamagnetic Iron Oxide Particle (SPIO)-Labeled Cells", *Magnetic Resonance in Medicine*, vol. 60, pp. 595-603, 2008.

[3] C. Billotey, C. Wilhelm, M. Devaud, J. C. Bacri, J. Bittoun, and F. Gazeau, "Cell internalization of anionic maghemite nanoparticles: Quantitative effect on magnetic resonance imaging", *Magnetic Resonance in Medicine*, vol. 49, pp. 646-654, 2003.

Magnetic Nanoparticles Interact with and Pass an *in vitro* Blood-Placenta Barrier Model

E. K. Müller[1], C. Gräfe[1], F. Wiekhorst[2], S. Dutz[3], A. Hochhaus[1], J. H. Clement[1]

[1] *Klinik für Innere Medizin II, Abt. Hämatologie & Internistische Onkologie, Universitätsklinikum Jena, Am Klinikum 1, 07747 Jena, Germany; mail to: elena.mueller@med.uni-jena,de*
[2] *Physikalisch-Technische Bundesanstalt, Abbestrasse 2–12, 10587 Berlin, Germany*
[3] *Institut für Biomedizinische Technik und Informatik, Technische Universität Ilmenau, Gustav-Kirchhoff-Straße 2, 98693 Ilmenau, Germany*

Introduction

Research activities concerning the application of nanomaterials in medicine have rapidly increased in the last years. Especially superparamagnetic iron oxide nanoparticles (SPIONs) are of great interest for example as drug delivery agents or contrast agents in MRI scans due to their unique physiochemical properties and functionalization. A prerequisite for any application of SPIONs is the knowledge about the impact of these nanoparticles onto the human body, whereby the interaction with biological tissues and cells plays a decisive role. [1, 2]

In pregnant women, the blood-placenta barrier (BPB) segregates the maternal and the foetal blood supply and is important for the bidirectional transfer of important substances such as oxygen, nutrients and hormones. On one hand SPIONs applied to pregnant women might penetrate the BPB or disrupt its barrier integrity as off-target effect. On the other hand, nanomaterials, like SPIONs, might offer the opportunity to selectively target the pregnant woman, the foetus or the placenta for the treatment of various complications and diseases during pregnancy. For all of these situations, the behavior of the particles in the BPB concerning interaction and passage through the interface and possible teratogenic effects should be investigated in more detail. [3, 4]

In this study, an *in vitro* model of the BPB was established and optimized to study the interaction and passage of three differently charged SPIONs through this interface.

Methods

For the establishment of a co-culture *in vitro* BPB model, the human choriocarcinoma trophoblastic cell line BeWo as well as primary placental pericytes (hPC-pl) were used, that were seeded on the apical and the basolateral site of PET transwell membranes (pore size 3 µm), respectively. Optimization of the seeding density and incubation time was confirmed by investigation of the barrier integrity using different methods: histologic cross sections, measurement of the transepithelial electrical resistance (TEER) and the molecular permeability as well as immunohistochemical staining of adherence molecules *zonula occludens-1* (ZO-1) and β-catenin.

The *in vitro* model was incubated with differently charged SPIONs: neutral starch-coated (D), cationic polyethyleniminecoated (PEI) and anionic carboxymethyldextran-coated (CMX) particles. The interaction and the cytotoxicity of the SPIONs with the two cell types was investigated independently for both cell types with the PrestoBlue® assay, real time cell analysis (RTCA) using the xCELLigence system, flow cytometry and microscopic analyses. The particles' impact on the cellular barrier integrity of the *in vitro* BPB model was investigated by afore mentioned methods. The passage of the SPIONs through the BPB model was quantified by two highly sensitive methods: magnetic particle spectroscopy and atomic absorption spectroscopy.

Results and Discussion

For the establishment of an *in vitro* BPB model, the co-culture of BeWo cells with pericytes was compared to a BeWo mono-culture regarding the formation of a cellular barrier. For different BeWo seeding densities, histologic cross sections showed the formation of a tighter and thinner cell layer for the co-culture (Fig. 1). TEER measurements and molecular permeability assays confirm this observation by showing a 2- and 3-fold increase compared to the mono-culture. Additionally, the visualization of the cell-cell-contact proteins ZO-1 and β-catenin by immunological staining show an enhanced expression again supporting the barrier-enhancing effect of co-cultured BPB towards mono-culture systems.

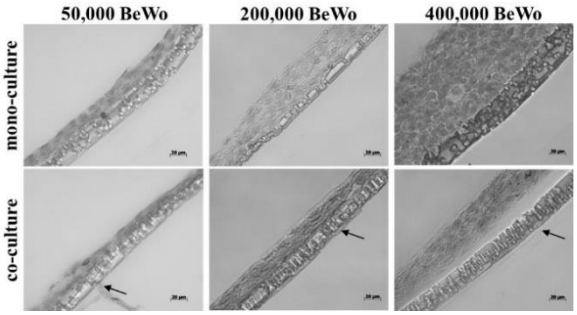

Figure 1: Histologic cross sections (15 µm) of the BPB transwell model (day 5 PS). The co-culture model (BeWo + pericytes) was compared to the BeWo mono-culture regarding different BeWo seeding densities. The basolateral pericyte cell layer is indicated by arrows. Cells were stained using Nuclear Fast Red.

Investigations of the cellular interaction and cytotoxicity of SPIONs with the two cell types revealed the influence of the particle charge and concentration, the incubation time as well as the cell type on these parameters. Especially cationic PEI-coated particles showed pronounced cytotoxicity and interaction capability especially in the pericytic cells.

The incubation of the transwell-based BPB model with the three different SPION types did not reveal major disruption of the barrier integrity, while a particle charge- and incubation time-dependent incorporation into the barrier's cell layers could be shown (Fig. 2). The quantification of the SPION distribution within the distinct compartments of the transwell BPB model showed that the BPB prevents the free passage of particles from the upper donor compartment into the lower acceptor compartment again confirming the high barrier integrity. However, minor amounts of particles in the range of 1 ng were detected in the lower compartment. Detection of SPIONs in the basolateral pericyte cell layer in the range of 4 ng indicates a transcellular passage of these particles through the BPB.

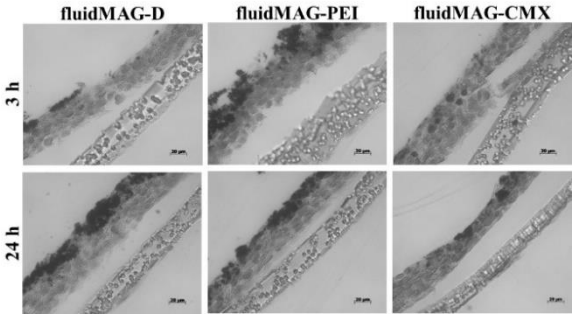

Figure 2: Histologic cross sections (15 µm) of the BPB transwell model (day 4/5 PS). Transwell models were incubated with 100 µg/cm^2 fluidMAG-D/PEI/CMX particles for 3 h or 24 h. Cells and SPIONs were stained using Nuclear Fast Red and Prussian Blue, respectively.

Conclusion

In conclusion, the established *in vitro* BPB model based on the co-culture of BeWo cells and pericytes on transwell inserts was shown to be a suitable model for the investigation of behavior and passage of SPIONs in this biological interface. Together with the possibility to sensitively quantify amounts of SPIONs in this model, a first prediction of the *in vivo* behavior of these particles is possible.

Acknowledgement

This work was supported by Deutsche Forschungsgemeinschaft (DFG) in the framework of the priority program 1681 (CL202/3-2, WI4230/8-2, DU1293/4-2).

References

[1] R.A. Revia, M. Zhang. *Materials Today*. **2016**, 19: 157-168
[2] K.M. Gharpure, S.Y. Wu, C. Li *et al., Clin Cancer Res*. **2015**, 21: 3121-2130
[3] C. Muoth, L. Aengenheister, M. Kucki *et al., Nanomedicine*. **2016**, 11:941-957
[4] T. Buerki-Thurnherr, U. von Mandach, P. Wick. *Swiss Med Wkly*. **2012**, 142:w13559

Magnetic tissue engineering of the vocal fold: generation of 3D cell constructs using superparamagnetic iron oxide nanoparticles

M. Pöttler,* E. Scheiber, [1]C. Bohr,[2] , M. Döllinger[2] , C. Alexiou,[1] S. Dürr[1,2]

[1] *Department of Otorhinolaryngology, Head and Neck Surgery, Section of Experimental Oncology and Nanomedicine (SEON), Else Kröner-Fresenius-Stiftungsprofessor, University Hospital Erlangen, Germany*
[2] *Department of Otorhinolaryngology, Head and Neck Surgery, Section of Phoniatrics and Pediatric Audiology, University Hospital Erlangen, Germany*

Introduction

The principles of biology and engineering are combined in tissue engineering to generate functional replacement for damaged tissue. Growing interest and new approaches in tissue engineering are promising solutions for overcoming the rejection of transplanted organs. Tissue engineering comprises the isolation of autologous cells from healthy tissue or stem cells, cultivation and proliferation of these cells and finally generation of 3D structures resembling natural tissue structures. Even though expertise of these methods in tissue engineering has been established, still there is scope for enhancement. In vivo tissue has complex cellular organization and defined arrangements of cells need to be established. Therefore, techniques to manipulate and remotely control cellular behavior can deliver a powerful tool for tissue engineering. Such a tool bargains Magnetic Tissue Engineering (MTE). [3,4] As the voice is the most important instrument of oral communication [1], tissue defects in this region lead to serious aggravation in quality of life. Hitherto, no satisfactory possibilities for vocal fold (VF) transplantation exist. [2] We aim for establishment of a functional VF transplant in a rabbit model by MTE using superparamagnetic iron oxide nanoparticles (SPION).

Methods

Rabbit vocal fold fibroblasts (VFF) were incubated for 24 h with different concentrations of SPIONs (20, 40 or 80 µg/cm^2). Vocal fold cell behavior under SPION treatment was tested extensively for adhesion, spreading and migration, which are important for formation of 3D structures. The possibility of magnetic guidance of SPION-loaded cells was tested in 2D. 1 x 10^5 SPION loaded VFFs were seeded in 6 well plates were a 24-well magnet plate was positioned below. Cells were allowed to adhesre for 24 h. To generate 3D VFF cell-constructs, 1 x 10^6 cells loaded with 20 µg/cm^2 SPIONs were placed in a 24- well plate with a magnet above to induce MTE.

Results

The effects of SPIONs on cell behavior were dose-dependent for adhesion, with good tolerability observed up to the nanoparticle concentration of 20 µg/cm^2, migration and spreading were not significantly influenced by SPION uptake up to 80 µg/cm^2. [6] Magnetically guidance of cells loaded with SPIONs was demonstrated in 2D with 20 and 40 µg/cm^2 with cells only growing in areas where a magnet is present. [5,6] (Fig.1) To establish a 3D structure of VFFs a magnet (0.7 T) was placed above the cell culture plate and cells loaded with 20 µg/cm^2 were able to form 3D cell construct after 24h. (Fig. 2)

Discussion

Here, we present first results of magnetic tissue engineering for voice rehabilitation. To develop 3D structures cell behavior must not be affected by SPION uptake. Therefore, cell features including adhesion, spreading and migration were proven to be intact after SPION treatment. As a proof of principle for magnetic cell guidance SPION loaded vocal

fold cells were allowed to "choose" either to grow on the side were a magnet or none was placed. Interestingly, 5 to 20 µg/cm^2 are sufficient to induce cell growth solitary at site of the magnet in 2D. Furthermore, magnetic cell guidance as only initiator for 3D cell formation was proven to work with very low amount of SPIONs. Next steps include the isolation of epithelial cell and establishment of 3D co-cultures, as well as the proof of functionality in a flow channel model of the rabbit larynx. Our results will constitute a solid basis for a successful transfer of this technique into humans, in order to provide an individual and personalized vocal fold implant. This is particularly important for patients, who suffer from dysphonia or even aphonia as a consequence of a vocal fold tissue defect, and will help to improve their quality of life.

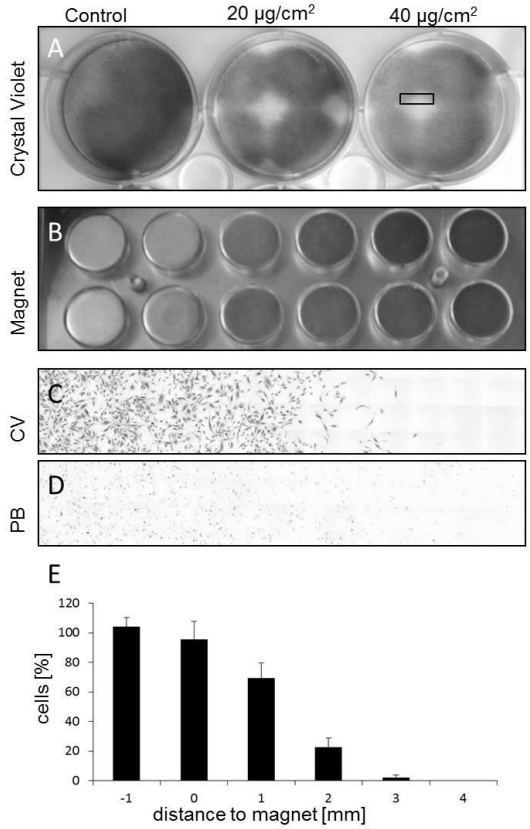

Fig. 1: 2D cell-control: A: Magnetic field induced VFF cell-growth ,control cells are not loaded with SPIONs, VFFs (SPION concentrations as indicated) only grow in magnetic zones. B: 24- well magnetplate. C und D: magnification of A (rectangle) with cells stained with Crystal Violet (C) and Prussian Blue (iron) (D). F: Cell concentrations of magnetisized VFFs in distance to magnet.

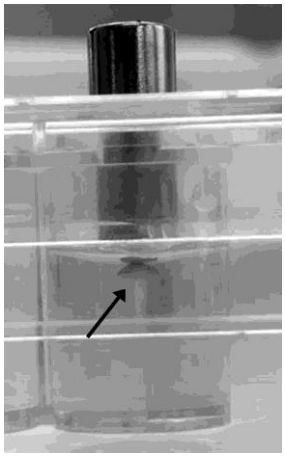

Fig. 2: 3D VFF cell construct (arrow) in 48 well plate after 24h. Magnet on top (outside of lid) retains magnet in well. Cells were incubated for 24 h with 20 µg/cm^2 SPION, before 1 x 10^6 cells were used for construct formation.

Acknowledgments

Deutsche Krebshilfe Nr.111332

References

[1] Rosanowski, F.; Grassel, E.; Hoppe, U.; Kollner, V. HNO 2009, 57, (9), 866-72.

[2] Ling, C.; Li, Q.; Brown, M. E., et al. Sci Transl Med 2015, 7, (314), 314ra187.

[3] Perea, H.; Aigner, J.; Heverhagen, J. T.; Hopfner, U.; Wintermantel, E. J Tissue Eng Regen Med 2007, 1, (4), 318-21.

[4] Horch, R. E.; Boos, A. M.; Quan, Y., et al. J Cell Mol Med 2013, 17, (10), 1197-206.

[5] Dürr S, Bohr C, Pöttler M, Lyer S, Friedrich RP, Tietze R, Döllinger M, Alexiou C, Janko C. Anticancer Res. 2016 Jun;36(6):3085-91.

[6] Pöttler M, Fliedner A, Schreiber E, Janko C, Friedrich RP, Bohr C, Döllinger M, Alexiou C, Dürr S.Nanoscale Res Lett. 2017 Dec;12(1):284.

The Life Cycle of Magnetic Nanoparticles: A Pharmaceutical Approach

M. Rabel[1], P. Warncke[1], J. Thamm[1], H.D. Kurland[2], C. Bergemann[3], C. Grüttner[4], D. Cialla-May[5], F.A. Müller[2], D. Fischer[1]

1 Friedrich Schiller University Jena, Department of Pharmaceutical Technology, Jena, Germany
2 Friedrich Schiller University Jena, Otto Schott Institute of Materials Research, Jena, Germany
3 chemicell GmbH, Berlin, Germany
4 micromod Partikeltechnologie GmbH, Rostock, Germany
5 Leibniz Institute of Photonic Technologies, Jena, Germany

Introduction

Iron oxide based magnetic nanoparticles (MNPs) for medical and pharmaceutical applications are usually coated with natural polymers such as starch or dextran. Besides possible biocompatibility concerns, the use of these MNPs is often limited due to their poor degradation behavior. Therefore, it is crucial to consider the whole life cycle of the MNP application.

Objectives

Consequently, MNPs with different natural, synthetic, and inorganic shell materials were tested throughout their entire life cycle, simulating the application as a MRI contrast agent (Fig. 1). The simulation started with the MNPs as they were synthesized, was continued with their storage and the injection process into the body associated with the formation of a biomolecule corona, and was completed with the aging and degradation of the MNPs.

Materials and Methods

The MNPs were characterized physicochemically regarding their hydrodynamic diameter, polydispersity index (PDI), surface charge and morphology using photon correlation spectroscopy, laser Doppler anemometry and electron microscopy. The storage stability was tested for up to 3 months in water, evaluating changes of these parameters. Moreover, the colloidal stability of the MNPs was tested in relevant test media (artificial lysosomal fluid, simulated body fluid, 5% glucose). The hemotoxicity was tested *in vitro*, using isolated sheep erythrocytes and *ex ovo* in a hen´s egg model (HET-CAV) [1]. The MNPs were aged and degraded in artificial lysosomal fluid (ALF, pH 4.5), simulating the conditions in lysosomes as well as in simulated body fluid (SBF, pH 7.4), representing the plasma compartment, over a period of up to 28 days. MNP degradation was analyzed by iron quantification and infrared spectroscopy.

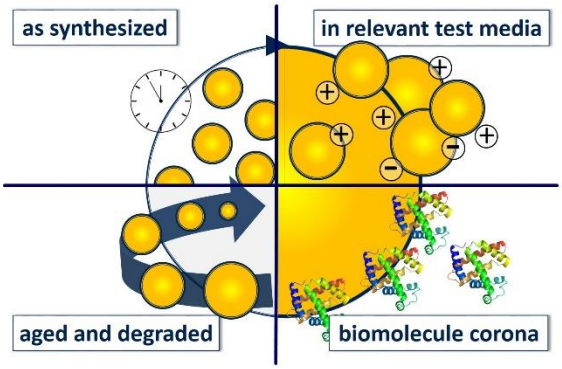

Fig. 1: The life cycle of magnetic nanoparticles (MNPs) for pharmaceutical and medical applications.

Results

All MNPs showed comparable hydrodynamic diameters of 150-200 nm with varying surface charges depending on the shell material. The aqueous MNP dispersions were stable over 3 months. The MNPs displayed a controllable colloidal stability in

relevant test media. Neutral MNPs were stable in all media, whereas charged MNPs tended to agglomerate in the presence of ions. MNP hemotoxicity was dependent on the surface characteristics of the MNPs with cationic MNPs being more toxic than others. A modification with a model protein corona (serum albumin) decreased the hemotoxic effects. To assess the biodegradation behavior of MNPs ALF and SBF were used, since they exhibit advantages compared to usually used citric acid buffers as they have a similar salt composition and pH value as in the *in vivo* situation. In SBF, all MNPs stayed stable over 28 days without iron mobilization from the core. No changes in the core/shell composition could be detected by electron microscopy and infrared spectroscopy. In contrast, in ALF all MNPs degraded in dependence on the biodegradability (natural > inorganic), water permeability, as well as acid/base character (basic > neutral > negative) of the shell material as it was shown by iron quantification. All organic coated MNPs fully degraded after 28 days, in contrast to the inorganic coated (silica) MNPs. Moreover, infrared spectroscopy indicated that MNP degradation was linked to a loss or degradation of the surface coating.

Conclusion

In conclusion, the surface characteristics of MNPs play an important role in the stability, hemotoxicity and biodegradation behavior of MNPs. This confirms the importance of a complete life cycle testing of MNPs.

Acknowledgments

The authors would like to thank M. Lucanus, L. Michel and J. Grabow for their excellent technical assistance. We acknowledge the Federal Ministry of Education and Research (project 03XP0003) for financial support.

Reference

[1] Schlenk F, Werner S, Rabel M, et al.: Archives of Toxicology **2017**, 1-16. doi: 10.1007/s00204-017-1968-z

Optical detection and biological characterization of magnetic particles using an *ex ovo* model

P. Warncke[1], R. Müller[2], O. Stranik[2], C. Bergemann[3], W. Fritzsche[2], D. Fischer[1]

[1] *Department of Pharmaceutical Technology, Institute of Pharmacy, Friedrich-Schiller-University Jena, Otto-Schott-Str. 41, 07745 Jena, Germany*
[2] *Leibniz Institute of Photonic Technology, Department of Nanobiophotonics, Albert-Einstein-Str. 9, 07745 Jena, Germany*
[3] *Chemicell GmbH, Eresburgstr. 22-23, 12103 Berlin, Germany*

Introduction

Iron oxide nanoparticles attracting high interest in medical applications as contrast agents, hyperthermia or magnetic drug targeting. Since the degradation of iron oxide particles is slow, the cytotoxicity of these particles is an intensively investigated parameter preferentially tested in cell cultures. Only limited information is available in 3D settings, especially under dynamic flow conditions in the blood stream. To mimic the complex *in vivo* situation, the hen's egg test offers a dynamic planar vascular network system, accessible by optical microscopy, for investigations after systemic particle injection.

Methods

Different magnetic fluorescent iron oxide particles or magnetic silica beads with varying surface characteristics were investigated regarding their flow characteristics and optical properties. Hemocompatibility was tested in a red blood cell assay. Optical investigations were performed using hen's egg chick area vasculosa (CAV) *in vivo*. Briefly, fertilized eggs were incubated for 72 h and transferred into petri dishes to obtain the planar vascular network. After systemic injection of the particles into the vitelline vein, the screening of the particle flow was performed under an optical microscope connected to a camera (AxioImager Z1.m, Carl Zeiss, Jena), operated in the dark field scattering or the fluorescence mode. A magnetic field was induced by a cylindrical NdFeB magnet or a Helmholtz coil setting next to the objective. Data analysis was realized with the image processing package Fiji and the SPT plugin TrackMate.

Results

Due to its planar surface, the hen's egg chick area vasculosa allowed the optical inspection of the whole blood vessel system. Fluorescent particles with emission wavelengths of the dye >500 nm and a particle size of 1 µm (in combination with a 10x objective) were optimal for optical detection due to the background fluorescence of the embryonic tissue. The hemocompatibility testing of these particles indicated their suitability for systemic administration. Despite different surface characteristics none of the particles showed disturbance of the erythrocyte membrane nor erythrocyte aggregation *in vitro*, whereas *in vivo* particle agglomeration in the vessels of the CAV was observed for particles without additional surface coatings. Tracking analysis in the presence of a magnetic field showed an increased hydrodynamic resistance that led to a decreased velocity and an increased particle size, indicating particle agglomeration. After removal of the magnetic field a partial disintegration could be observed. As *in vitro* in microfluidic channels these effects were not detectable they were suggested as surface interactions of particles with the complex blood environment. In conclusion, the shell less

hen’s egg test offers an entire optical accessible vascular network for dynamic observations of the particle flow in complex biological media and to study the effect of the particle behavior in the presence of a magnetic field.

Acknowledgments

The work was supported by the Federal Ministry of Education and Research (BMBF 03XP0003 - NanoBEL).

Influence of Sterilisation and Preservation Procedures on the Integrity of Protein Coated Magnetic Nanoparticles

A. Weidner[1], S. Wojahn[1], C. Gräfe[2], J.H. Clement[2], S. Dutz[1]

[1] *Institut für Biomedizinische Technik und Informatik (BMTI), Technische Universität Ilmenau*
[2] *Klinik für Innere Medizin II, Abteilung Hämatologie und Internistische Onkologie, Universitätsklinikum Jena*

Introduction

For a potential application of protein coated magnetic nanoparticles (MNP) in animals or humans, one has to guarantee that the particles are free from biological pathogens or any biological contamination. Additionally, after this sterilisation, it is important to bring the particles into a condition, which makes them storable for several weeks. For these purposes, several procedures like freezing, lyophilisation, autoclaving, and UV sterilisation were evaluated with regard to their effect on the composition of the protein coating.

Methods

The iron oxide MNP were prepared as described before [1]. To produce the protein coating, the particles were incubated at 37°C for 10 min in fetal calf serum (FCS) serving as natural protein source. Afterwards they have been magnetically washed with distilled water and possible aggregates have been dispersed by ultrasonication [2].
The prepared protein-coated MNP have been applied to the following preservation and sterilisation methods:

- freezing at -15°C
- deep freezing at -80°C
- lyophilisation (with and without PEG or TMAH as additives)
- autoclaving (121°C for 20 min)
- UV-sterilisation ($\lambda \sim 200$ - 280 nm for 150 to 240 min).

Possible effects on the particles and protein coating like degradation, agglomeration or cross-linking have been investigated by size measurement via dynamic light scattering (DLS). Additionally, the zeta potential was used as an indicator for surface protein amount and composition [3]. To determine the composition of the protein coating, a sodium dodecyl sulfate polyacrylamide gel electrophoresis (SDS-PAGE) and a grey value intensity analysis by means of ImageJ [4] was performed.

Results

After freezing at -15°C and thawing the sample after two, four and six weeks, DLS shows a significant agglomeration for all storing times. Results of SDS-PAGE reveal an increase in smaller sized proteins, which may be due to the degradation of high-molecular weight proteins. The zeta potential is stable at -30 mV. For deep freezing at -80°C the agglomeration does not appear, but similar degradation effects can be observed. Therefore, both methods are rated as improper for a long-term storage of protein coated MNP.
The lyophilisation of protein coated MNP with PEG as additive and re-dispersion after one, three and six weeks leads for all respective times to a similar particle size and particle size distribution compared to the original sample, whereas the plain particles show slight agglomeration. The TMAH-added samples show instability and big agglomerates as well as a fraction of very small protein fragments. This behaviour was confirmed by zeta potential measurements and SDS-PAGE. A protein degradation of the protein coating on the surface of the MNP could be concluded for these samples.
During autoclaving, the results for DLS and the zeta potential of the samples did not change significantly, but SDS-PAGE reveals damages of the entire integrity of the proteins. All typical peaks are vanished and only one large agglomeration in the region of 55 kDa can be observed, what is a clear

indication for the denaturation and extensive degradation of the proteins in the coating. Resulting from these findings it can be stated that, the standard autoclaving protocol is not suitable for the sterilisation of protein coated magnetic nanoparticles since a degradation of the corona proteins occurs.

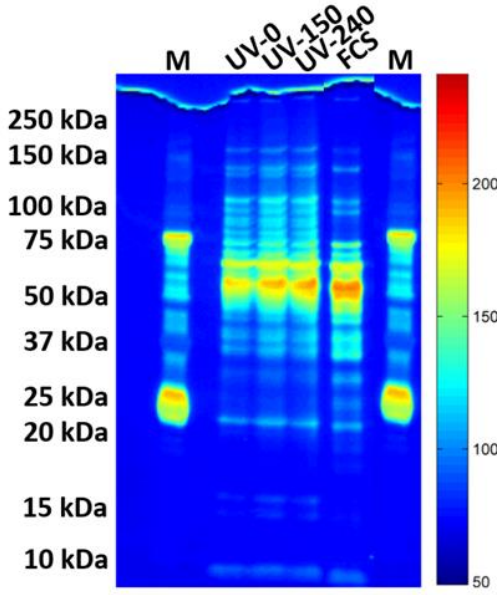

Figure 1: SDS-PAGE of original sample (UV-0) as well as samples exposed to UV radiation for 150 minutes (UV-150) or 240 minutes (UV-240).

After UV sterilisation for 150 and 240 min a stable zeta potential of -30 mV as well as very similar results for SDS-PAGE show, that there are no major changes in composition and amount of the protein coating (see Fig. 1). Resulting from all these findings it can be concluded, that the exposure to UV radiation of 200-280 nm for up to 240 minutes, causes no relevant change of protein content and composition. Thus, the UV sterilisation is a suitable procedure for the sterilisation of protein coated magnetic nanoparticles.

Conclusion

We could show that freezing and deep freezing lead to the degradation of large proteins and agglomeration. Thus, they are only suitable for short term storage. Autoclaving is not suitable at all, as it damages the integrity of the proteins of the protein corona.
In conclusion, only UV sterilisation and lyophilisation were suitable for sterilisation and conservation of the protein coated MNP.

Acknowledgements

This work was supported by Deutsche Forschungsgemeinschaft (DFG) via SPP 1681 (FKZ: DU 1293/4-2, CL202/3-2).

References

[1] S. Dutz, J.H. Clement, D. Eberbeck, Th. Gelbrich, R. Hergt, R. Müller, J. Wotschadlo, M. Zeisberger. Ferrofluids of magnetic multicore nanoparticles for biomedical applications. J. Magn. Magn. Mater. 2009, 321/10, 1501–1504

[2] A. Weidner, C. Gräfe, M. v.d. Lühe, H. Remmer, J.H. Clement, D. Eberbeck, F. Ludwig, R. Müller, F.H. Schacher, S. Dutz. Preparation of Core-Shell Hybrid Materials by Producing a Protein Corona around Magnetic Nanoparticles. Nanoscale Research Letters 2015, 10, 282

[3] C. Gräfe, A. Weidner, M. v.d. Lühe, C. Bergemann, F.H. Schacher, J.H. Clement, S. Dutz. Intentional formation of a protein corona on nanoparticles: Serum concentration affects protein corona mass, surface charge, and nanoparticle–cell interaction. Int J Biochem Cell Biol., 2016, 75, 196-202

[4] Schneider, C.A., Rasband, W.S. & Eliceiri, K.W. NIH Image to ImageJ: 25 years of image analysis. Nat. Methods, 2012, 9, 671–675

Long-term Stable Measurement Phantoms for Quantitative Magnetic Particle Imaging

L. Wöckel[1], V.C. Behr[2], C. Grüttner[3], O. Kosch[4], A. Mattern[1], P. Vogel[2,5], J. Wells[4], F. Wiekhorst[4], S. Dutz[1]

[1] *Institute of Biomedical Engineering and Informatics (BMTI), Technische Universität Ilmenau, Ilmenau*
[2] *Department of Experimental Physics 5 (Biophysics), University of Würzburg, Würzburg*
[3] *micromod Partikeltechnologie GmbH, Rostock*
[4] *Physikalisch-Technische Bundesanstalt Berlin, Berlin*
[5] *Department of Diagnostic and Interventional Radiology, University Hospital Würzburg, Würzburg*

Introduction

Since the first description of the MPI principle in 2005 [1], a variety of laboratory MPI scanners have been reported at locations all over the world [2]. In 2014 the first commercial scanners were brought onto the market by Bruker Biospin. These scanners enable the reconstruction of the spatial distribution of magnetic nanoparticles (MNP) within tissue, which is of major importance for many applications of MNP in biomedicine.

To enable researchers to explore the potential of this promising novel imaging modality, the detection limits and image resolutions of the present MPI scanners have to be assessed as major performance determining parameters. For this, well-defined and comparable magnetic structures are needed to perform comparison studies between the MPI setups of different laboratores. Up to now, each laboratory uses its own measurement phantoms [3, 4]. Mostly, these phantoms consist of MNP at a certain concentration filled into containers of different volume. Such phantoms often exhibit no long-term stability, and thus do not allow ring test studies between different labs and scanners. In this study, we developed dedicated phantoms to monitor and assess relevant imaging properties of an MPI scanner. In particular, the spatial resolution, the capability for MNP quantification of and furthermore, the long-term behavior of the used MNP-matrix combinations are addressed.

Methods

First, we aimed to establish combinations of MNPs and matrix materials suitable for the preparation of such phantoms. The main requirements for these combinations are good imaging properties of the tracer particles used, and a homogenous and agglomeration-free distribution of these particles within the selected matrix. Ideally, this matrix is long-term stable and guarantees a constant image quality of the designed phantoms over a long time period. For these studies, the following MNP types were used

- FeraSpin-R, nanoPET-Pharma Berlin
- fluidMag-D50, chemicell Berlin
- Ferucarbotran, Meito Sangyo. Co. Nagoya, Japan
- Perimag, micromod Partikeltechnologie Rostock
- SEON^{LA}, SEON Erlangen

and the synthetic polymer Elastosil (RT 604, Wacker Chemie AG) was tested for its suitability in the preparation of dedicated measurement phantoms. The obtained combinations were checked for their mechanical stability by means of mechanical load tests (shore-A). The homogeneity of MNP distribution within the matrix was determined by optical investigation of the samples with a microscope. The influence of embedding the MNP in a polymer matrix on the MPI performance of the particles was tested by means of MPS. The most promising MNP-

matrix combination was used to manufacture measurement objects of different shape (cylinders, cubes) and different size embedded in a phantom matrix with an overall geometry of a cylinder with D = 50 mm and H = 60 mm. The resulting test phantoms were evaluated for their suitability to simulate MNP loaded areas within a nonmagnetic matrix by means and MPI at PTB (Bruker BioSpin preclinical MPI-scanner) and University of Würzburg (Traveling-Wave MPI) [5].

Results

The transfer of MNP from aqueous suspensions into organic silicones was a challenging and critical part of the phantom preparation. We established a procedure by using ethanol or isopropyl for this transfer, resulting in no alteration of the mechanical properties (shore-A) of the Elastosil.

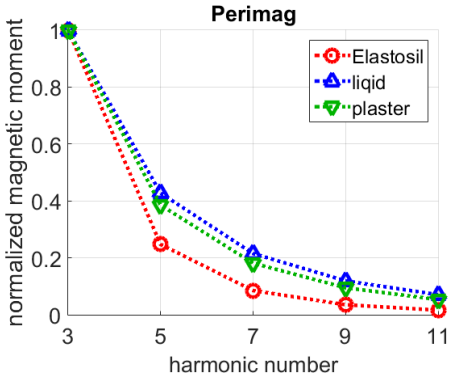

Figure 1: MPS measurements of Perimag embedded into different materials.

The MPS measurements revealed a decrease of the higher harmonics after embedding the MNP into the polymer (see figure 1). This is explained by an immobilization of the particles in the matrix, which inhibits the Brown rotation of the particles. For smaller particles (SEON^{LA}, fluidMag-D50) which show a smaller proportion of Brownian contribution, this decrease is less pronounced. In repeated MPS measurements, no changes of the magnetic properties were found for all particle types immobilized in Elastosil, and thus they show a long-term stable behavior for up to now six months.

From all tested materials, the combination Perimag/Ethanol/Elastosil was the most promising one regarding long-term stability and signal performance and was used for the preparation of the phantoms. The imaging of the prepared phantoms was successful down to a Fe-concentration of 10 mmol(Fe)/l, and reconstruction quality increased with increasing concentration, which will be demonstrated in the presentation.

Conclusions

In summary, we have developed suitable combinations of MNP and Elastosil for the manufacture of long-term stable MPI phantoms. The prepared phantoms show constant magnetic and mechanical properties for the duration of the study and can be imaged by MPI. Ongoing work is focused on more structured measurement phantoms.

Acknowledgments

The authors thank M.Sc. Mathias Fritz (TU Ilmenau) for assistance during microscopy. This work was supported by Deutsche Forschungsgemeinschaft (FKZ: DU 1293/6-1 and TR408/9-1).

References

[1] B. Gleich, and R. Weizenecker, Nature, vol. 435, no. 7046, pp. 1214-1217, Jun 30, 2005.

[2] N. Panagiotopoulos, R. L. Duschka, M. Ahlborg et al., International journal of nanomedicine, vol. 10, pp. 3097-114, 2015.

[3] T. Knopp, and T. Buzug, Magnetic Particle Imaging: An Introduction to Imaging Principles and Scanner Instrumentation, Berlin Heidelberg Springer-Verlag, 2012.

[4] J. J. Konkle, P. W. Goodwill, O. M. Carrasco-Zevallos et al., IEEE Transactions on Medical Imaging, vol. 32, no. 2, pp. 338-347, Feb, 2013.

[5] Vogel et al. Traveling wave Magnetic Particle Imaging, IEEE TMI, 33(2), 400-7, 2014.

Meltable magnetic biocomposites for controlled release

Mengbo Zhou[1], Robert Müller[2], Andrea Dellith[2], Thomas Heinze[1]

1 Institute of Organic Chemistry and Macromolecular Chemistry, Friedrich Schiller University of Jena, Humboldtstraße 10, D-07743 Jena, , Germany.
2 Leibniz-Institute of Photonic Technology. (IPHT), P.O.B. 100239, D-07702 Jena, Germany.

This work proofs the principle of using meltable polysaccharide based biopolymer as a magnetically remote controlled matrix for drug release. A biocompatible composite from a meltable polysaccharide ester and functional nanoparticles is developed, which can be softened under an induced alternating magnetic field (AMF). Thus, it allows a release of active pharmaceutical ingredients. These systems could be suitable alternative path compared to hydrogel composites embedded with magnetic particles as remote controlled biomaterials [1].
A new approach towards the fabrication of biocompatible composites suitable for remote melting is presented. For that purpose, fatty acid esters of dextran with adjustable melting points in the range of 30 to 140 °C were synthesized. Esterification of the polysaccharide by activation of the fatty acids with iminium chloride guaranteed mild reaction conditions leading to high quality products as confirmed by FTIR- and NMR spectroscopy as well as by gel permeation chromatography [2]. A method for the preparation of magnetically responsive bionanocomposites was developed consisting of combined dissolution/suspension of the dextran ester and oleic acid hydrophobized magnetite nanoparticles (MNPs) in an organic solvent followed by homogenization with ultrasonication, casting of the solution, drying, and melting of the composite for a defined shaping. This process leads to a uniform distribution of MNPs in nanocomposite as revealed by scanning electron- and optical microscopy [3].
Green fluorescent protein (GFP) and Rhodamine B (RhB) were loaded separately as model drugs in the composite disks (Fig. 1). The thermoplastic property of magnetic composite makes the fabrication to desired geometry like casting method possible. The application of an AMF heated the magnetic particles and resulted in a temperature increase above the melting range that leads to an increased diffusion of model drugs (Fig.2).

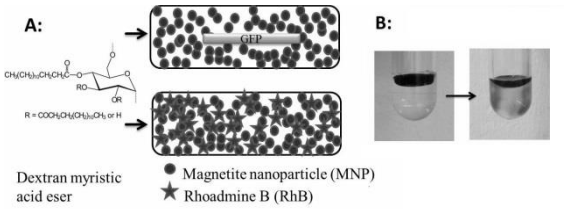

Fig. 1. **A**: Scheme of magnetic biocomposite from magnetite nanoparticle and dextran myristic acid ester containing green fluorescence protein or Rhodamine B, **B**: Gradual heating generated with an AC field resulting in release of RhB

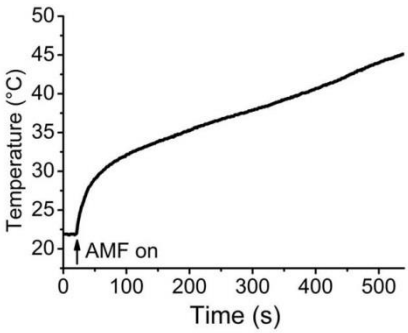

Fig. 2. Temperature increase (measured with a fiber optical sensor) in the biocomposite disk (1 wt.% MNP) surrounded by 0.5 mL water and subjected to continuous alternating magnetic field (20 kA/m, 400 kHz).

It is shown that the application of an AMF can accelerate continuously the diffusion of RhB from the composite. A steady increase of released RhB was found by treatment at 42°C. In comparison to the external heat-

ing in water bath, AMF generates heating inside of magnetic composite. Three cycles of AMF heating has doubled the amount of released RhB compared to control samples (Fig. 3). The GFP composite design is different from the RhB composite (Fig. 2). The GFP can be blocked in the composite, when no external stimulus was applied. The release started after the sample was heated in the water bath at 45°C. The reason is that the GFP cannot penetrate the polymer layer (approx. 1 mm thickness) when the polymer is in solid state [4]. The application of AMF can lead to a continuous release of GFP from the composite and induces a release of a stepwise accelerating behavior (Fig. 4).

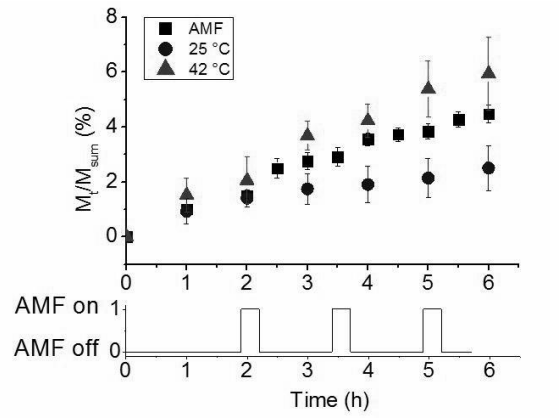

Fig.3. Cumulative released mass of Rhodamine B from composites in 6 hours; squares, 1 wt.% MNP under exposure to alternating magnetic field for 12 min duration; triangles, 1 wt.% MNP, heated externally at 42°C and circles, 1 wt.% MNP, control sample at 25°C in phosphate buffered saline. M_t represents the cumulative mass released at time t. M_{sum} represents the total mass loaded.

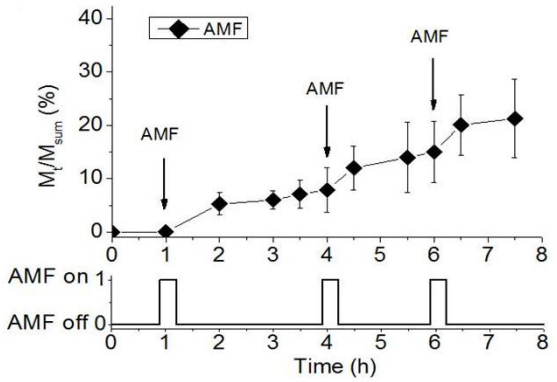

Fig.4. Cumulative released mass of green fluorescent protein (1 wt.% MNP under exposure to alternating magnetic field for 12 min interval) in phosphate buffered saline. M_t represents the cumulative mass released at time t. M_{sum} represents the total mass loaded.

Conclusion

The release behavior of meltable and biocompatible nanocomposites loaded with model drugs under alternating magnetic field was studied. The novel composite can be potentially applied as drug carrier in the field of controlled release applications.

Acknowledgments

The financial support of the German Science Foundation (DFG, priority program SPP 1681, contracts HE2054/14-2 and MU2382/4-2) is acknowledged.

References

[1] N. S. Satarka, J. Z. Hilt, Acta Biomater. 4, 11-16, 2008.

[2] T. Liebert, J. Wotschadlo, P. Laudeley, T. Heinze, Biomacromolecules 12, 3107-3113, 2011.

[3] M. Zhou, T. Liebert, R. Müller, A. Dellith, C. Gräfe, J. H. Clement, T. Heinze, Biomacromolecules 16, 2308-2015, 2015.

[4] R. Müller, M. Zhou, A. Dellith, T. Liebert, T. Heinze, J. Magn. Magn. Mater. 431, 289-293, 2017.

List of Participants

Christoph Alexiou

Universityhospital Erlangen
ENT-Clinic, Section of Experimental Oncology and Nanomedicine (SEON)

Waldstrasse 1
91054 Erlangen
E-mail: christoph.alexiou@uk-erlangen.de

Günter K. Auernhammer

Max Planck Institute for Polymer Research
Physics at Interfaces

Ackermannweg 10
55128 Mainz
E-mail: auhammer@mpip-mainz.mpg.de

Christoph Balceris

TU Braunschweig
Institut für Elektrische Messtechnik und Grundlagen der Elektrotechnik

Hans-Sommer-Str. 66
38106 Braunschweig
E-mail: c.balceris@tu-bs.de

Olga Baun

University of Mainz
Physics

Staudingerweg 7
55099 Mainz
E-mail: obaun@uni-mainz.de

Tatiana Becker

Technische Universität Ilmenau
Technical Mechanics Group

Max-Planck-Ring 12
98693 Ilmenau
E-mail: tatiana.becker@tu-ilmenau.de

Silke Behrens

Karlsruher Institut für Technologie
Institut für Katalyseforschung und -technologie

Hermann-von-Helmholtz-PLatz 1 1
76344 Eggenstein-Leopoldshafen
E-mail: silke.behrens@kit.edu

Peter Blümler

University of Mainz
Physics

Staudingerweg 7
55099 Mainz
E-mail: bluemler@uni-mainz.de

Dmitry Borin

TU Dresden
George-Baehr-Str. 3
1069 Dresden
E-mail: dmitry.borin@tu-dresden.de

Helmut Brand

Universitaet Bayreuth
Physik

Universitaetsstr 30
95440 Bayreuth
E-mail: brand@uni-bayreuth.de

Joachim Clement

Jena University Hospital
Hematology / Oncology

Am Klinikum 1
7747 Jena
E-mail: joachim.clement@med.uni-jena.de

Johanna Demut

Universitätsklinikum Jena
Abteilung Hämatologie und internistische Onkologie

Am Klinikum 1
7747 Jena
E-mail: johanna.demut@med.uni-jena.de

Eike Dohmen

Technische Universität Dresden
Chair of Magnetofluiddynamics, Measuring and Automation Technology

George-Bähr-Str. 3
1099 Dresden
E-mail: eike.dohmen@tu-dresden.de

Sebastian Draack

TU Braunschweig
Inst. f. Elektr. Messtechnik u. Grdl. d. Elektrotechnik

Hans-Sommer-Straße 66
38106 Braunschweig
E-mail: s.draack@tu-bs.de

Silvio Dutz

TU Ilmenau
Gustav-Kirchhoff-Straße 2
98693 Ilmenau
E-mail: silvio.dutz@tu-ilmenau.de

Ekateina Elfimova

Ural Federal University
Lenin 51
620000 Ekaterinburg
Russia
E-mail: Ekaterina.Elfimova@urfu.ru

Birgit Fischer

Universität Hamburg
Physikalische Chemie

Grindelallee 117
20146 Hamburg
E-mail: birgit.fischer@chemie.uni-hamburg.de

Ralf Friedrich

HNO-Klinik / Universitätsklinikum Erlangen
SEON

Glückstrasse 0
91054 Erlangen
E-mail: r.p.friedrich@gmx.de

Lisa Fruhner

Forschungszentrum Jülich GmbH
Jülich Centre for Neutron Science

Wilhelm-Johnen-Strasse 1
52428 Jülich
E-mail: l.fruhner@fz-juelich.de

Philipp Gebhart

TU Dresden
IFKM

George-Bähr-Str. 0
1069 Dresden
E-mail: gebhart.philipp@googlemail.com

Philipp Globig

Universitätsklinikum Jena
Klinik für Innere Medizin II, Abt. Hämatologie & Internistische Onkologie

Am Klinikum 1
7747 Jena
E-mail: philipp.globig@med.uni-jena.de

Christine Gräfe

Universitätsklinikum Jena
Hämatologie & Internistische Onkologie

Am Klinikum 1
7747 Jena
E-mail: christine.graefe@med.uni-jena.de

Micha Gratz

Universität des Saarlandes
Campus 0
66123 Saarbrücken
E-mail: micha.gratz@uni-saarland.de

Thomas Gundermann

Institute of Fluid Mechanics/ TU-Dresden
Magnetofluiddynamics, Measuring and Automation Technologies

George-Bähr-Str. 3
1069 Dresden
E-mail: thomas.gundermann@tu-dresden.de

Martin Hähsler

Karlsruhe Institute of Technology
Institute of Catalysis Research and Technology (IKFT)

Hermann-von-Helmholtz-Platz 1
76344 Eggenstein-Leopoldshafen
E-mail: martin.haehsler@kit.edu

Melissa Hermes

Institute of Physical Chemistry Cologne
Department of Chemistry

Luxemburgerstr. 116
50939 Köln
E-mail: melissa.hermes@uni-koeln.de

Stephan Hinrichs

University of Hamburg
Physical Chemistry

Grindelallee 117
20146 Hamburg
E-mail: stephan.hinrichs@chemie.uni-hamburg.de

Patrick Ilg

University of Reading
Department of Mathematics and Statistics

Whiteknights 0
0 Reading
United Kingdom
E-mail: p.ilg@reading.ac.uk

Thomas Ilzig

Technische Universität Dresden
Chair of Magnetofluiddynamics, Measuring and Automation Technology

George Bähr Straße 3
1069 Dresden
E-mail: thomas.ilzig@tu-dresden.de

Larisa Iskakova

Urals Federal University
Mathematical physics

Lenina ave. 51
620083 Ekaterinburg
Russia
E-mail: Larisa.Iskakova@urfu.ru

Alexey Ivanov

Ural Federal University
Department of Mathematical Physics

Lenin Av. 51
620000 Ekaterinburg
Russian Federation
E-mail: Alexey.Ivanov@urfu.ru

Karl Alexander Kalina

Institute of Solid Mechanics / TU Dresden
Chair of Computational and Experimental Solid Mechanics

George-Bähr-Straße 0
1069 Dresden
E-mail: karl.kalina@tu-dresden.de

Karin Koch

University of Cologne
Department for Physical Chemistry

Luxemburger Str. 116
50939 Köln
E-mail: karin.koch@uni-koeln.de

Patrick Kreissl

ICP, Universität Stuttgart
Allmandring 3
70569 Stuttgart
E-mail: pkreissl@icp.uni-stuttgart.de

Matthias Kundt

Universität zu Köln
Institut für physikalische Chemie, Department für Chemie

Luxemburger Straße 116
50939 Köln
E-mail: matthias.kundt@uni-koeln.de

Stefan Lampaert

Delft University of Technology
Mekelweg 2
0 Delft
The Netherlands
E-mail: s.g.e.lampaert@tudelft.nl

Joachim Landers

Universität Duisburg-Essen
Lotharstr. 1
47057 Duisburg
E-mail: joachim.landers@uni-due.de

Adrian Lange

TU Dresden
Lehrstuhl für Magnetofluiddynamik

George-Bähr-Straße 3
1062 Dresden
E-mail: adrian.lange@tu-dresden.de

Maik Liebl

Physikalisch-Technische Bundesanstalt
Abbestrasse 43071
10587 Berlin
E-mail: maik.liebl@ptb.de

Modesto T Lopez-Lopez

University of Granada
Applied Physics

Campus de Fuentenueva 0
18071 Granada
Spain
E-mail: modesto@ugr.es

Niklas Lucht

Institute of Physical Chemistry
University of Hamburg
Chemistry

Grindelallee 117
20146 Hamburg
E-mail: niklas.lucht@chemie.uni-hamburg.de

Frank Ludwig

TU Braunschweig
Institut für Elektrische Messtechnik und Grundlagen der Elektrotechnik

Hans-Sommer-Str. 66
38106 Braunschweig
E-mail: f.ludwig@tu-bs.de

Stefan Lyer

Universitätsklinikum Erlangen
ENT-Department, Section of Experimental Oncology and Nanomedicien

Glückstraße 0
91054 Erlangen
E-mail: stefan.lyer@uk-erlangen.de

Yeimy Mabel Martinez Triana

Universität zu Köln
Department of Chemie

Luxemburger Str. 116
0 Cologne
E-mail: ymartin1@smail.uni-koeln.de

Andreas Menzel

Heinrich Heine University Dusseldorf
Theoretical Physics II: Soft Matter

Universitätsstraße 1
40225 Düsseldorf
E-mail: menzel@hhu.de

Benedikt Mues

RWTH Aachen University
Applied Medical Engineering

Pauwelsstr. 20
52074 Aachen
E-mail: benedikt.mues@rwth-aachen.de

Robert Müller

IPHT Jena
Albert-Einstein-Str. 9
7745 Jena
E-mail: robert.mueller@ipht-jena.de

Annemarie Nack

Universität Rostock
Chemie

Dr. Lorenz Weg 2
18059 Rostock
E-mail: Annemarie.Nack@uni-rostock.de

Ekaterina Novak

Ural Federal University
Lenina St. 51
620000 Ekaterinburg
Russia
E-mail: ekaterina.novak@urfu.ru

Stefan Odenbach

TU Dresden
Magnetofluiddynamics, Measuring and Automation Technology

George-Bähr-Str. 3
1062 Dresden
E-mail: stefan.odenbach@tu-dresden.de

Hendrik Paysen

Physikalisch-Technische Bundesanstalt (PTB)
8.23 Metrology for Magnetic Nanoparticles

Abbestraße 43071
10587 Berlin
E-mail: hendrik.paysen@ptb.de

Tilen Potisk

University of Bayreuth
Theoretical Physics III

Universitaetsstrasse 30
95440 Bayreuth
E-mail: tilen.potisk1@gmail.com

Marina Pöttler

HNO-Kinik Erlangen
Sektion für experimentelle Onkologie und Nanomedizin (SEON)

Glückstr. 0
91054 Erlangen
E-mail: marina.poettler@uk-erlangen.de

Elena Pyanzina

Ural Federal University
Lenin av. 51
620000 Ekaterinburg
Russia
E-mail: elena.pyanzina@urfu.ru

Martin Rabel

Friedrich-Schiller-University Jena
Pharmaceutical Technology

Otto-Schott-Straße 41
7745 Jena
E-mail: martin.rabel@uni-jena.de

Bart Jan Ravoo

Westfälische Wilhelms-Universität Münster
Organisch-Chemisches Institut

Corrensstrasse 40
48149 Münster
E-mail: b.j.ravoo@uni-muenster.de

Hilke Remmer

TU Braunschweig
Institut für Elektrische Messtechnik und Grundlagen der Elektrotechnik

Hans-Sommer-Str. 66
38106 Braunschweig
E-mail: h.remmer@tu-bs.de

Pedro A. Sanchez

University of Vienna
Computational Physics, Faculty of Physics

Sensengasse 43313
1090 Vienna
Austria
E-mail: pedro.sanchez@univie.ac.at

Sarah Schatte

Technische Universität Berlin
Physikalische Chemie / Molkeulare Materialwissenschaften

Straße des 17. Juni 124
10623 Berlin
E-mail: s.schatte@tu-berlin.de

Philipp Scheerer

Universitätsklinikum Jena
Klinik für Innere Medizin 2 Unive

Am Klinikum 1
7747 Jena
E-mail: Philipp.Scheerer@med.uni-jena

Henrik Schmidt

Max-Planck-Institut für Polymerforschung Mainz
Ackermannweg 10
55116 Mainz
E-mail: schmidt@mpip-mainz.mpg.de

Malte Schümann

Technische Universität Dresden
Chair of Magnetofluiddynamics, Measuring and Automation Technology

George-Bähr-Str. 3
1069 Dresden
E-mail: Malte.Schuemann@tu-dresden.de

Julian Seifert

Universität zu Köln
Chemie, Physikalische Chemie

Luxemburger Straße 116
50939 Köln
E-mail: julian.seifert@uni-koeln.de

Ahmad Shaaban

Institut für physikalische chemie/Universität zu Köln
Department Chemie

Luxemburger Str. 116
50939 Köln
E-mail: ahmad.shaaban@uni-koeln.de

Erik Siebert

Technische Universität Dresden
Chair of Magnetofluiddynamics, Measurement- and Automation Technology

George-Bähr-Str. 3
1062 Dresden
E-mail: erik.siebert@gmail.com

Ioana Slabu

RWTH Aachen University
Applied Medical Engineering

Pauwelsstr. 20
52074 Aachen
E-mail: slabu@ame.rwth-aachen.de

Anastasia Storozhenko

Southwest State University
Regional Centre of Nanotechnology

50 let Oktyabrya 94
305040 Kursk
Russia
E-mail: storogenko_s@mail.ru

Andreas Tschöpe

Universität des Saarlandes
Experimentalphysik

Campus 0
66123 Saarbrücken
E-mail: a.tschoepe@nano.uni-saarland.de

Thilo Viereck

Inst. f. Elektr. Messtechnik, TU Braunschweig
Hans-Sommer-Str. 66
38106 Braunschweig
E-mail: t.viereck@tu-bs.de

Regine von Klitzing

TU Darmstadt
Physics

Alarich-Weiss-Strasse 10
64287 Darmstadt
E-mail: klitzing@fkp.tu-darmstadt.de

Joachim Wagner

Universität Rostock
Chemie

Dr. Lorenz Weg 2
18059 Rostock
E-mail: joachim.wagner@uni-rostock.de

Thomas Wallmersperger

TU Dresden
IFKM

George-Bähr-Str. 0
1069 Dresden
E-mail:
thomas.wallmersperger@tu-dresden.de

Paul Warncke

Friedrich-Schiller-University Jena
Department of Pharmaceutical Technology

Otto-Schott-Str. 41
7745 Jena
E-mail: paul.warncke@uni-jena.de

Samira Webers

University of Duisburg-Essen
Faculty of Physics

Lotharstraße 1
47057 Duisburg
E-mail: samira.webers@uni-due.de

Rudolf Weeber

ICP, Universität Stuttgart
Allmandring 3
70569 Stuttgart
E-mail: Rudolf.Weeber@icp.uni-stuttgart.de

Andreas Weidner

TU Ilmenau
BMTI

Gustav-Kirchhoff-Straße 2
98693 Ilmenau
E-mail: andreas.weidner@tu-ilmenau.de

Heiko Wende

University of Duisburg-Essen
Faculty of Physics

Lotharstr. 1
47048 Duisburg
E-mail: heiko.wende@uni-due.de

Frank Wiekhorst

Physikalisch-Technische Bundesanstalt
8.23 Metrology for Magnetic Nanoparticles

Abbestrasse 43071
10587 Berlin
E-mail: frank.wiekhorst@ptb.de

Emilia Wisotzki

Leibniz Institute of Surface Modification
Permoserstr. 15
4318 Leipzig
E-mail: emilia.wisotzki@iom-leipzig.de

Marcus Witt

TU Darmstadt
Festkörperphysik

Alarich-Weiss-Straße 10
64287 Darmstadt
E-mail: witt@fkp.tu-darmstadt.de

Lucas Wöckel

TU-Ilmenau
BMTI

Gustav-Kirchhoff Str. 2
98693 Ilmenau
E-mail: lucas.woeckel@tu-ilmenau.de

Mengbo Zhou

University of Jena
humboldtstr. 9
7749 Jena
E-mail: mengbo.zhou@uni-jena.de

Klaus Zimmermann

TU Ilmenau
Fakultät für Maschinenbau

Max-Planck-Ring 12
98693 Ilmenau
E-mail: klaus.zimmermann@tu-ilmenau.de

Andrey Zubarev

Ural Federal University
Mathematical

Lenin 51
620000 Ekaterinburg
Russia
E-mail: A.J.Zubarev@urfu.ru